Applied Science

Section

Journal of Research and Applications (JRA), UCSMTLA, 2019 Volume-01, Issue-01

Article ID - JRA190006

FABRICATION OF GRAPHENE AND GRAPHENE/PVA/Ag NANOCOMPOSITE FILMS AS SEMICONDUCTORS FROM WASTE PLASTIC BOTTLES

April Cho [1], Zin Mar Aung [2]

[1] MSc Student, Department of Chemistry, Meiktila University, Myanmar

[2] Associate Professor, Department of Chemistry, Meiktila University, Myanmar

[1] *Aprilcho269@gmail.com*

ABSTRACT

This research work focuses on the potential of utilizing "waste-treats-waste" by the synthesis of graphene using waste plastic bottles as source materials. It is studying the reproducible and affordable method for advanced applying of graphene and graphene based nanocomposites from waste plastic bottles by using pyrolysis method. The synthesized graphene is characterized by X-ray Diffraction analysis (XRD), Ultra–violent spectroscopy (UV), Scanning Electron Microscopy (SEM) and Thermogravimetric-Diffractional Thermal Analysis (TG-DTA). Moreover, the powerful modification of graphene/PVA/silver nanocomposite films was synthesized as modern semiconductors for advanced applyings in physical chemistry. Thus, the waste plastic bottles can be used to valuable carbon-based nanomaterials for use in electrical applications.Thus, it can be reduced the air, water and land pollution to the environment.

KEYWORDS*: graphene (Gr), polyvinyl alcohol (PVA), waste plastic bottles (WPB)*

1. INTRODUCTION

1.1 Waste Plastic Bottles

Nowadays, Myanmar has been facing with challenges of waste as a result of increasing income and consumption levels, urban population growth, and lack of effective waste treatment and disposal options. The level of air pollution, soil pollution, water pollution and global warming is increasing with the development of industries, population growth and weakness management of plastic wastes.

The disposal of plastic wastes represents as major challenge for all over the world in developing countries for waste and environmental management. The industrialization, rapid urbanization, economic growth and changes in consumption patterns have been accompanied by immense challenges in managing the country's solid waste. Because, the plastic has the insolubility about 300 years in the nature. Waste plastic bottles, one of the most common abundant industrial and municipal wastes and as an excellent candidate in the synthesis of carbon-based-materials, carbon microspheres, carbon nanotubes or activated carbon (Premakumara and Hengesbaugh, 2016).

Fig1. Waste Plastic Bottles

Graphene, the first truly 2D material, is a monolayer of carbon atoms bonded through sp^2 hybridization to form a regular hexagonal honeycomb lattice. Each atom has four bonds: one sigma bond with each of its three neighbors and one pi bond that is oriented out of plane. These atoms are about 1.42 A° apart. It's the thinnest material and more electrically conductive than copper about 1000,000 and it conducts heat than diamond at room temperature. Graphene is the last of a long string of continuous advances in the science of carbon and a gapless semiconductor with a linear low-frequency energy dispersion relation for charge carries (Wang, and Shi, 2015).

Graphene sheets in solid form usually show evidence in diffraction for graphite's (002) layering. This is true of some single-walled nanostructures. However, unlayered graphene with only (hkl) rings has been found in the core of presolar graphite onions. Electron diffraction patterns showed the expected honeycomb lattice. Suspended graphene showed "rippling of the flat sheet, with amplitude of about one nanometer.

Moreover, graphene is an excellent additive to significantly enhance mechanical, thermal, and electrical properties of polymer materials. The unique properties of graphene include high mechanical stiffness and strength, high specific surface area, high flexibility, high electrical conductivity, high carrier mobility, high thermal conductivity and optical transparency (Amollo et al*.,* 2017*)*. Confinement of graphene, combined with enhanced exchange properties within aqueous environment, is the key for the development of biosensors, biomedical devices, and water remediation applications (Abudabbus, 2017). Graphene can be applied in various applications such as transparent conductors, actuators nanocomposites, chemical sensors, biomedical applications, energy research, nanoelectronic devices. Graphene is a promising material for the preparation of graphene/polymer composites with enhanced electrical, mechanical, thermal, and gas barrier properties at extremely low loading ratio due to its unique structure.

The development of green processes for the synthesis of nanoparticles is evolving into a significant field. Chemical, Physical and Biological methods of these nanoparticles can be synthesized.

Silver nanoparticles are between 1 nm and 100 nm in size and have gained a lot of future research concern. Biological synthesis of nanoparticles was synthesized by some researchers and testing for antimicrobial activities. Silver nanoparticles are capable of applying in electronic and communication, health care, water treatment, environmental treatment, biotechnology and pharmaceuticals, food agriculture and catalysis.

Polyvinyl alcohol (PVA) is the world's largest volume, synthetic, water soluble polymer. PVA is classified into two classes namely: partially hydrolyzed and fully hydrolyzed. Partially hydrolyzed PVA is used in the food (Abudabbus*,* 2017). PVA is an odorless and tasteless, translucent, white or cream colored granular powder. It is used as a moisture barrier film for food supplement tablets and for foods that contain inclusions or dry food with inclusions that need to be protected from moisture uptake. It is soluble in water, slightly soluble in ethanol, but insoluble in other organic solvents. PVA is a water soluble and biodegradable polymer with excellent chemical resistance and an interesting material for biomedical application.

PVA/Gr composite films were used to produce Gr/PVA/Ag composites, respectively by electrochemical reduction of Ag^+ at a constant voltage, by in situ synthesis of silver nanoparticles within the PVA and PVA/Gr matrix, respectively (Abudabbus, 2017*)*. Graphene nanosheets are of considerable scientific and technological interest due their potential applications in structural, thermal, electronic and various other nanotechnologies (Jiang and Wang, 2011).

In this research work, as first step graphene is made from waste plastic bottles by using pyrolysis method. As second step, silver nanoparticle solution is prepared from Tiawan papaya fruit as reducing agent with the help of silver nitrate solution. After two steps, graphene/PVA/Ag nanocomposite films are prepared by combining graphene, PVA and silver nanoparticles with suitable ratios to obtain strong conductivity as semiconductors in physical chemistry.

2. EXPERIMENT

2.1 Materials and Methods

Polyethylene tetrapathalate (PET) bottles were selected among various waste plastic bottles in Meiktila Township. Ripen Taiwan papaya fruit was used as reducing agent. Polyvinyl alcohol (PVA), 0.003 M silver nitrate ($AgNO_3$**)** solution, deionized water and distilled water were applied as chemicals.

Fabrication of graphene were analyzed by XRD, UV, SEM and TG-DTA analysis as well as graphene/PVA/Ag nanocomposite films were analyzed by SEM and TG-DTA analysis. Resistances of prepared graphene/PVA/Ag nanocomposite films were determined by AVO (Ampere-Voltage-Ohm) meter.

2.2 Preparation of Graphene and Graphene / PVA/Ag Nanocomposite Films

Graphene was prepared from waste plastic bottles by using pyrolysis method. Firstly, waste plastic bottles were cleaned with distilled water and then they were cut into pieces with a belnder. These pieces were sieved with 100 mesh size sieves. Finally, graphene powder was obtained from sealed crucible containing these pieces by heating about 850°C for one hour in an electrical furnace.

Fig2. Graphene (a) sheet (b) powder

After preparation of graphene, silver nanoparticle solutions were made from ripen papya fruit to prepare graphene/PVA/Ag nanocomposite films.

Silver nanoparticle solution was made from ripen papaya fruit pulp extract with silver nitrate solution as reducing agents. Ripen papaya fruit pulp extract solution was prepared by mixing papaya fruit pulp and deionized water with (1:4) weight byvolume (w/v) ratio in the first step. And then, silver nitrate solution was poured down into these papaya fruit pulp solutions with (10:3) volume by volume ratio (v/v). Therefore, silver nanoparticle solution was obtained after few minutes at room temperature.

For fabrication of grapheme / PVA / Ag nanocomposite films, 1.0 g graphene powder and 3.0 g polyvinyl alcohol was weighed and put into a beaker. Then, silver nanoparticle solution and deionized water were poured down into it with volume by volume ratio (v/v). According to Table 2, the various ratios of graphene/PVA/Ag nanocomposite films were prepared by varying volumes of silver nanoparticle solution and deionized water.

Fig3. Ripen Taiwan papaya (a) fruit pulp (b) fruit pulp extract solution and (c) silver nanoparticle solution

Fig 4 Photographs of prepared graphene/ PVA/Ag nanocomposite films

3. RESULTS AND DISCUSSION

3.1 Preparation and Analysis of Graphene Powder from Waste Plastic Bottles

Graphene powders were synthesized from waste plastic bottles by pyrolysis method at 850 °C for one hour. The yield percentage of prepared graphene powder is shown in Table 1. It was found that average yield percent of prepared graphene powder is 10.542 %.

Table 1 Yield Percentage of Prepared raphene powder

No	Pieces of waste plastic bottles (g)	Graphene sheet (g)	Yield %
1	69.70	7.62	10.93
2	68.68	7.23	10.53
3	62.59	6.42	10.26
4	70.0	7.39	10.56
5	70.0	7.30	10.43
	Average yield %		10.542

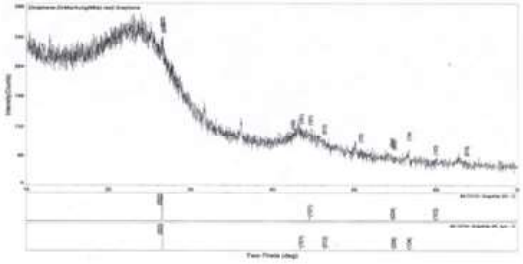

Fig5. XRD pattern of prepared graphene powder

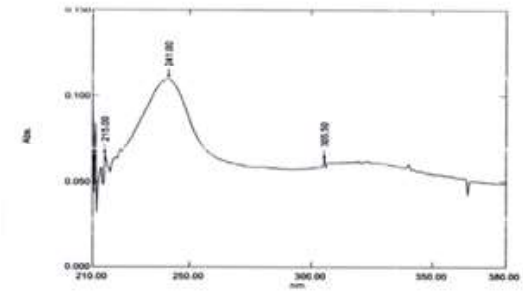

Fig6. UV-Visible spectrum of prepared graphene powder

Graphene was analyzed by XRD to obtain the crystallite size of prepared graphene powder. At (002), (100) and (101) peaks, a broad band was observed two-theta value between 20 and 30. Moreover, graphene was analyzed by UV to prove that it was build up with conjugated double bonds. As well as SEM analysis showed the surface morphology of prepared graphene powder and TG-DTA analysis was provided that thermal stability of graphene until 600°C under nitrogen gas. Therefore, these analyses can be revealed that the prepared powder is graphene powder.

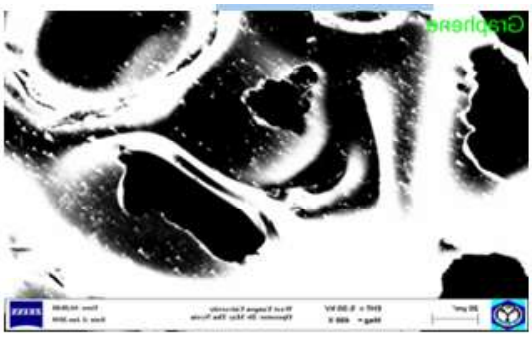

Fig7 SEM analysis of prepared grapheme powder

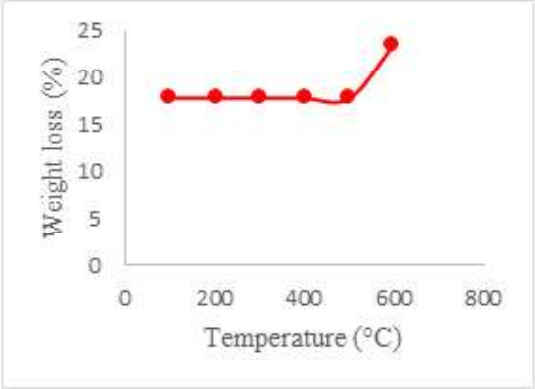

Fig 8 TG-DTA analysis of prepared graphene powder

3.2 Analysis of Silver Nanoparticles and Graphene/PVA/Ag Nanocomposite Film

Silver nanoparticle solution was prepared by mixing ripen papaya fruit pulp extract solution and silver nitrate solution with volume by volume ratio (v/v). It was characterized by UV-Vis spectroscopy to obtain the maximum wavelength ($»_{max}$) nearly at 418 nm and it was revealed that the wavelength of brown color silver nanoparticle solution was between (400-480 nm). However, it was analyzed by XRD to know the crystallite size and the size of prepared silver nanoparticles was (14-18 nm) and average crystallite size was16.41 nm. The structure of crystallite arrangement is face centered cubic (f.c.c) structure. Therefore, the prepared solution is silver nanoparticle solution.

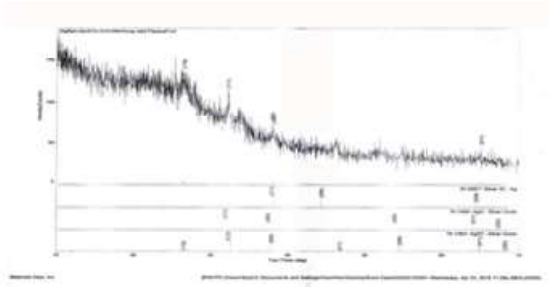

Fig10 XRD pattern for prepared silver nanoparticles

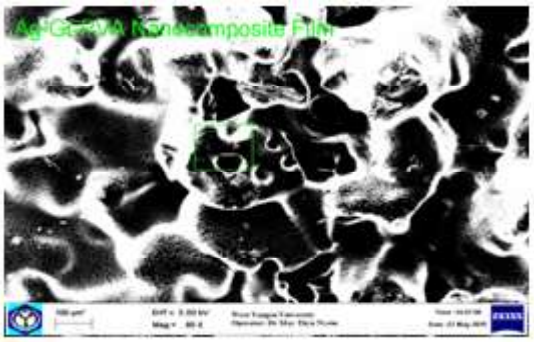

Fig 11 SEM microphotograph of Gr/PVA/Ag nanocomposite film

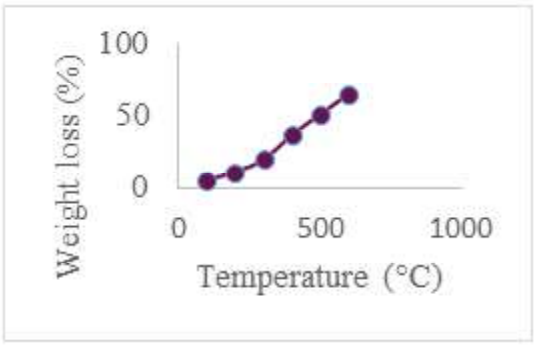

Fig 12 TG-DTA thermogram of Gr/PVA/Ag nanocomposite film

Graphene/PVA/Ag nanocomposite film was analyzed by SEM to detect the surface morphology and the surface is more uniform, flexible and stronger binding capacity than that of prepared graphene powder. Also it was characterized by TG-DTA which was given the high conductivity with the help of silver nanoparticles. Therefore, prepared graphene/ PVA/ Ag nanocomposite film is more suitable than prepared graphene powder to apply as semiconductors for electronic devices in physical chemistry.

3.3 Application of Prepared Nanocomposite Films

In the electronic field, these graphene/ PVA/Ag nanocomposite films can be applied for biosensors, semiconductors, catalysis, electro-chemical and communications, water treatment and electronic devices. For advanced applying of graphene based nanocomposite films as semiconductor, resistances were determined with AVO (Ampere-Voltage-Ohm) meter. The film F containing 1.0 g graphene, 3 g PVA and 100 mL silver nanoparticle solution, was possessed the lowest resistance value about 0.478 &!. Because the resistance is the reverse of conductance, this film has higher conductance.

Table 2 Resistances for Prepared Graphene/ PVA/ Ag Nanocomposite Films

Films	Volume of AgNPs solution (mL)	Deionized water (mL)	Resistance (□)
A	50	50	0.613
B	60	40	0.550
C	70	30	0.520
D	80	20	0.507
E	90	10	0.504
F	100	00	0.478

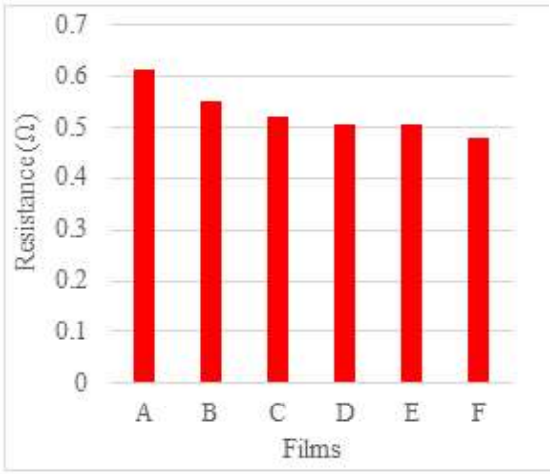

Fig13. Comparison the resistances of prepared graphene/PVA/Ag nanocomposite films

A= graphene (1.0 g) + 3 g PVA + (50 mL) Ag NPs+ (50 mL) D.I
B= graphene (1.0 g) + 3 g PVA+ (60 mL) Ag NPs + (40 mL) D.I
C= graphene (1.0 g) + 3 g PVA+ (70 mL) Ag NPs + (30 mL) D.I
D= graphene (1.0 g) + 3 g PVA + (80 mL) Ag NPs + (20 mL) D.I
E= graphene (1.0 g) + 3 g PVA+ (90 mL) Ag NPs + (10 mL) D.I
F= graphene (1.0 g) + 3 g PVA+ (100 mL) Ag NPs + (0 mL) D.I

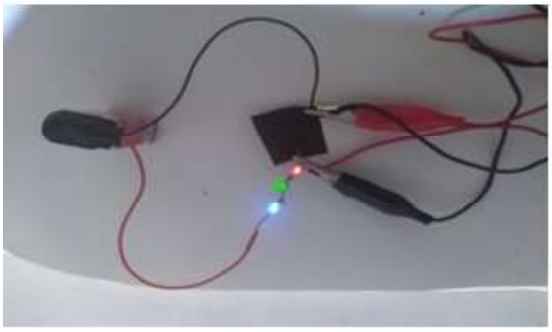

Fig14 Application of graphene/PVA/Ag nanocomposite films

4. CONCLUSION

Prepared graphene powders via recycled PET plastic bottles are used as precusor for graphene/ PVA/Ag nanocomposite films that they can be applied as semiconductors. In this research work, the waste plastic bottles can be reduced and reused to produce graphene and graphene nanocomposites by using affordable method. Therefore, not only it can be reduced environmental pollution but also commercially produced graphene as advanced applyings.

ACKNOWLEDMENT

We feel million thanks to committee chair person, Rector Dr. Mie Mie Khin, for permission of JRA publication.

We would like to express our profound gratitude to Professor, Dr Ni Ni Aung, Head of the Department of Chemistry and Dr Ni Ni Sein, Professor, Meiktila University, for their invaluable guidance, providing all of the departmental facilities and constant encouragement.

REFERENCES

[1] "Quick Study on Waste Management in Myanmar," p. 23.

[2] W. Xiluan and G. Shi, "Introduction to the chemistry of graphene," *Phys. Chem. Chem. Phys. PCCP*, vol. 17, Oct. 2015.

[3] A. A, G. T. Mola, and V. Nyamori, "Graphene for Thermoelectric Applications: Prospects and Challenges," *Crit. Rev. Solid State Mater. Sci.*, vol. 43, p. 133, Apr. 2017.

[4] J.-W. Jiang, J.-S. Wang, and B.-S. Wang, "Minimum thermal conductance in graphene and boron nitride superlattice," *Appl. Phys. Lett.*, vol. 99, no. 4, p. 043109, Jul. 2011.

Journal of Research and Applications (JRA), UCSMTLA, 2019 Volume-01, Issue-01

Article ID - JRA190015

SYNTHESIS AND IDENTIFICATION OF NAA(1-NAPHTHALENE ACETIC ACID) FROM NAPHTHALENE BALL

Khin Mooh Theint [(1)], Tin Myint Htwe[(2)]

[(1)]University of Technology (Yatanarpon Cyber City) Mandalay, Myanmar

[(2)] Mandalay Technological University, Mandalay, Myanmar

[(1)]khinmoohtheint@gmail.com

ABSTRACT

NAA (1-naphthalene acetic acid; $C_{12}H_{10}O_2$),is used to stimulate root formation in cuttings of woody and herbaceous plants to prevent premature flowers and fruit drop in apples, pears, grapes, guavas, mangoes, melons, citrus fruits, cucumbers, cotton, soya beans, etc. Among the various kinds of plant growth regulators, 1-naphthalene acetic acid especially encourages the root development of the plants. In this work, NAA was successfully synthesized from naphthalene which was extracted from naphthalene ball. The purity of naphthalene, a-chloromethyl naphthalene, a-naphthyl acetonitrile and 1-naphthalene acetic acid were also confirmed by Thin Layer Chromatography, UV and FT-IR spectroscopic methods. The yield percent of NAA based on naphthalene was found to be 21%. The yield percent of naphthalene from naphthalene ball is found to be 39.17%.

KEYWORDS*: naphthalene, 1-naphthalene acetic acid, plant growth regulator, root development, spectroscopic methods*

1. INTRODUCTION

1-naphthalene acetic acid (NAA) is an organic compound with the formula $C_{12}H_{10}O_2$. This colorless solid is soluble in organic solvents. It features a carboxyl methyl group (CH_2CO_2H) linked to the "1-position" of naphthalene. NAA is a synthetic plant hormone in the auxin family and is an ingredient in many commercial plant rooting horticultural products; it a rooting agent and used for the vegetative propagation of plants from stem and leaf cuttings. It is also used for plant tissue culture[1] . The hormone NAA does not occur naturally, and, like all auxins, is toxic to plants at high concentrations NAA is widely used in agriculture shown to greatly increase cellulose fiber formation in plants paired with another phytohormone. [2] NAA has been shown to greatly increase cellulose fiber formation in plants when paired with another phytohormone called gibberellic acid. Because it is in the auxin family it has also been understood to prevent premature dropping and thinning of fruits from stems. It is applied after blossom fertilization. Increased amounts can actually have negative effects however, and cause growth inhibition to the development of plant crops. It has been used on many different crops including apples, olives, oranges, potatoes, and various other hanging fruits. In order for it to obtain its desired effects it must be applied in concentrations ranging from 20–100 μg/mL[4]. NAA present in the environment undergoes oxidation reactions with hydroxyl radicals and sulfate radicals. Radical reactions of NAA were studied using pulse radiolysis technique. Hydroxyl adduct radical was formed as the intermediate during the reaction of hydroxyl radical with NAA. The intermediate naphthyl methyl radical was formed during the reaction of sulfate radical anion with NAA [4]. In micro propagation of various plants, NAA is typically added to a medium containing nutrients essential to the plants' survival. It is added to help induce root formation in various plant types. It can also be applied by spraying it onto plants and which is typical in agricultural use. It is prohibited in many areas to use it in high concentrations due to the health concerns towards humans and other animals. The synthetic auxins are used in commercial applications largely because they are resistant to oxidation by enzymes that degrade IAA. In addition to their

greater stability, the synthetic auxins are often more effective than IAA in specific applications. The synthetic auxins are favored in commercial applications because of their low cost and greater chemical stability. Synthetic auxins such as Indole butyric acid (IBA) and 1-Naphthalene acetic acid (NAA) have proven most effective. IBA and /or NAA are more stable than indole acetic acid (IAA) [5]. In the present work, NAA was synthesized from naphthalene.

In this case, naphthalene was prepared from naphthalene ball. The prepared NAA was checked by TLC and identified by UV and IR spectroscopic methods.

2. EXPERIMENT

In this work, naphthalene ball was used as naphthalene source.There are four reaction steps involved in this synthesis.They are

First step: Extraction of naphthalene from naphthalene ball

Second step: Preparation of a-chloromethyl naphthalene

from naphthalene

Third step : Preparation of a-naphthyl acetonitrile from

a- chloromethyl naphthalene

Fourth step :Preparation of 1-naphthalene acetic acid

(NAA) from a- naphthyl acetonitrile

Step (1)

The source of naphthalene was the naphthalene balls that can be purchased easily in markets. The pure naphthalene could be separated by sublimation.

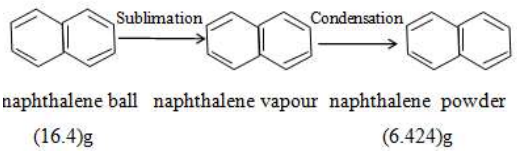

Fig 1. The reaction step for the extraction of naphthalene from naphthalene ball

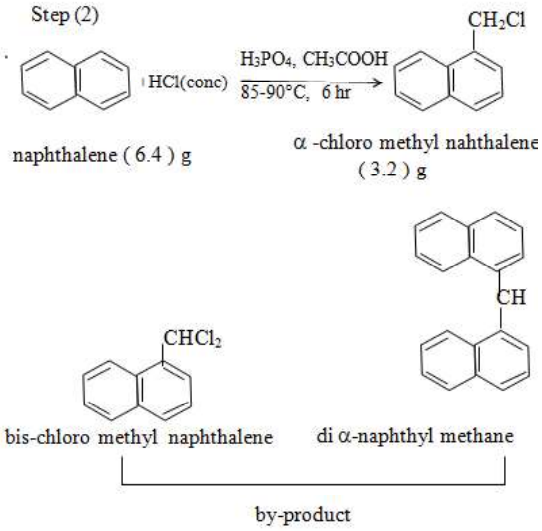

Fig 2. The reaction step for the preparation of a -chloro methyl naphthalene from naphthalene

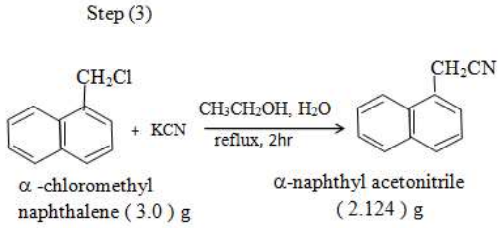

Figure 3. The reaction step for the preparation of a-naphthyl acetonitrile from a-chloro methyl naphthalene

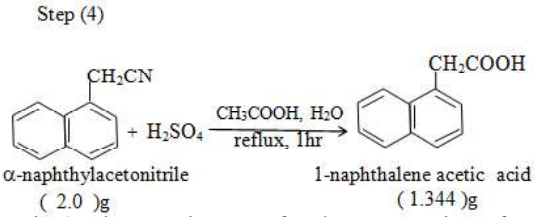

Fig 4. The reaction step for the preparation of 1-naphthalene acetic acid from a- naphthyl acetonitrile

The resulting naphthalene was collected and stored in a sealed glass bottle for further investigation and synthesis.[5] Fig1.In each step, isolation, purification and characterization by molecular spectroscopy such as UV and FT-IR were carried out. The precursor naphthale, a -chloro

methyl naphthalene, a - naphthyl acetonitrile and the final product NAA were also checked by thin layer chromatography and confirmed by determination of melting points. The solvent system used for TLC was carbon tetrachloride or n-hexane for naphthalene and benzene, acetone, acetic acid (15:6:1) v/v for NAA. Fig 7.The FT-IR spectrum and Ultra-Violet data of the isolated NAA were also recorded.

3. RESULTS AND DISCUSSION

Naphthalene was prepared from naphthalene ball. Table1 shows the yield percents of naphthalene from it. The results are given as an average of six experimental determinations. In this work, naphthalene obtained from naphthalene ball was used as precursor to synthesize 1-naphthalene acetic acid (NAA). The synthesis of NAA from coal tar was also carried out because coal tar is more abundant. It is also a waste effluent of steel mill and can be purchased locally.

Table1.Yield Percent of Naphthalene from Naphthalene ball

Experimental Yield (%)	Literature Value[8]
39.17 %	98.6%

Table 2. shows the characteristic properties of naphthalene from naphthalene ball. The melting point of naphthalene from naphthalene ball is found to be nearly agree with the literature value. The other characteristic properties of naphthalene are also found to be nearly the same. Therefore, the naphthalene from naphthalene ball was used as precursor in the synthesis of 1-naphthalene acetic acid (NAA).

According to UV data, the absorption peaks at 215.79 and 274.70 nm which are almost consisted with those of the literature value 218 and 275 nm [6]. The UV absorption spectrum of naphthalene from naphthalene ball was depicted in Fig 5.

Naphthalene samples were identified by Fourier Transform Infra-Red spectroscopy.Fig6. is FT-IR spectra of naphthalene samples from naphthalene ball. FT-IR spectrum revealed the presence of symmetric stretching C-H of ring, asymmetric and symmetric stretching vibration, over tone and combination bands of aromatic ring, C=C ring skeleton vibration (aromatic ring) and ring stretching

Table2. Characteristic Properties of Naphthalene

	Naphthalene from Naphthalene ball	
Properties	Experimental Work	Literature
Melting Point	80.3°C	81°C
Colour	White	White
Odour	Strong smell	Strong smell
Solubility	Benzene, chloroform cyclohexane, n-hexane	Benzene,chloroform cyclohexane, n-hexane

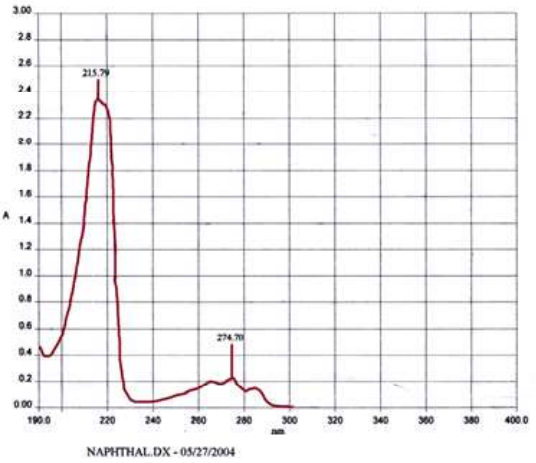

Fig5. UV spectrum of naphthalene

at 3047.85, 2980.12, 1650, 1591.94, 1500 and C-H bending in plane, C-H out of plane bending and C=C bending (out of plane ring at 1387.68, 958.80 and 481.28cm^{-1}.These absorptions were in agreement with literature values [6,7] thus, naphthalene from naphthalene ball source is pure.

Peak Report
File: C:\FIRST\TMP\KMT-5.RAS
Title: Sample for 1
Filter: Three Point Center of Gravity

cm-1	%T	cm-1	%T	cm-1	%T	cm-1	%T
471.28	15.55	481.28	15.15	779.83	7.05	958.80	19.77
1387.68	17.46	1591.94	19.02	3047.85	12.23		

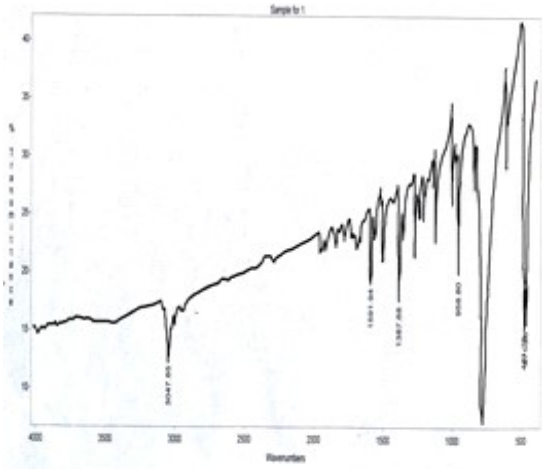

Fig6. FT - IR spectrum of naphthalene

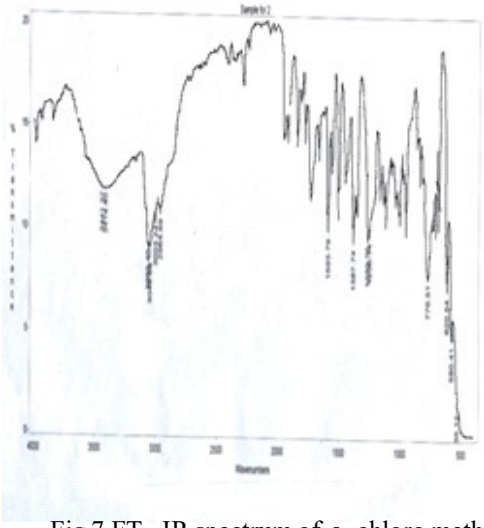

Fig 7.FT - IR spectrum of a -chloro methyl naphthalene

α - chloromethyl naphthalene samples prepared from naphthalene ball sources were characterized by taking FT-IR spectrum and by determining its melting point. The melting point of prepared a- chloromethyl naphthalene compound is (28.6°C) and the melting points of a- chloromethyl naphthalene were agreeable with the literature values (26 - 29°C)[9].

The yield percents of a- chloromethyl naphthalene from naphthalene is 50.0%. Fig 7 is the FT-IR spectra of -chloromethyl naphthalene. FT-IR spectrum of a-chloromethyl naphthalene revealed the presence of symmetric stretching C-H of alkene indicates at 3441.37 and 3414.40 cm^{-1}, asymmetric stretching CH_2 at 3065.46 cm^{-1} aromatic ring at 3003.24cm^{-1}, asymmetric CH_3 at 2964.69cm^{-1}, C=C ring stretching at 1593.79 cm^{-1} , C-H bending (in plane) at 1387.74,1270.76 and 1256.14 cm^{-1}, C-Cl stretching at 776.51cm^{-1} and C=C bending (out of plane) at 580.41 cm^{-1}.These absorptions were in agreement with literature values .

Peak Report
File: C:\FIRST\TMP\KMT.RAS
Title: Sample for 2
Filter: Three Point Center of Gravity

cm-1	%T	cm-1	%T	cm-1	%T	cm-1	%T
412.18	0.10	422.91	0.09	440.18	0.06	453.75	0.02
469.11	0.07	535.12	1.42	580.41	4.70	620.54	7.03
776.51	7.73	1256.14	9.62	1270.76	9.48	1387.74	9.28
1593.79	9.82	2964.69	10.60	3003.24	10.28	3048.69	8.44
3065.46	9.11	3414.40	11.82	3441.37	11.89		

α -naphthyl acetonitrile samples prepared from naphthalene ball sources were characterized by taking FT-IR spectrum and by determining its melting point. The melting point of prepared a-naphthyl acetonitrile compound is (30°C) and the melting points of a-naphthyl acetonitrile were agreeable with the literature values(33 - 35°C).[9] The yield percents of a- naphthyl acetonitrile based on the weight of a-chloromethyl naphthalene is 70.8% and the yield percents of a- naphthyl acetonitrile based on the weight of naphthalene is 33.2%. Fig 8 is the FT-IR spectra of a-naphthyl acetonitrile. FT-IR spectrum of a-naphthyl acetonitrile revealed the presence of aromatic C-H stretching indicates at 3047.95 cm^{-1}, nitrile, C°N at 2264.4cm^{-1}, overtone and combination bonds (weak) at1732.31cm^{-1}, ring stretching (very variable intensity) at 1592.03 cm^{-1} ,

C-H in plane bending, usually weak at 1387.56, 1273.28 and 1120.23cm^{-1}, out of plane bending of C-H at 958.55cm^{-1} , C-H out of plane bending indicates at 854.46, 781.9 and 626.7cm^{-1}.These absorptions were in agreement with literature values . Fig 8.

Peak Report
File: C:\FIRST\TMP\NAPH.RAS
Title: Sample for -Naphthyl acetonitrile
Filter: Three Point Center of Gravity

cm-1	%T	cm-1	%T	cm-1	%T	cm-1	%T
471.48	3.10	480.39	2.56	783.90	0.44	958.55	3.17
1387.56	1.91	1503.47	2.38	1592.03	2.18	3047.95	0.74

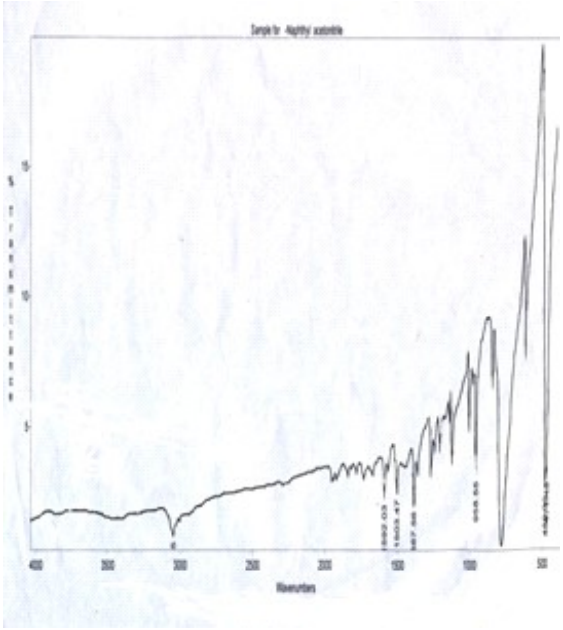

Fig8. FT-IR spectrum of a-Naphthylacetonitrile

1) Stationary phase : Silica gel
2) Mobile phase: Benzene: Acetone: Acetic acid (15:6:1)
3) Visualization :UV 254 nm
4) R_f value : 0.85

Fig9. Thin Layer Chromatograph of 1-naphthalene acetic acid (Authentic sample, synthesized sample)

1-naphthalene acetic acid ($C_{12}H_{10}O_2$), melting point (128°C) and the melting points of 1-naphthalene acetic acid were agreeable with the literature values(129-135°C) . Fig 9. shows Thin Layer Chromatograph of synthesized 1-naphthalene acetic acid comparing with standard sample. According to UV data, the absorption peaks at 223 and 280.25 nm which are almost consisted with those of the literature value 218 and 275 nm. The yield percent of 1-naphthalene acetic acid based on a- naphthyl acetonitrile is 67.2%. The yield percents of 1-naphthalene acetic acid based on naphthalene is 21%. Fig10. show FT-IR spectrum of 1-naphthalene acetic acid. It revealed the presence of COOH and intense O–H and three adjacent hydrogen C-H out of plane bending vibration of a substituted naphthalene indicate at 1217.69, and at 931.34,792.36 cm^{-1}, Fig11.[13][14]

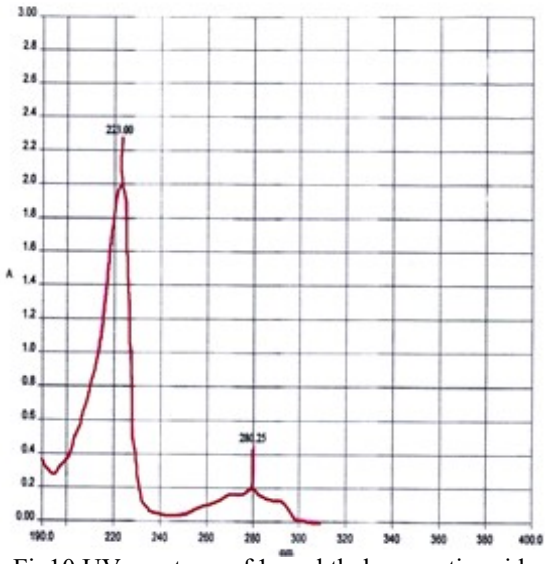

Fig10.UV spectrum of 1-naphthalene acetic acid

Peak Report
File: C:\FIRST\TMP\KMT-6.RAS
Title: Sample for Pure NAA
Filter: Three Point Center of Gravity

cm-1	%T	cm-1	%T	cm-1	%T	cm-1	%T
539.04	29.33	623.72	33.27	778.20	4.90	792.95	16.96
931.52	20.61	1159.41	27.77	1184.36	17.68	1217.69	5.61
1250.06	14.41	1268.06	22.79	1292.55	24.64	1327.80	22.23
1410.47	11.50	1597.94	24.08	1692.14	1.91	2535.75	22.63
2644.63	19.28	2728.03	19.06	2913.53	12.68	2947.35	13.75
3012.60	12.68	3057.65	11.66				

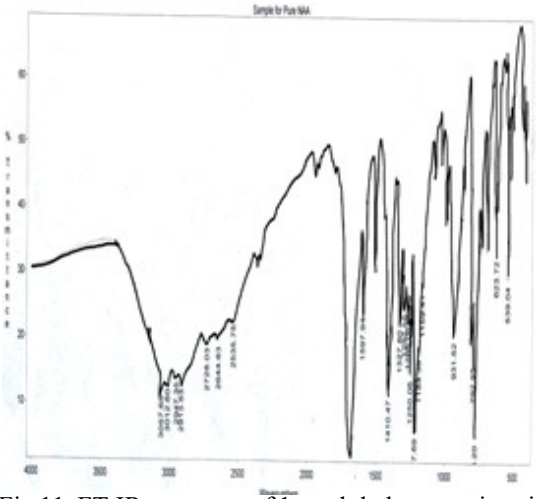

Fig 11. FT-IR spectrum of 1-naphthalene acetic acid

4. CONCLUSION

In this work, 1-naphthalene acetic acid was successfully synthesized from naphthalene ball. NAA was checked by TLC and identified by UV and FT-IR absorption spectroscopy. The yield percent of naphthalene from naphthalene ball is found to be 39.17%.The yield percent of NAA based on the precursor, naphthalene was found to be 21%.

Many NAA-based plant growth regulators are in the market. Dip 'N Grow®, AGRONAA are such products.

The former contains 1% IBA and 0.5% NAA and the latter 4.5% 1-naphthalene acetic acid plus solvents and other inert ingredients [11]. Many experiments were done on plant growth regulators. In Myanmar, all sorts of legumes are cultivated and exported every year. Actually Myanmar is the second largest legumes exporting country in the world since 2002. At least 18 varieties of legume was cultivated and among them, exported soy bean was 4% and that of cow pea was also nearly 4% of the total export. Varieties of legumes were exported to neighboring countries such as India, Pakistan, Indonesia, Singapore, Malaysia and Japan. As the market demand is increasing, Myanmar should also increase its legume cultivation. In the hope to fulfill this novel ambition, this research work was performed for the synthesis of NAA from readily available sources, naphthalene ball. For further research work, the synthesis of 1-naphthalene acetic acid from readily available source, coal tar and application of NAA with soy beans and cow peas in soil and aqueous medium were also carried out.

ACKNOWLEDGMENT

I wish to acknowledge my deepest gratitude to Rector (acting) Dr Aung Win, University of Technology Yadanarpon Cyber City, for allowing to carry out this research paper.

I would like to thank Dr.Reenu, Pro rector, who give me all kinds of useful helps.

I wish to convey my sincere and deepest gratitude to my research supervisors, Dr.Tin Myint Htwe, Retired Professor and Head, Department of Engineering Chemistry, Mandalay Technological University and Dr.Toe Shein, Retired Professor and Head, Department of Engineering Chemistry, Yangon Technological University for his close supervision, helping me for my research , invaluable advice, guiding me at each step and generous encouragement of this research work.

Grateful thanks are also due to Dr. Phyu Phyu Win, Deputy Director General, Department of Research and Innovation (Yangon) Department for invaluable advice and all kinds of useful helps for this paper.

REFERENCES

[1] H. Morikawa and M. Takahashi, "Cultured cells of Australian laurel, Pittosporaceae and a method for culturing tissues by using said cultured cells," US20020137206A1, 26-Sep-2002.

[2] "Tomlin, C.D.S. (2006) The Pesticide Manual, A World Compendium, 14th Edition British Crop Protection Council. Alton, Hampshire, 186-187. - References - Scientific Research Publishing." [Online]. Available: https://www.scirp.org/

(S(lz5mqp453edsnp55rrgjct55))/reference/ReferencesPapers.aspx?ReferenceID=1880037. [Accessed: 10-Dec-2019].

[3] "Determination of 1 naphthylacetic acid in commercial formulations - Technische Informationsbibliothek (TIB)." [Online]. Available: https://www.tib.eu/en/search/id/springer%3Adoi~10.1007%252FBF01242657/Determination-of-1-naphthylacetic-acid-in-commercial/. [Accessed: 10-Dec-2019].

[4] "Radical chemistry of glucosamine naphthalene acetic acid and naphthalene acetic acid: a pulse radiolysis study - Shibin - 2014 - Journal of Physical Organic Chemistry - Wiley Online Library." [Online]. Available: https://onlinelibrary.wiley.com/doi/abs/10.1002/poc.3285. [Accessed: 10-Dec-2019].

[5] "(PDF) Hopkins W.,Huner N.-Introduction to plant physiology-2008.pdf | Susmita Das - Academia.edu." [Online]. Available: https://www.academia.edu/24551123/Hopkins_W._Huner_N.-Introduction_to_plant_physiology-2008.pdf. [Accessed: 10-Dec-2019].

[6] "Organic Chemistry 3rd Third Edition: Robert Neilson Boyd Robert Thornton Morrison: Amazon.com: Books." [Online]. Available: https://www.amazon.com/Organic-Chemistry-Neilson-Thornton-Morrison/dp/B000IXV40E. [Accessed: 10-Dec-2019].

[7] "PhotochemCAD Chemicals." [Online]. Available: https://omlc.org/spectra/PhotochemCAD/index.html. [Accessed: 10-Dec-2019].

[8] E. Pretsch, P. Bühlmann, and C. Affolter, *Structure Determination of Organic Compounds: Tables of Spectral Data*, 3rd completely rev. and enlarged ed. 2000. Corr. 2nd printing edition. Berlin/ ; New York: Springer, 2000.

[9] A. P. Vogel, *A text-book of practical organic chemistry including qualitative organic analysis.* London: Longman, 1972.

[10] K. Theint and T. Htwe, "Synthesis of NAA (2-(1-Naphthyl) Ethanoic Acid) from Coal Tar and Application of Plant Hormone with Soy Bean and Cow Pea in Aqueous Medium," p. 6, 2012.

[11] "The Myanmar Times," *The Myanmar Times*. [Online]. Available: https://www.mmtimes.com/. [Accessed: 10-Dec-2019].

Journal of Research and Applications (JRA), UCSMTLA, 2019 Volume-01, Issue-01

Article ID - JRA190017

ISOLATION OF A PURE ORGANIC COMPOUND AND DETERMINATION OF ACUTE TOXICITY OF ETHANOLIC PLANT EXTRACT FROM *Cassia Renigera* WALL (NGU - ZAT)

Chaw Theingi Khin[(1)]

[(1)] University of Technology (Yatanarpon Cyber City), Myanmar

[(1)]*chawchaw97.cc@gmail.com*

ABSTRACT

In this paper, one of Myanmar indigenous medicinal plants, namely *Cassia renigera* Wall. (Ngu-zat) was selected for preliminary phytochemical screening and antibacterial activity tests. The acute toxicity of 95% ethanolic root extract of *Cassia renigera* Wall (Ngu-zat) was tested by Litchfield and Wilcoxon on ICR mice. Furthermore, a pure organic compound could be isolated from the root of Ngu-zat by using advanced separation techniques such as Thin Layer and Column Chromatography. This isolated compound was rechecked by phytochemical screening and antimicrobial activity tests by agar-well diffusion method. The functional groups of this pure organic compound were identified by FT-IR spectroscopic method.

KEYWORDS: *agar- well diffusion method, Cassia renigera Wall., FT-IR spectroscopic method*

1. INTRODUCTION

Plants are rich source of antioxidants, which is evinced through many reports on medicinal plants with antioxidant potential. Many plants possess antioxidant activity because they contain antioxidative phyto-chemicals such as phenolic compounds, which may reduce the risk of cancer, cardiovascular disease and many other diseases, as well as reduce the antioxidative damage of cellular components. They play a key role as antioxidants due to the presence of phenolic groups (hydroxyl substituents next to their aromatic structure), which enable them to scavenge free radicals. In recent decades, the phytochemical constituents of plants have received much attention due to their potential utilization in the nutraceutical and drug industries [1].

Cassia renigera Wall (Ngu-zat) commonly known as Burmese pink cassia is a beautiful ornamental tree fit for garden and as avenue trees. Though names Burmese pink cassia, the tree is found widely in India, and almost all tropical regions of the world. Pink cassia trees grow quickly and will be in full bloom in four to five years. The leaves fall off with the beginning of flowering season. The flowering season immediately precedes monsoon season and wraps the tree with a pink blanket. The flowers fall away at the beginning of rains [2].

In this research work, the acute toxicity of ethanolic extract of *Cassia renigera* Wall (Ngu-zat) could be determined. A pure organic compound could also be isolated from the root of Ngu-zat by using advanced chromatographic techniques such as column and thin layer, respectively.

1.1 Botanical Description

Family - Caesalpiniaceae

Common name - Burmese Pink Cassia
Botanical name - *Cassia renigera* Wall.

Myanmar name - Ngu-zat

Medicinal uses - For adenopathy, burning sensations, leprosy, skin diseases, syphilis and tubercular glands.

Part used - Root

Fig1. Flowers and plant of *Cassia renigera* Wall.

1.2 Aim

The aim of this research work is to isolate the pure organic compound from the root of *Cassia renigera* Wall (Ngu-zat) and to determine the acute toxicity of ethanolic crude extract of this root.

2. MATERIALS AND METHODS

2.1 Sample collection

The root of Ngu-zat for experiment was collected from Patheingyi Township, Mandalay Region, Myanmar. The samples were cut into small pieces and allowed to dry in air. Then the dried pieces were stored in a well-stoppered bottle and used throughout the experiment.

2.2 Phytochemical Tests for *Cassia renigera* Wall (Ngu-zat)

The phytochemical tests of the root of Ngu-zat were tested by test tube methods [3].

2.3 Antibacterial Activities of *Cassia renigera* Wall (Ngu-zat)

The antibacterial activities of the root of Ngu-zat were tested by using agar well diffusion method on three selected organisms.

2.4 Determination of Acute Toxicity of Ethanolic Extract of Root of *Cassia renigera* Wall (Ngu-zat)

2.4.1 Materials

Different concentrations of ethanolic extracts of *Cassia renigera* Wall (Ngu-zat) root, 40 Institute of Cancer Research (ICR) of both sexes (body weight 25-30g), Mouse cages, Animals balance, Distilled water, Drinking water bottles, Surgical gloves and masks, Cannula, Picric acid for marking.

2.4.2 Preparation of Plant Extract

The air dried root samples were coarsely powdered. The powdered 20 gm was then mixed 100 mL of 95% ethanol and kept at room temperature for 36 hours. The mixture was then filtered and the filtrate was free from the solvent under partial vacuum at 40°C. Extracts were stored in a refrigerator and used throughout the acute toxicity test.

2.4.3 Method

A total of 40 ICR mice of both sexes (body weight 25-30 g) used in this study were randomly divided into four groups with 10 animals in each. Three were tested groups and one was control group. 10 ICR mice in each group were fasted overnight before administration of the ethanol extract of root of *Cassia renigera* Wall. The acute toxicity study was carried out with an oral administration of ethanol extract of *Cassia renigera* Wall at increasing doses of 2 g/kg, 4 g/kg and 8 g/kg on the three test groups and 10mL/kg of distilled water on control group. After administering the extract orally, each group containing mice was kept in individual cage with free access to food and water and was observed toxic effects daily for two weeks. The median lethal dose (LD_{50}) was determined from the number of animals surviving at the end of two weeks periods [4].

Fig 2. ICR mice of both sexes and dministrationof ethanolic extract solution to the experimental mice

2.5 Extraction and Isolation of A Pure Organic Compound (CTK-1)

2.5.1 Materials, Methods and Instruments

Commercial grade reagents from BDH, MERCK, etc, were used in this research work. Analytical and preparative TLC was performed by using precoated silica gel plates (Merck co Inc, Kiesel gel $60F_{254}$). Silica gel (60, 70 to 230 Mesh ASTM) was used for column chromatography.

The following advanced instruments were used in the characterization of the samples and identification of the pure compound.

1. UV-Lamp (Lambda-40, Pekin Elmer Co. England)

2. FT-IR spectrometer, Shimadzu, Japan

2.5.2 Column Separation of Crude Extract

Air dried sample (500)g was percolated with EtOH (1000 mL) for two months. The percolated solution was evaporated and then extracted with (150 mL) of ethyl acetate. When ethyl acetate extract was concentrated, the crude sample (2.35 g) was obtained.

The crude extract (2.35g) was separated by column chromatographic method using silica gel (70-230 mesh) as an adsorbent and various ratios of n-hexane and ethyl acetate ranging from non-polar to polar were used as eluent. Totally (202) fractions were obtained. Each and every fractions were checked by TLC. The same R_f value fractions were combined. Ten combined fractions were obtained. The fraction (X) was checked by TLC for purity. It gives one spot on TLC and UV active. It was recrystallized by 40% ethylacetate in n-hexane for two times. The pale orange needle shape crystal (15.8 mg) was obtained. The yield percent of this pure compound was found to be (0.67%) based upon the EtOAc crude extract.

2.5.3 Phytochemical Test for Pure Organic Compound (CTK-1)

A small amount of pure crystal (CTK-1) was boiled with ethanol in a water-bath for a few minutes. The mixture of 1% $FeCl_3$ and 1% $K_3[Fe(CN)_6]$ solution was added to it [3].

2.5.4 Antimicrobial Activities of Pure Organic Compound (CTK-1)

Pure compound was rechecked the antimicrobial activities by using agar well diffusion method on six selected organisms.

2.5.5 Functional Groups Identification of Pure Organic Compound (CTK-1)

FT-IR spectrum of pure compound (CTK-1) was measured at Department of Chemistry, University of Mandalay, Myanmar. **3.** RESULTS AND DISCUSSION

3.1 The Results of Phytochemical Test for *Cassia renigera* Wall (Ngu-zat)

According to table (1), the root of Ngu-zat consists of alkaloid, flavonoid, steroid, terpene, glycoside, reducing sugar, polyphenol and saponin respectively.

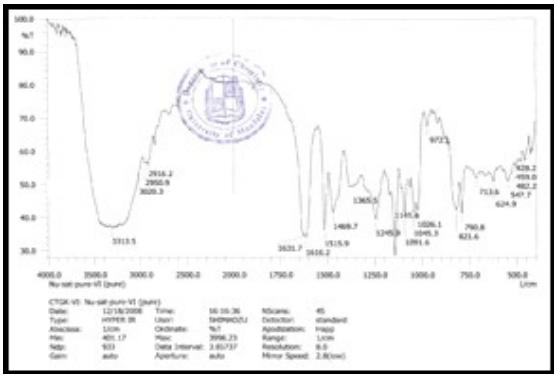

Fig 3. FT-IR Spectrum of Pure Organic Compound (CTK-1)

Table 1 Phytochemical Tests for *Cassia renigera* Wall (Ngu-zat)

No.	Constituents	Reagent used	Observation	Inference
1.	Alkaloid	(i) Dragendroff's reagent	Orange ppt	+
		(ii) Mayer's reagent	Cream color	+
2.	Flavonoid	EtOH, Mg turning, Conc: HCl	Red color	+
3.	Steroid	Pet-ether, Conc: H_2SO_4, acetic anhydride	Reddish brown color	+
4.	Terpene	$CHCl_3$, Conc H_2SO_4, acetic anhydride	Red color	+
5.	Glycoside	10% lead acetate	White ppt	+
6.	Reducing sugar	Benedict's solution	Red ppt	+

7.	Polyphenol	1% $FeCl_3$, 1%$K_3[Fe(CN)_6]$	Bluish green color	+
8.	Saponin	EtOH, Conc: H_2SO_4	Frothing	+
9.	Lipophilic	0.5 M KOH	-	-
10.	Tannin	1% $FeCl_3$	-	-

(+) = presence of constituents

(–) = absence of constituents

3.2 The Results of Antibacterial Activities of *Cassia renigera* Wall (Ngu-zat)

The results of the antibacterial activities of the root of Ngu-zat are tabulated in Table (2).

Table 2 Antibacterial Activities of *Cassia renigera* Wall (Ngu-zat)

Sample	Organisms	n-hexane	EtOAc	EtOH
Ngu-zat	*S. aureus*	–	++	++
	E. coli	–	++	++
	S. typhi	–	++	++

Agar well ~ 7 mm

(+) ~ 7 mm – 11 mm *S. aureus* = *Staphylococcus aureus*

(++) ~ 12 mm – 16 mm *E. coli* = *Esherichia coli*

(+++) ~ 17 mm above *S. typhi* = *Salmonella typhi*

According to this table, the ethyl acetate and ethanol extracts of this plant respond the medium activities on all tested organisms.

Staphylococcus aureus Esherichia col *Salmonella typhi*

Fig 4. Antibacterial activities of *Cassia renigera* Wall

3.3 The Results of Acute Toxicity Test

The ethanolic extract of root of Ngu-zat was tested for acute toxicity on albino mice. Acute toxicity study was evaluated by the method of Litchfield and Wilcoxon (1949) [4]. These results are shown in Table (3).

The mice treated with 2 g/kg, 4 g/kg, 8 g/kg doses of ethanolic extract of *Cassia renigera* Wall (Ngu-zat) were kept under observation for 2 weeks. All the mice were alived and did not show any toxic symptons such as body weight loss and restlessness. Therefore the median lethal dose (LD_{50}) was more than 8 g/kg.

Table 3 AcuteToxicity Test of 95 % Ethanolic Extract of *Cassia renigera* Wall (Ngu-zat)

Group	Treatment (g/kg)	No. of mice used	No. of mice death	No. of mice survived	% death
I	2	10	0	10	0
II	4	10	0	10	0
III	8	10	0	10	0
IV	10 ml/kg (vehicle)	10	0	10	0

Table (4) presents commonly used terms for toxicities along with the dose equivalents both in rats and humans.

Table4. Commonly used Terms for Toxicities

Commonly used terms	LD_{50} (single oral does per kg in mice)	Probable lethal does for man
Extremely toxic	1.5 mg or less	65 mg
Highly toxic	1.5-75 mg	4 g
Moderately toxic	70-700 mg	30 g

Slightly toxic	0.75-7 g/ kg	250 g
Practically nontoxic	7-21 g/kg	1 kg
Relatively harmless	21 g/kg or more	> 1 kg

According to Table (3) and (4), it was found that 8 g/kg of ethanol extract of Ngu-zat was practically non-toxic.

3.4 The Result of Phytochemical Test for Pure Organic Compound (CTK-1)

Phytochemical Test for Pure Organic Compound gives the bluish green color solution which indicates the presence of polyphenol.

3.5 The Result of Antimicrobial Activities of Pure Organic Compound (CTK-1)

The results of the antimicrobial activities of the pure compound are shown in table (5).

Table 5 Antimicrobial Activities of Pure Organic Compound (CTK-1)

Sample	Organisms					
	I	II	III	IV	V	VI
Pure Compound (CTK-1)	++	++	+	++	++	+

Organisms

Agar well - 10 mm

10 mm ~ 14 mm (+)

15 mm ~ 19 mm (++)

20 mm above (+++)

I. *Bacillus subtilis*

II. *Staphylococcus aureus*

III. *Pseudomonas eruginosa*

IV. *Bacillus pumalis*

V. *Candida albicans*

VI. *E. Coli*

According to this table, the pure compound (CTK-1) responds medium activities on four tested organisms, such as *Bacillus subtilis, Staphylococcus aureus, Bacilluspumalis, Candida albicans* and low activities on other two organism.

Bacillus subtilis *Staphylococcus aureus* *Candida albicans*

Pseudomonus aeruginosa *Bacillus pumalis* *E. coil*

Fig 5. Antimicrobial Activities of Pure Organic Compound (CTK-1)

3.6 FT-IR Assignments of Pure Organic Compound (CTK-1)

The resulting functional groups are tabulated in Table (6).

Table 6 The Absorption Peaks and their Assignments of Pure Compound (CTK-1)

Absorption peaks (cm^{-1})	Assignments
3315.5	O–H stretching vibration of alcohol group
3020.3	C–H stretching vibration of sp^2 hydrocarbon
2950.9, 2916.2	Unsymmetrical and symmetrical C–H stretching vibration of sp^3 hydrocarbon
1631.7, 1616.2	C=C ring skeletal stretching vibration of aromatic benzene ring.
1469.7	C–H in plane bending vibration of allylic hydrocarbon

1245.9	C–C–O stretching vibration of alcohol group
1091.6, 1045.3	C–O–C stretching vibration of ether group.
972.1, 821.6	C–H out of plane bending vibration of trans or E and cis or Z alkenic group.

The FT-IR spectrum of pure organic compound (CTK-1) isolated from Ngu-zat was measured at the Department of Chemistry, University of Mandalay and it is shown in Figure (3).

In this spectrum, the broad band at 3313.5 cm^{-1} indicates the O–H stretching vibration of alcohol group. The peaks at 2950.9 cm^{-1} and 2916.2 cm^{-1} are the unsymmetrical and symmetrical C–H stretching vibrations of sp^3 hydrocarbons. The peaks which appear at 1631.7 cm^{-1} and 1616.2 cm^{-1}indicate the presence of the C = C ring skeletal stretching vibration of aromatic benzene ring.The band which occurs at1469.7cm^{-1}should be the C–H in plane vibration of allylic hydrocarbon.

The peak at 1245.9 cm^{-1} represents the C–C–O stretching vibration of alcohol group. The two bands at 1091.6 cm^{-1} and 1045.3 cm^{-1} express the presence of C–O–C stretching vibration of ether functional group.

In addition, the C–H out of plane bending vibration of trans or E and cis or Z alkenic groups could be observed at 972.1 cm^{-1} and 821.6 cm^{-1} [5].

4. CONCLUSIONS

In this research work, Myanmar indigenous medicinal plant *Cassia regnigera* Wall. (Ngu-zat) was tested by preliminary phytochemical screening. As mentioned in Table (1), the root of Ngu-zat contains alkaloid, flavonoid, steroid,terpene, glycoside, reducing sugar, polyphenol and saponin compounds.

Moreover, the antibacterial activities of various solvent extracts of root of Ngu-zat were tested by agar-well diffusion method on three selected organisms such as *Staphylococcus aureus*, *Escherichia coli* and *Salmonella typhi*. As described in Table (2), ethylacetate extract of this plant responds medium activities on all tested organisms. Hence, it was selected for detailed chemical investigation.

In addition, the 95 % ethanolic extract of root of Ngu-zat was tested for acute toxicity on ICR mice. This extract did not show any toxic symptoms when tested for acute toxicity (LD_{50}) up to maximum dose of 8g/kg, so it was practically non-toxic.

A pure organic compound (CTK-1) was isolated from the root of Ngu-zat by using Thin Layer and Column Chromatographic techniques. Pale orange needle shaped crystal (15.8 mg, 0.67 %) was obtained from the column separation. This isolated compound was rechecked by phytochemical screening and antimicrobial activities tests.Pure compound gives rise to positive for polyphenol test and it responds medium activities on four tested organisms and low activities on remaining two organisms, such as *Pseudomonas aeruginosa* and *E. coli.*

The functional groups of pure organic compound (CTK-1) was identified by FT-IR spectroscopic method. It contains alcohol group, sp^3 and sp^2 hydrocarbons, allylic hydrocarbon, ether group, trans or E and cis or Z alkenenic group. From these experimental results, pure compound (CTK-1) may be polyphenol and bioactive compound.

ACKNOWLEDGEMENT

I would like to express my deepest thanks to Rector, Dr Aung Win, , University of Technology (Yatanarpon Cyber City), for his permission to present this research paper. I wish to express my special thanks to my supervisor, Dr Myint Myint Sein (Retired Professor), Head of Department of Chemistry, University of Mandalay for her valuable guidance, and encouragement throughout this research work. Finally, I also thank to Dr Khin Mooh Theint (Professor and Head), Department of Engineering Chemistry, from UT-YCC for her kind helps.

REFERENCES

[1] C. Rice-Evans, N. Miller, and G. Paganga, "Antioxidant properties of phenolic compounds," *Trends Plant Sci.*, vol. 2, no. 4, pp. 152–159, Apr. 1997.

[2] A. Chevallier, *The Encyclopedia of Medicinal Plants: A Practical Reference Guide to over 550 Key Herbs and Their Medicinal Uses*. New York/ : Boston: DK Publishing, 1996.

[3] J. B. Harborne, *Phytochemical Methods: A Guide to Modern Techniques of Plant Analysis*. Springer Netherlands, 1973.

[4] J. T. Litchfield and F. Wilcoxon, "A simplified method of evaluating dose-effect experiments," *J. Pharmacol. Exp. Ther.*, vol. 96, no. 2, pp. 99–113, Jun. 1949.

[5] "Spectrometric Identification of Organic Compounds 6th Ed (1)," *Scribd*. [Online]. Available: https://www.scribd.com/doc/270382005/Spectrometric-Identification-of-Organic-Compounds-6th-Ed-1. [Accessed: 13-Dec-2019].

[6] A. Nagathein, "Pon Pya Ah Bea Dan, Myanmar Version, Mingalar Press, Yangon." 1971.

[7] *Organic Chemistry With Infotrac 5th edition by McMurry, John (1999) Hardcover*, 5 edition. Brooks/Cole Pub Co, 1600.

[8] M. N. Chatterjea and R. Shinde, *Textbook of Medical Biochemistry: Eighth Edition*. JP Medical Ltd, 2011.

Journal of Research and Applications (JRA), UCSMTLA, 2019 Volume-01, Issue-01

Article ID - JRA190018

REMOVAL OF LEAD FROM THE WASTE WATER DISCARDED FROM BATTERY FACTORY BY USING GROUNDNUT, GROUNDNUT CHARCOAL AND GROUNDNUT ASH

Hla Myint Htwe[1]

[1] Technological University (Mandalay), Engineering Chemistry

[1]*drhlamyinthtwe@gmail.com*

ABSTRACT

In this work, the waste water from Naung-yoe Battery Factory, Chanmyathazi Township, Mandalay Region, was collected. The groundnut, groundnut charcoal and groundnut ash were used as adsorbents in removal toxic metal lead (Pb). The optimum pH was selected by volumetric analysis using standard EDTA and xylenol orange as indicator. In addition, the amount of lead removal capacities were investigated by using various mesh size and various amount of groundnut, groundnut charcoal and groundnut ash.

KEYWORDS: *lead, groundnut, groundnut charcoal, groundnut ash, EDTA*

1. INTRODUCTION

Environmental pollution is one of the most serious problem facting humanity and other life forms on our planet today.

Environmental pollution is defined as the contamination on the physical and biological components of the earth/atmosphere system to such an extent that normal environmental processes are adversely affected [1].

Some of the main causes of pollution include industrial emissions, poor disposal of wastes, mining, deforestation, use of fossil fuels and agricultural activities. Pollution can affect air, land and water bodies throughout the world. (Web-1).

Domestic household, industrial and agricultural practices produce wastewater that can cause pollution of many lakes and rivers. (Web-2)

An important source of water pollutants is industrial discharge water. Most industrial waste waters are discharged directly into natural water systems without proper management process.

Unfortunately, the existence of large dosage of heavy metals in these effuents represents the greatest challenge in water purification, where exceeding the allowed concentration limit of these metals in the human body can end up the acute or chronic, death. [2].

Like other heavy metals, lead is one of major pollutans in waste water. It is used as a major raw material in battery manufacturing and wastewater from this industry can contain high concentration of lead about 0.50-25.00 mg/L. Lead may contaminate surface and drinking water from industrial effluents (eg. lead-acid, battery), waste incinerators and utilities. Lead affects the central nervous system and inhibits the ability to synthesizer red blood cell.

Several approaches have been employed to remove heavy metal ions from waste water. However, generally, the adsorption process has been proved convenient in terms of cost, simplicity and flexibility. [2]

Groundnut is one of the major agricultural wastes. It is a fibrous materials containing cellulose as the major constituent. Agricultural by product materials appear as effective and cheap sorbents for removal of heavy metals from wastewater. In this research work, groundnut (500 g), groundnut charcoal (150g) and groundnut ash (100 g) were used as adsorbents for the removal of lead from battery factory wastewater.

2. EXPERIMENT

2.1 Sample collection

The waste water sample was collected from Naung Yoe battery factory, Chanmyathazi Township, Mandalay Region.

2.2 Determination of the pH value of waste water sample

The pH of the waste water was determined by using pH meter. The results were shown in Table (1).

2.3 Determination of optimum pH for the lead solution

The waste water sample prepared was to obtain the variable pH values by using ammonia solution. Then, each waste water having pH values 1-6 was titrated with 0.001 M EDTA solution using xylenol orange as indicator. The effect of pH on the waste water was determined. The results were shown in Table (2). From the results, the optimum pH was found to be 5. Therefore, the waste water sample was treated to get pH 5 by using ammonia solution and this prepared solution was used throughout the research work.

2.4 Preparation of adsorbent

Among the many kinds of adsorbents, groundnut was selected as adsorbent for the study.

Groundnut sample was collected from Bomgwin village, Kyaukse township, Mandalay Region.

500 g of groundnut was grinded by using motar and pastel. And then these groundnut were passed served through 40, 60, 80 and 100 mesh size sieves.

Three different mesh sizes groundnut sample such as 40> mesh >60, 60> mesh >80, 80> mesh >100 were obtained.

500g of groundnut was heated in electric furnace at 400ºC about 30 minutes to obtain charcoal. After burning, the charcoal was cooled at room temperature. The groundnut charcoal was grinded and served to set three different mesh sizes denoted as ($GN\,C_1$, $GN\,C_2$, $GN\,C_3$)

1000 g of groundnut was heated in electric furnace at 800ºC about 30 minutes to obtain white colour of ash. After burning, the ash was cooled at room temperature and sieved to obtain three different mesh sizes denoted as ($GN\,A_1$, $GN\,A_2$, $GN\,A_3$).

Fig. 1 Three different adsorbent (groundnut, groundnut charcoal and groundnut ash)

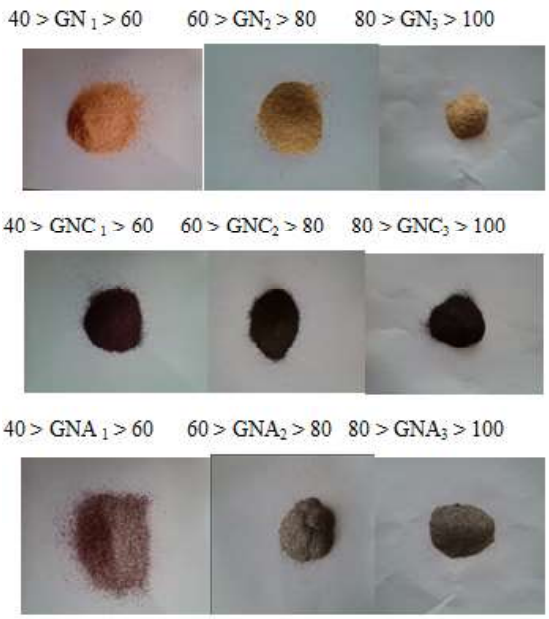

Fig2. Three different sizes of adsorbent (groundnut, groundnut charcoal and groundnut ash)

2.5 Determination of lead removal capacity of groundnut

0.215 g cotton was put in the coloum 2 cm diameter and 70 cm length. Groundnut sample, GN_1 (40> GN_1> 60 mesh) 1 g was added over the cotton. Then, 25 ml of prepared waste water was added into the coloum. The waste water sample was passed through the adsorbent slowly and steadily along the coloum at room temperature. The flow rate of the sample was 10 drops per minute. The filtrate was collected until no drop comes out from the coloum. One drop of xylenol orange indicator was added into 5 cm^3 of filtrate in a conical flask to obtain wine red colour solution. A few drop of dilute nitric acid was added in this solution to obtain yellow colour

solution. A small amount of hexamine powder was added in this solution to obtain wine red colour solution. This prepared solution was titrated with 0.001 M EDTA solution to reach the end point of lemon yellow colour solution. To known the effect of amount of groundnut on removal of lead, the various amounts of adsorbent, groundnut, were used in the range of (1-10) g. The results were shown in Table (3). For groundnut samples, GN_2 ($60 > GN_2 > 80$ mesh), and GN_3 ($80 > GN_3 > 100$ mesh), similar procedures were performed and the results were described in Table (4) and (5).

2.6 Determination of lead removal capacity of groundnut charcoal

0.215 g cotton was put in the coloum 2 cm diameter and 70 cm length. Groundnut charcoal sample, GNC_1 ($40 > GNC_1 > 60$ mesh) 1 g was added over the cotton. Then, 25 ml of prepared waste water was added into the coloum. The waste water sample was passed through the adsorbent slowly and steadily along the coloum at room temperature. The flow rate of the sample was 10 drops per minute. The filtrate was collected until no drop comes out from the coloum. One drop of xylenol orange indicator was added into 5 cm^3 of filtrate in a conical flask to obtain wine red colour solution. A few drop of dilute nitric acid was added in this solution to obtain yellow colour solution. A small amount of hexamine powder was added in this solution to obtain wine red colour solution. This prepared solution was titrated with 0.001 M EDTA solution to reach the end point of lemon yellow colour solution. To known the effect of amount of groundnut charcoal on removal of lead, the various amounts of adsorbent, groundnut charcoal, were used in the range of (1-10) g. The results were shown in Table (6). For groundnut charcoal samples, GNC_2 ($60 > GNC_2 > 80$ mesh), and GNC_3 ($80 > GNC_3 > 100$ mesh), similar procedures were performed and the results were described in Table (7) and (8).

2.7 Determination of lead removal capacity of groundnut ash

0.215 g cotton was put in the coloum 2 cm diameter and 70 cm length. Groundnut ash sample, GNA_1 ($40 > GNA_1 > 60$ mesh) 1 g was added over the cotton. Then, 25 mL of prepared waste water was added into the coloum. The waste water sample was passed through the adsorbent slowly and steadily along the coloum at room temperature. The flow rate of the sample was 10 drops per minute. The filtrate was collected until no drop comes out from the coloum. One drop of xylenol orange indicator was added into 5 cm^3 of filtrate in a conical flask to obtain wine red colour solution. A few drop of dilute nitric acid was added in this solution to obtain yellow colour solution. A small amount of hexamine powder was added in this solution to obtain wine red colour solution. This prepared solution was titrated with 0.001 M EDTA solution to reach the end point of lemon yellow colour solution. To known the effect of amount of groundnut ash on removal of lead, the various amounts of adsorbent, groundnut ash, were used in the range of (1-10) g. The results were shown in Table (9). For groundnut ash samples, GNA_2 ($60 > GNA_2 > 80$ mesh), and GNA_3 ($80 > GNA_3 > 100$ mesh), similar procedures were performed and the results were described in Table (10) and (11).

3. ANALYSIS

3.1 pH value of the waste water sample

pH value of the waste water discarded from Battery factory was determined and the results were shown in Table (1).

Table1. pH Values of Waste Water Sample

No	pH
1	0.5
2	0.5
3	0.5

According to this table, pH of the waste water discarded from Battery factory was found to be 0.5. The discarded waste water is too acidic.

3.2 Determination of optimum pH for the solution containing lead

The waste water sample (pH 0.5) was prepared to obtain various pH values. The observation was made for the titration of waste water solution contains lead standard EDTA solution. The results were shown in Table (2).

Table2. Titration of 5 mL Waste Water Solution with Standard 0.001 M EDTA Solution

No	pH	The colour after the addition of indicator xylenol orange	The colour after the addition of dilute nitric acid	The colour after the addition of hexamine	Remark
1	1	Yellow	Yellow	-	-
2	2	Red	Red	-	-
3	3	Red	Red	-	-
4	4	Red	Red	-	-
5	5	Wine Red	Yellow	Wine Red	Lemon Yellow (True colour change)
6	6	Wine Red	Wine Red	-	-

- = no true colour changes

From Table (2), pH 5 solution gave the true colour change during the titration. The optimum pH for the solution that contains lead found to be 5. This pH value agrees the literature value.

Therefore, the waste water sample was prepared to get pH 5 by using ammonia solution. The prepared solution was used through the research work.

3.3 Determination of Lead Removal Capacity of Groundnut for the Waste Water Discarder from Battery Factory

To determine the lead removal capacity, groundnut, groundnut charcoal and groundnut ash were used as adsorbents and filtration method was used. Lead removal capacity of various amount of three different mesh sizes groundnut samples of were determined for the waste water sample from Battery Factory and the results were described in Table (3), Table (4) and Table (5).

Table3. Removal of Lead from Waste Water Sample by using Groundnut ($40 > GN_1 > 60$ mesh)

No	Amount of groundnut used (g)	Amount of removal of Lead (mg)	Removal percentage (%)
1	1	0.43514	26.24998
2	2	0.47658	28.74982
3	3	0.51802	31.24969
4	4	0.60090	36.24945
5	5	0.64235	38.74994
6	6	0.68379	41.24982
7	7	0.72523	43.74970
8	8	0.80812	48.75006
9	9	0.82884	49.99910
10	10	0.93244	56.24969

Table4. Removal of Lead From Waste Water Sample by using Groundnut ($60 > GN_2 > 80$ mesh)

No	Amount of groundnut used (g)	Amount of removal of Lead (mg)	Removal percentage (%)
1	1	0.51802	31.24970
2	2	0.55947	33.75018
3	3	0.62163	37.49910
4	4	0.66307	39.99988
5	5	0.70451	42.49976
6	6	0.76668	46.25018
7	7	0.80812	48.75006
8	8	0.87028	52.49988
9	9	0.91172	54.99976
10	10	1.03605	62.49910

Table5. Removal of Lead from Waste Water Sample by using Groundnut ($80 > GN_3 > 100$ mesh)

No	Amount of groundnut used (g)	Amount of removal of Lead (mg)	Removal percentage (%)
1	1	0.55947	33.75018
2	2	0.62163	37.49910
3	3	0.66307	39.99988
4	4	0.72523	43.74970
5	5	0.76668	46.25018

6	6	0.80812	48.75006
7	7	0.84956	51.24994
8	8	0.91172	54.99976
9	9	0.95317	57.50024
10	10	1.05677	63.74994

From Table (3), (4) and (5), it can be seen that the increase in amount of groundnut used increases the amount of removal of Lead from the waste water.

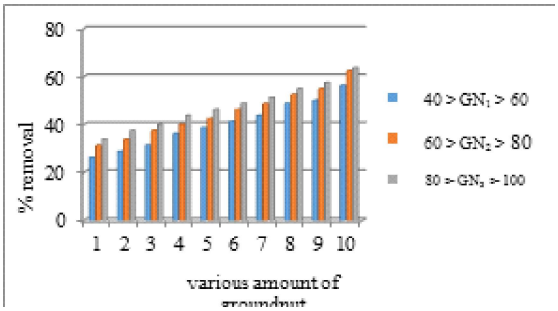

Fig 3. The Percent Removal of Lead by Various Amount and Various Size of Groundnut

According to Table (3), (4), (5) and Figure (3), it was found that the smaller the mesh size of groundnut, the more adsorption can occur and the more amount of Lead can be removed.

3.4 Determination of Lead Removal Capacity of Groundnut Charcoal

Lead removal capacity of various amount of three different mesh sizes groundnut charcoal samples of were determined for the waste water sample from Battery Factory and the results were described in Table (6), Table (7) and Table (8).

Table6. Removal of Lead from Waste Water Sample by using Groundnut Charcoal ($40 > GNC_1 > 60$ mesh)

No	Amount of groundnut charcoal used (g)	Amount of removal of Lead (mg)	Removal percentage (%)
1	1	0.62118	37.47285
2	2	0.66307	37.49910
3	3	0.80812	48.75006
4	4	0.82284	49.99910
5	5	0.84956	51.24994
6	6	0.91172	54.99976
7	7	1.01533	61.25006
8	8	1.05677	63.74994
9	9	1.16038	70.00024
10	10	1.24326	74.99910

Table7. Removal of Lead from Waste Water Sample by using Groundnut Charcoal ($60 > GNC_2 > 80$ mesh)

No	Amount of groundnut charcoal used (g)	Amount of removal of Lead (mg)	Removal percentage (%)
1	1	0.66308	40.00048
2	2	0.70458	42.50398
3	3	0.87038	52.50591
4	4	0.95318	57.50084
5	5	1.03608	62.50181
6	6	1.09828	66.24404
7	7	1.13965	68.74969
8	8	1.24328	75.00120
9	9	1.30584	78.75343
10	10	1.40903	85.00012

Table8. Removal of Lead from Waste Water Sample by using Groundnut Charcoal ($80 > GNC_3 > 100$ mesh)

No	Amount of groundnut charcoal used (g)	Amount of removal of Lead (mg)	Removal percentage (%)
1	1	0.70451	42.49976
2	2	0.74596	45.00024
3	3	0.91172	54.99976
4	4	1.01533	61.25006
5	5	1.07749	64.99988
6	6	1.16038	70.00024
7	7	1.22254	73.75006
8	8	1.30542	78.74981
9	9	1.36759	82.50024
10	10	1.42975	86.25005

From Table (6), (7) and (8), it can be seen that the increase in amount of groundnut charcoal used increases the amount of removal of Lead from the waste water.

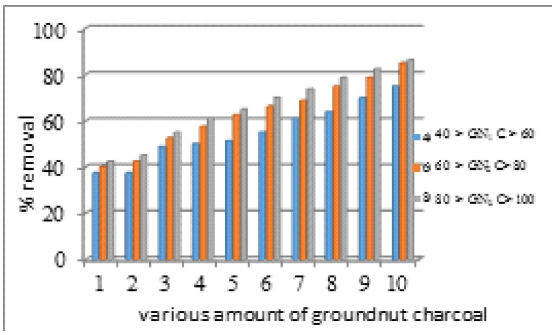

Fig4. The Percent Removal of Lead by Various Amount and Various Size of Groundnut Charcoal

According to Table (6), (7), (8) and Figure (4), it was found that the smaller the mesh size of groundnut charcoal, the more adsorption can occur and the more amount of Lead can be removed.

4.5 Determination of lead removal capacity of Groundnut ash

Lead removal capacity of various amount of three different mesh sizes groundnut ash samples of were determined for the waste water sample from Battery factory and the results were described in Table (9), Table (10) and Table (11).

Table 9. Removal of Lead from Waste Water Sample by using Groundnut Ash (40 >GNA_1 > 60 mesh)

No	Amount of groundnut ash used (g)	Amount of removal of Lead (mg)	Removal percentage (%)
1	1	0.47658	28.74982
2	2	0.51802	31.24969
3	3	0.62163	37.49910
4	4	0.66307	39.99988
5	5	0.70451	42.49976
6	6	0.76668	46.25018
7	7	0.84956	51.24994
8	8	0.90812	54.78258
9	9	1.05677	63.74994
10	10	1.09821	66.24981

Table10. Removal of Lead from Waste Water Sample by using Groundnut Ash (60 > $GN A_2$ > 80 mesh)

No	Amount of groundnut ash used (g)	Amount of removal of Lead (mg)	Removal percentage (%)
1	1	0.55947	33.75018
2	2	0.60090	36.24945
3	3	0.64235	38.74994
4	4	0.70451	42.49976
5	5	0.80812	48.75006
6	6	0.84956	51.24994
7	7	0.95317	57.50024
8	8	0.99461	60.00012
9	9	1.09821	66.24981
10	10	1.22254	73.75006

Table11. Removal of Lead from Waste Water Sample by using Groundnut Ash (80 > $GN A_3$ > 100 mesh)

No	Amount of groundnut ash used (g)	Amount of removal of Lead (mg)	Removal percentage (%)
1	1	0.60090	36.24945
2	2	0.64235	38.74994
3	3	0.68379	41.24982
4	4	0.76668	46.25018
5	5	0.82884	49.99910
6	6	0.91172	54.99976
7	7	1. 01533	61.25006
8	8	1.07749	64.99988
9	9	1.20038	74.41325
10	10	1.24326	74.99910

From Table (9), (10) and (11), it can be seen that the increase in amount of groundnut ash used increases the amount of removal of Lead from the waste water.

According to Table (9) (10), (11) and Figure (5), it was found that the smaller the mesh size of groundnut ash, the more adsorption can occur and the more amount of Lead can be removed.

The amount of removal of lead from the waste water sample was compared by using same mesh size of groundnut, groundnut charcoal and groundnut ash.

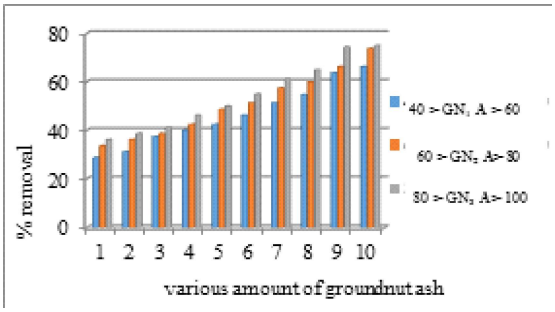

Fig5. The Percent Removal of Lead by Various Amount and Various Size of Groundnut Ash

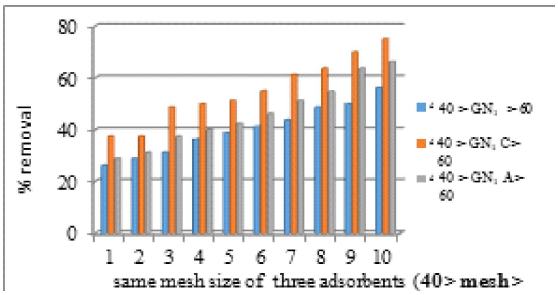

Fig6. The Effect of Same Mesh Size of Three Adsorbents (40 > mesh > 60)

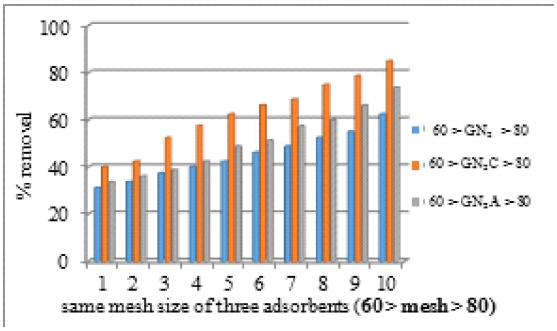

Fig7. The Effect of Same Mesh Size of Three Adsorbents (60 > mesh > 80)

From Figure (6), (7) and (8) it was found that groundnut charcoal can adsorb more lead and the amount of removal of lead was greater than that of others.

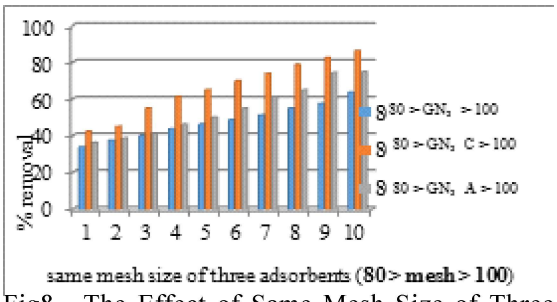

Fig8. The Effect of Same Mesh Size of Three Adsorbents (80 > mesh > 100)

IV. CONCLUSION

The waste water discarded from battery factory contains some extent of toxic lead metal that can pollute the environment (soil, water, etc.). In this research work, the removal of toxic metal lead was studied by using groundnut, groundnut charcoal and groundnut ash as adsorbents by applying filtration method.

The pH of the sample solution was measured by pH meter and pH of the original waste water sample was found to be 0.5 (very acidic). The amount of lead removal was selected by volumetric analysis using standard EDTA and xylenol orange as indicator.

The optimum pH was determined and found that it was 5. Therefore, the waste water sample was prepared to obtain pH 5. The experiments were carried out at room temperature and flow rate of the sample was 10 drops per minute.

To known the effect of amount of groundnut on removal of lead, the various amounts of adsorbent, groundnut, were used in the range of (1-10)g. The increase in amount of groundnut used increases the amount of removal of lead from the waste water. The smaller the mesh size of groundnut, the more adsorption can occur and the more amount of lead can be removed. Groundnut charcoal can adsorb the amount of removal of lead was greater than that of others.

Therefore, this sample groundnut can be used for the removal of metal ion (Pb^{2+}) from polluted water.

ACKNOWLEDGMENT

I would like to express my gratitude to Dr Aye Kyaw, Rector of Yadanabon University, Dr Khin Ma Ma Tin and Dr Myinzu Min, Pro-rectors of Yadanabon University, for providing necessary resources. I owe

a great deal of gratitude to Professor Dr Hlaing Hlaing Myat, Head of Department of Chemistry, Yadanabon University for her invaluable suggestions, guidance and encouragement throughout[1] this [2]research.

REFERENCES

[1] "Environmental Management | Science Direct." [Online]. Available: https://www.sciencedirect.com/book/9780128119891/environmental-management. [Accessed: 12-Dec-2019].

[2] A. M. Mohammad, T. A. Salah Eldin, M. A. Hassan, and B. E. El-Anadouli, "Efficient treatment of lead-containing wastewater by hydroxyapatite/chitosan nanostructures," *Arab. J. Chem.*, vol. 10, no. 5, pp. 683–690, Jul. 2017.

[3] "Research Gate," *Research Gate*. [Online]. Available: https://www.researchgate.net/press. [Accessed: 12-Dec-2019].

Journal of Research and Applications (JRA), UCSMTLA, 2019 Volume-01, Issue-01

Article ID – 190027

Solving the Problems with Some Application of Derivatives

Kyi Sint

Department of Mathematics, TU(Pakokku),Myanmar

dawkyisint1971@gmail.com

ABSTRACT

There are many different way of mathematics rules. Among them, we express finding the extreme values for the optimization problems that changes in the particle life with the derivatives. The derivative is the exact rate at which one quantity changes with respect to another. And them, we can compute the profit and loss of a process that a company or a system. Variety of optimization problems are solved by using derivatives. There were use derivatives to find the extreme values of functions, to determine and analyze the shape of graphs and to find numerically where a function equals zero.

KEYWORDS: *first order derivatives, second order derivatives, differentiation rules, related rate, optimization problems.*

1. INTRODUCTION

In this paper, some basic definitions and notations of derivatives are firstly introduced. Next, some differentiation rules are presented. Moreover, related rates with some examples are also presented. Finally, some applications of derivatives are mentioned by using the closed interval method and the second derivative test.In calculus we have learnt that when y is the function of x, the derivative of y with respect to x (i.e $\frac{dy}{dx}$) measures rate of change in y with respect x. Geometrically, the derivative is the slope of curve at a point on the curve. The derivative is often called as the "instantaneous" rate of change. The process of finding the derivative is called as differentiation.

2. FIRSR AND SECOND ORDER DERIVATIVES

If $y = f(x)$ is a differentiable function, then its derivative $f'(x)$ is also a function. If f' is also differentiable, then we can differentiate f to get a new function of x denoted by f''. So $f'' = (f')'$ .The function is called the second derivative of because it is the derivative of the first derivative.

There are many ways to denote the derivative of a function, where the independent variable is x and the dependent variable is y. Some common alternative

$$f'(x) = y' = \frac{dy}{dx} = \frac{df}{dx} = \frac{\mathrm{d}}{\mathrm{dx}} f(x) = D(f)(x) = D_x f(x).$$

$$f''(x) = y'' = \frac{d^2y}{dx^2} = \frac{d}{dx}\left(\frac{dy}{dx}\right) = \frac{dy'}{dx} = \frac{df'(x)}{dx} = D^2(f)(x) = D_x^2 f(x).$$

The symbols $\frac{d}{dx}$ and D indicate the operation of differentiation.

3. SOME EXAMPLES OF DERIVATIVES

3.1. Example

Let $u = f(t)$ be the number of people in the labor force at time t in a given industry. Let $v = g(t)$ be the average production per person in the labor force at time t. The total production is then $y = uv$.

(a)If the labor force is growing at the rate of 4% per year and the production per worker is growing at the rate of 5% per year, we can find the rate of growth of the total production, y.

(b) If the labor force is decreasing at the rate of 2% per year while the production per person is increasing at the rate of 3% per year. Is the total production increasing, or is it decreasing, and at what rate?

(a) $u = f(t)$ be the number of people in the labor force at time t be the average production per person in the labor force at time t.

The total production

The total production $y = uv$

If the labor force is growing at the rate of 4% per year, $\frac{du}{dt} = 0.04\,u$

If the production per worker is growing at the rate of 5% per year, $\frac{dv}{dt} = 0.05v$

The rate of growth of the total production is

$$\frac{dy}{dt} = \frac{d}{dt}(uv)$$
$$= u\frac{dv}{dt} + v\frac{du}{dt}$$
$$= u \times 0.05v + v \times 0.04u$$
$$= 0.05uv + 0.04uv$$
$$- 0.09uv - 0.09y$$

The rate of growth of the total production is 9% per year.

(b)If the labor force is decreasing at the rate of 2% per year, $\frac{du}{dt} = -0.02\,u$

If the production per person is increasing at the rate of 3% per year, $\frac{dv}{dt} = 0.03v$

The rate of the total production is

$$\frac{dy}{dt} = \frac{d}{dt}(uv)$$
$$= u\frac{dv}{dt} + v\frac{du}{dt}$$
$$= u \times 0.03v + v \times (-0.02u)$$
$$= 0.01uv$$
$$= 0.01y.$$

The total production is increasing at 1% per year.

3.2. Example

We use the derivatives to solve a variety of optimization problems in business, physics, mathematics, and economics. A triangle has two sides a = 1 cm and b = 2cm. How fast is the third side c increasing when the angle α between the given sides is 60˚ and is increasing at the rate of 3˚ per second?

By given,

$$a = 1cm,\ b = 2cm,\ \alpha = 60°,\ \frac{d\alpha}{dt} = 3°$$

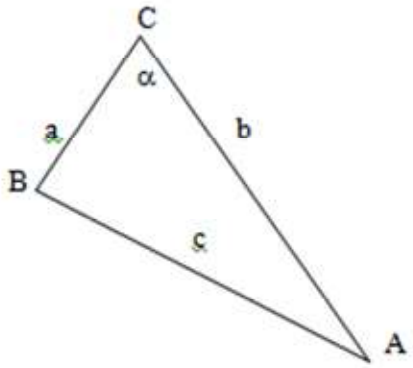

Fig1. Triangle Shape

According to the law of cosines,

$$c^2 = a^2 + b^2 - 2ab\cos\alpha$$

We differentiate both sides of this equation with respect to time t,

$$\frac{d}{dt}(c^2) = \frac{d}{dt}(a^2 + b^2 - 2ab\cos\alpha)$$

$$2c\frac{dc}{dt} = -2ab(-\sin\alpha)\frac{d\alpha}{dt}$$ (a and b are constants)

$$\frac{dc}{dt} = \frac{ab\sin\alpha}{c}\frac{d\alpha}{dt}$$

Calculate the length of the side c

$$c = \sqrt{a^2 + b^2 - 2ab\cos\alpha}$$
$$= \sqrt{1^2 + 2^2 - 2 \times 1 \times 2\cos 60°}$$
$$= \sqrt{1 + 4 - 2} \quad = \sqrt{3}\ \text{cm}$$

Now we know all quantities to determine the rate of change $\frac{dc}{dt}$:

$$\frac{dc}{dt} = \frac{ab\sin\alpha}{c}\frac{d\alpha}{dt}$$

$$= \frac{1\times 2\sin 60^\circ}{\sqrt{3}} \times 3$$

$$= \frac{2\frac{\sqrt{3}}{2}}{\sqrt{3}} \times 3 = 3\,cm/sec\,.$$

4. APPLICATIONS OF DERIVATIVES

Derivatives have various applications in Mathematics, Science, and Engineering. The closed interval method is a way to solve a problem within a specific interval of a function. The solutions found by the closed interval method will be at the absolute maximum or minimum points on the interval, which can either be at the endpoints or at critical points. We say that x = c is a critical point of the function $f(x)$ if $f(c)$ exist and if either of the following are true. $f'(c) = 0$ or $f'(c)$ doesn't exist.If a point is not in the domain of the function then it is not a critical point.

4.1. Example

A management company is going to build a new apartment complex. They know that if the complex contains x apartments the maintenance costs for the building, landscaping etc. will be

$$C(x) = 4000 + 14x - 0.04\,x^2$$

The land they have purchased can hold a complex of at most 500 apartments. How many apartments should the complex have in order to minimize the maintenance costs?

All we really need to do here is determine the absolute minimum of the maintenance function and the value of x that will give the absolute minimum.

$$C(x) = 4000 + 14x - 0.04\,x^2\,,$$
$$0 \le x \le 500$$

First, we'll need the derivative and the critical point that fall in the range $0 \le x \le 500$

$$C'(x) = 14 - 0.08x$$

$$C'(x) = 0 \quad \text{when} \quad 14 - 0.08\,x = 0$$

$$x = 175$$

The critical point is $x = 175$

Since the cost function

$$C(x) = 4000 + 14x - 0.04\,x^2\,,$$
$$0 \le x \le 500$$

We can find the minimum value by the closed interval method:

$C(0) = 4000, C(175) = 5225,\ and\ \ C(500) = 1000$

From these evaluations we can see that the complex should have 500 apartments to minimize the maintenance costs.

4.2. Example

We need to enclose a rectangular field with a fence. We have 500 feet of fencing material and a building is on one side of the field and so won't need any fencing. Determine the dimensions of the field that will enclose the largest area.

In this problem we want to maximize the area of a field and we know that will use 500 ft of fencing material. So, the area will be the function we are trying to optimize and the amount of fencing is the constraint. The two equations for these are,

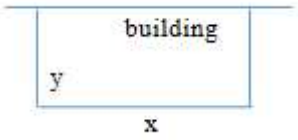

Fig 2. Rectangular Feild

Maximize: $A = xy$

Constraint: $500 = x + 2y$

$$x = 500 - 2y$$

Substituting this into the area function gives a function of y. $A(y) = (500 - 2y)\,y$

$$= 500y - 2y^2$$

Now we want to find the largest value this will have on the interval $[0,250]$.The first derivative is

$$A'(y) = 500 - 4y$$

$A'(y) = 0$ when $500 - 4y = 0$

$$y = 125$$

We can find the maximum value by the closed interval method,

$$A(0) = 0,\ A(250) = 0,\ A(125) = 31250\ ft^2$$

The largest possible area is $31250\ ft^2$.

$$y = 125 \Rightarrow x = 500 - 2(125) = 250$$

The dimensions of the field that will give the largest area, subject to the fact that we used exactly $500ft$ of fencing material, are 250 x 125.

5. SECOND DERIVATIVES TEST

Suppose f' is continuous on open interval that contains x = c.

1.If $f'(c) = 0$ *and* $f''(c) < 0$, then f has a local maximum at x = c.

2. $f'(c) = 0$ *and* $f''(c) > 0$, then f has a local minimum at x = c.

3. $f'(c) = 0$ *and* $f''(c) = 0$, then the test fails. The function f may have a local maximum, a local minimum, or neither.See [1].

5.1. Example

A printer need to make a poster that will have a total area of 200 in^2 and will have 1inch margins on the sides, a 2 inch margin on the top and a 1.5 inch margin on the bottom. What dimensions will give the largest printed area?

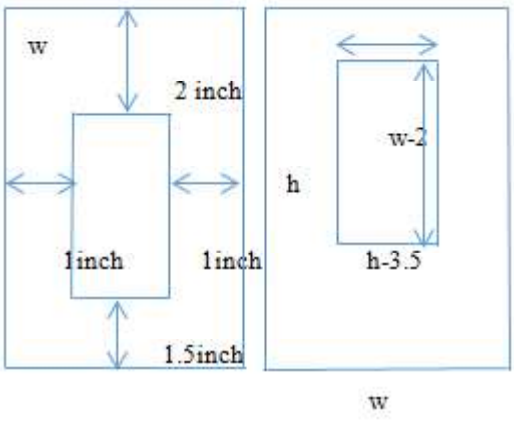

Fig 3. Poster

The constraint is that the overall area of the poster must be 200 in^2 while we want to optimize the printed area. (i.e the area of the poster with the margins taken out).

Let's define the height of the poster to be h and the width of the poster to be w. Here is a new sketch of the poster and we can see that once we've taken the margins into account the width of the printer area is w-2 and the height of the printer area is h-3.5.

Here are equations that we'll be working with

Maximize: $A = (w - 2)(h - 3.5)$

Constraint: $200 = wh \Rightarrow h = \frac{200}{w}$

Solving the constraint for h and plugging into the equation for the printed area gives,

$$A(w) = (w - 2)\left(\frac{200}{w} - 3.5\right)$$

$$= 200 - 3.5w - \frac{400}{w} + 7$$

$$= 207 - 3.5w - \frac{400}{w}$$

The first and second derivatives are

$$A'(w) = -3.5 + \frac{400}{w^2} = \frac{400-3.5w^2}{w^2}$$

$$A''(w) = -\frac{800}{w^3}$$

From the first derivative, we have the following two critical points (w = 0 is not critical point because the area function does not exit there).

$$w = \pm\sqrt{\frac{400}{3.5}} = \pm 10.6904$$

However, since we're dealing with the dimensions of a piece of paper we know that we must have w > 0 and so only 10.6904 will make sense. Also notice that provided w > 0 the second derivative will always be negative and so we know that the maximum printed area will be at w = 10.6904 inches.

The height of the paper that gives the maximum printed area is then

$$h = \frac{200}{10.6904} = 18.7084 \text{ inches.}$$

5.2. Example

A 600 m^2 rectangular field is to be enclosed by a fence and divided into two equal parts by another fence parallel to one of the sides. What dimensions for the outer rectangle will require the smallest total length of fence? How much fence will be needed?

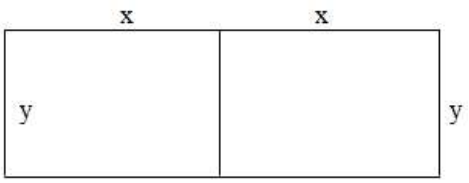

Fig 4. Rectangular Field

In this problem we want minimize the total length of fence and we know that will use 600m^2 rectangular field.

Minimize: $P = 4x + 3y$ (x and y are the sides of the rectangle)

Constraint : $600 = 2xy$

Solving the constraint for y and plugging into the equation for the total length of fence gives,

$$P(x) = 4x + 3\left(\frac{600}{2x}\right)$$

$$= 4x + \frac{900}{x}$$

The first and second derivatives are

$$P'(x) = 4 - \frac{900}{x^2} = \frac{4x^2-900}{x^2}$$

$$P''(x) = \frac{1800}{x^3}$$

From the first derivative, we have the following two critical points (x=0 is not a critical point because the function does not exist there).

$$x = \pm\sqrt{\frac{900}{4}} = \pm 15$$

However, since we're dealing with the dimensions of rectangle we know that we must have x > 0 and so only 15 will make sense.

Also notice that provided x > 0 the second derivative will always be positive and so we know that the minimum fence will be at x = 15 m.

The other side of rectangle is

$$y = \frac{600}{2\times 15} = 20 \text{ m}$$

The dimensions of the outer rectangle are

30 m by 20 m.

$$P = 4 \times 15 + 3 \times 20 = 120 \text{ m.}$$

120 meters of fence will be needed.

6. CONCLUSION

We have use the derivatives to find the extreme values of a process in social life. In the study of the differential equations, we should know critical points because it is main point to find the extreme values. We compute increase or decrease function during a interval in our social environments. We use the derivative to determine the maximum and minimum values of particular function (e.g. cost, strength, amount of material used in a building, profit, loss, etc.)

ACKNOWLEDGEMENTS

We would like to thank to Dr Myint Myint Khaing,Pro-Rector of Technological University (Pakokku) and Professor Dr Khin Myo Htun, Head of the Department of Engineering Mathematics, Technological University (Pakokku) for their kind permission for the submission of this paper.

REFERENCES

[1] "Thomas' Calculus Early Transcendentals | George B. Thomas Jr., Maurice D. Weir, Joel R. Hass | download." [Online]. Available: https://it.b-ok2.org/book/2295761/8d99df. [Accessed: 12-Dec-2019].

[2] "The qualitative theory of ordinary differential equations' - Google Search."

[3] D. W. Jordan and P. Smith, *Nonlinear ordinary differential equations: an introduction for scientists and engineers*, 4th ed. Oxford [England]: New York/ : Oxford University Press, 2007.

Journal of Research and Applications (JRA), UCSMTLA, 2019 Volume-01, Issue-01

Article ID - JRA190028

Solving the Problems in Social Life with Double Integrals

Kay Thi Win[(1)],KhinMyoHtun[(2)], Ngwe Kyar Su Khaing[(3)]

[(1)(3)]Technological University (Yamethin), Myanmar

[(2)]Technological University (Pakokku), Myanmar

[(1)]kaythiwin357@gmail.com, [(2)]khinmyohtun18@gmail.com, [(3)]ngwekhaingjune@gmail.com

ABSTRACT

There are many different rules for mathematics field. Among them, we express the solving problems for practical life with integration methods. There are integrals, double integrals, triple integrals, etc. Among these method, we use the double integrals method to find the volume and area of a region between two curves and between line and curves that design of engineering. We define and evaluate double integrals over bounded regions in the plane which are more general than rectangles. These double integrals are also evaluated as iterated integrals, with the main practical problem being that of determining the limits of integration. We can find the volume and area of the various shape by using the integration methods. For example, volume andarea of the leaf and area of the cardioid shape, etc. We can compute that number of people in the region bounded during the interval by using the integration method.

KEYWORDS: *volume by double integration, area by double integration and average values, double integrate a polar form.*

1. INTRODUCTION

We consider the integral of a function of two variables $f(x,y)$over a region in the plane and the integral of a function of three variables $f(x,y,z)$ over a region in space. To define the double integral of a function over a bounded, nonrectangular region R, this paper is organized with some basic definitions and notations. This paper present finding the volume with double integrals and finding the area with double integrals. And then we stated the double integral in polar form. We express finding the volume and area of the various shapes of the graph in social life. By using the integration methods to solve the problems in our social environment. In this paper, we used double integrals to solve the problems that submit the examples.

2.SOME BASIC DEFINITIONS

2.1.Definition

If R is a region like the one shown in the xy-plane, bounded 'above' and 'below' by the curve $y = g_2(x)$ and $y = g_1(x)$ and on the sides by the lines $x = a$ and $x = b$.The cross-sectional area [1],

$$A(x) = \int_{y=g_1(x)}^{y=g_2(x)} f(x,y)\,dy.$$

2.2.Definition

If $f(x,y)$ is positive and continuous over R, the volume of the solid region between R and the surface $z = f(x,y)$ to be $\iint_R f(x,y)\,dA$.

Integrating $A(x)$ from $x = a$ to $x = b$ to get the volume [2] as an iterated integral,

$$V = \int_a^b A(x)\,dx = \int_a^b \int_{g_1(x)}^{g_2(x)} f(x,y)\,dy\,dx.$$

3. FUBINI'S THEOREM (STRONGER FORM)

Let $f(x,y)$ be continuous on a region R.

1. If R is defined by
$a \le x \le b, g_1(x) \le y \le g_2(x)$, with g_1 and g_2 continuous on [a, b], then(By using vertical cross-sections),

$$\iint_R f(x,y)\,dA = \int_a^b \int_{g_1(x)}^{g_2(x)} f(x,y)\,dy\,dx.$$

2. If R is defined by
$c \le y \le d, h_1(y) \le x \le h_2(y)$, with h_1 and h_2 continuous on [c, d], then(By using horizontal cross-sections),

$$\iint_R f(x,y)\,dA = \int_c^d \int_{h_1(y)}^{h_2(y)} f(x,y)\,dx\,dy.$$

4. SOME EXAMPLES OF FINDING VOLUME

4.1. Example

The volume of a region such as tunnel shapes that lies the function $f(x,y) = \frac{x\,e^{2y}}{4-y}$ and x-axis between $0 \le x \le 2$ and $0 \le y \le 4 - x^2$ can be computed.

$$f(x,y) = \frac{x\,e^{2y}}{4-y}$$

$$\int_0^2 \int_0^{4-x^2} \frac{x e^{2y}}{4-y} dy\,dx = \int_0^4 \int_0^{\sqrt{4-y}} \frac{x e^{2y}}{4-y} dx\,dy.$$

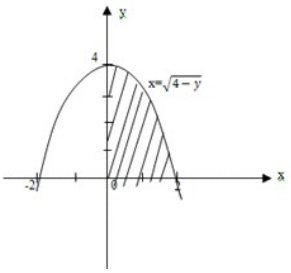

Fig.1 The region of tunnel shape.

By using horizontal cross-sections,

$$\int_0^4 \int_0^{\sqrt{4-y}} \frac{x e^{2y}}{4-y} dx\,dy = \int_0^4 \left[\frac{x^2 e^{2y}}{2(4-y)}\right]_{x=0}^{x=\sqrt{4-y}} dy$$

$$= \int_0^4 \frac{e^{2y}}{2}\,dy$$

$$= \left[\frac{e^{2y}}{4}\right]_0^4 = \frac{e^8 - 1}{4}.$$

4.2. Example

The volume of the region that triangle shape under the ladder in the xy-plane bounded by the x-axis and the line $y = x$ and $x = 1$ and whose top lies in the plane $f(x,y) = x - y + 2$.

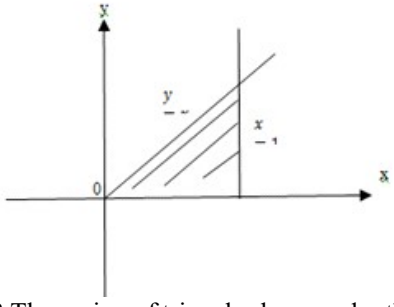

Fig.2 The region of triangle shape under the ladder

$$f(x,y) = x - y + 2$$

By using the vertical cross-sections,

Volume, $V = \int_0^1 \int_0^x (x - y + 2)\,dy\,dx$

$$= \int_0^1 \left[xy - \frac{y^2}{2} + 2y\right]_{y=0}^{y=x} dx$$

$$= \int_0^1 \left(x^2 - \frac{x^2}{2} + 2x\right) dx$$

$$= \int_0^1 \left(\frac{x^2}{2} + 2x\right) dx$$

$$= \left[\frac{x^3}{6} + x^2\right]_0^1$$

$$= \frac{1}{6} + 1 = \frac{7}{6}.$$

By using the horizontal cross-sections,

$$\text{Volume,V} = \int_0^1 \int_y^1 (x - y + 2)\,dx\,dy$$

$$= \int_0^1 \left[\frac{x^2}{2} - xy + 2x\right]_{x=y}^{x=1} dy$$

$$= \int_0^1 \left(\frac{5}{2} + \frac{y^2}{2} - 3y\right) dy$$

$$= \left[\frac{5y}{2} + \frac{y^3}{6} - \frac{3y^2}{2}\right]_0^1$$

$$= \left[\frac{5}{2} + \frac{1}{6} - \frac{3}{2}\right]$$

$$= \frac{15+1-9}{6} = \frac{7}{6}.$$

4.3. Example

We will design a can to build at a high place. Therefore, we should volume of the under a can. The volume of a region between the curve $f(x, y) = 3\cos x$ bounded by the x-axis on $(0 \le y \le \sec x \text{ and } -\frac{\pi}{3} \le x \le \frac{\pi}{3})$ can find.

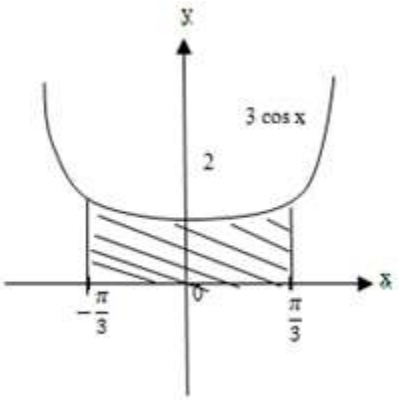

Fig3. The region between the curve and the x-axis

$$\int_{-\frac{\pi}{3}}^{\frac{\pi}{3}} \int_0^{\sec x} (3\cos x)\,dy\,dx$$

$$= \int_{-\frac{\pi}{3}}^{\frac{\pi}{3}} [3\cos x \,.\, y]_{y=0}^{y=\sec x}\,dx$$

$$= \int_{-\frac{\pi}{3}}^{\frac{\pi}{3}} (3\cos x.\sec x)\,dx$$

$$= \int_{-\frac{\pi}{3}}^{\frac{\pi}{3}} (3)\,dx$$

$$= 3[x]_{-\frac{\pi}{3}}^{\frac{\pi}{3}}$$

$$= 2\pi.$$

5. AREA BY DOUBLE INTEGRATION

5.1. Definition

The **area** of a closed, bounded plane region R is

$$Area, A = \iint_R dA.$$

5.2. Definition

For an integrable function of two variables defined on a bounded region in the plane, the average value [3] is the integral over the region divided by the area of the region.

$$Average\ value\ of\ f\ over\ R = \frac{1}{area\ of\ R} \iint_R dA.$$

5.3. SOME EXAMPLE OF FINDING AREA

5.3.1. Example

An engineering design for a building that parabola shape region. He will compute enclosed area by using the integration method. The area of the region R enclosed by the parabola shape $x = y^2$ and the line $y = x + 2$,can be computed.

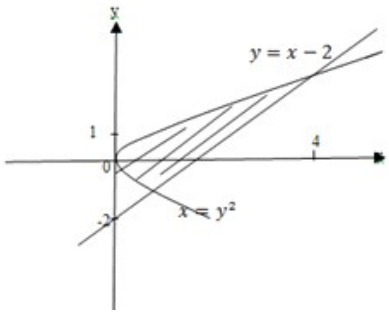

Fig4. The region enclosed by the parabola and the line

By given , $x = y^2$ and $y = x - 2$.

If $x = y^2$ then $y = y^2 - 2$.

$y^2 - y - 2 = 0$

$$(y - 2)(y + 1) = 0$$

$y = 2$ *and* $y = -1$.

Region: $y^2 \le x \le y + 2 , -1 \le y \le 2$.

Area,A=$\iint_R dA$.

$$= \int_{-1}^{2} \int_{y^2}^{y+2} dx\, dy$$

$$= \int_{-1}^{2} [x]_{y^2}^{y+2} dy$$

$$= \int_{-1}^{2} [y + 2 - y^2]\, dy$$

$$= \left[\frac{y^2}{2} + 2y - \frac{y^3}{3}\right]_{-1}^{2}$$

$$= \left[2 + 4 - \frac{8}{3}\right] - \left[\frac{1}{2} - 2 + \frac{1}{3}\right]$$

$$= \frac{10}{3} + \frac{7}{6} = \frac{20+7}{6} = \frac{27}{6} = \frac{9}{2}.$$

5.3.2. Example

The area of the regions R can be computed. The following function $\int_0^1 \int_{x^2-1}^{0} dy\, dx + \int_0^4 \int_0^{\sqrt{x}} dy\, dx$.

$$\int_0^1 \int_{x^2-1}^{0} dy\, dx + \int_0^4 \int_0^{\sqrt{x}} dy\, dx$$

$$= \int_0^1 [y]_{x^2-1}^{0} dx + \int_0^4 [y]_0^{\sqrt{x}} dx$$

$$= \int_0^1 [-x^2 + 1]\, dx + \int_0^4 [\sqrt{x}]\, dx$$

$$= \left[-\frac{x^3}{3} + x\right]_0^1 + \left[\frac{x^{\frac{3}{2}}}{\frac{3}{2}}\right]_0^4$$

$$= -\frac{1}{3} + 1 + \frac{16}{3}$$

$$= \frac{-1+3+16}{3} = 6.$$

5.3.3. Example

Finding the average values of $f(x, y) = \cos(x + y)$ over the rectangle $0 \le x \le \pi , 0 \le y \le \pi$.

$$\iint_R dA = \int_0^{\pi} \int_0^{\pi} \cos(x + y)\, dy\, dx$$

$$= \int_0^{\pi} [\sin(x + y)]_0^{\pi} dx$$

$$= \int_0^{\pi} [\sin(x + \pi) + \sin x]\, dx$$

$$= [-\cos(x + \pi) - \cos x]_0^{\pi}$$

$$= [-\cos(2\pi) - \cos \pi] - [-\cos(\pi) - 1]$$

$$= [-1 + 1] - [1 - 1] = 0.$$

Area of rectangle $= \pi \times \pi = \pi^2$.

$$Average\ value\ of\ f\ over\ R = \frac{1}{area\ of\ R}\iint_R dA.$$

Average value of f over R= $\frac{1}{\pi^2} \times 0 = 0.$

6. DOUBLE INTEGRAL IN POLAR FORM

Area differential in polar coordinates,

$dA = r\,dr\,d\theta.$

$$\iint_R f(r,\theta)dA = \int_{\theta_1}^{\theta_2}\int_{r_1}^{r_2} f(r,\theta)rdr\,d\theta$$

6.1.Example

We can compute values of area everything in our environment of daily life. There are many tree that having many leaf. We compute the area enclosed by the one leaf of the rose

$r = 2\cos 3\theta$ over the region R:$-\frac{\pi}{6} \le \theta \le \frac{\pi}{6}$.

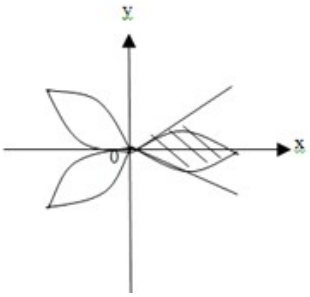

Fig5.The area enclosed by the one leaf of the rose

Area,A=$\iint_R dA.$

$$= \int_{-\frac{\pi}{6}}^{\frac{\pi}{6}}\int_0^{2\cos 3\theta} r\,dr\,d\theta$$

$$= \int_{-\frac{\pi}{6}}^{\frac{\pi}{6}}\left[\frac{r^2}{2}\right]_0^{2\cos 3\theta} d\theta$$

$$= \frac{1}{2}\int_{-\frac{\pi}{6}}^{\frac{\pi}{6}}[4(\cos 3\theta)^2]\,d\theta$$

$$= 4\int_0^{\frac{\pi}{6}}\left[\frac{1+\cos 6\theta}{2}\right]d\theta$$

$$= 2\left[\theta + \frac{\sin 6\theta}{6}\right]_0^{\frac{\pi}{6}}$$

$$= 2\left[\left(\frac{\pi}{6} + \frac{\sin \pi}{6}\right) - 0\right] = \frac{\pi}{3}.$$

6.2. Example

The area of the region, R of a piece of moon. The area of the region that lies inside the cardioid $r = 1 + \cos\theta$ over the region R:$0 \le \theta \le \frac{\pi}{2}$ and outside the circle $r = 1$ can be stated.

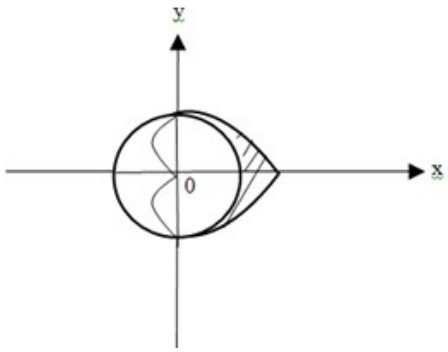

Fig 6.The region lies inside the cardioid and outside the circle

Area,A=$\iint_R dA.$

$$= 2\int_0^{\frac{\pi}{2}}\int_1^{1+\cos\theta} r\,dr\,d\theta$$

$$= 2\int_0^{\frac{\pi}{2}}\left[\frac{r^2}{2}\right]_1^{1+\cos\theta} d\theta$$

$$= \int_0^{\frac{\pi}{2}} [1 + 2\cos\theta + \cos^2\theta - 1]\, d\theta$$

$$= \int_0^{\frac{\pi}{2}} \left[2\cos\theta + \frac{1+\cos 2\theta}{2}\right] d\theta$$

$$= \left[2\sin\theta + \frac{\theta}{2} + \frac{\sin 2\theta}{4}\right]_0^{\frac{\pi}{2}}$$

$$= \left[\left(2 + \frac{\pi}{4} + 0\right) - 0\right]$$

$$= \frac{8+\pi}{4}.$$

7. CONCLUSION

There are many different rules for mathematics researcher. Among them, integration method is very important method. Specially for engineering because they are compute in imaginary for their design that is, volume of system and area of design for their practical life. Define and evaluate double integrals over bounded regions in the plane which are more general than rectangles. These double integrals are also evaluated as iterated integrals, with the main practical problem being that of determining the limits of integration. By using the integration method: integrations, double integrations and triple integrations, computed for solving the problems in daily life.

ACKNOWLEDGMENT

Firstly, I would like to thank my senior in the department that all of my duty region. I want to thank all of my teacher for their teaching, kindness and her urge wrote this research paper well.I am also indebted to all the teachers at my department who permitted me and friends who gives me all kind of encouragement and necessary help to write this research paper. I wish to report my family for their helping. To get a journal provide all of teachers and all of my friends.

REFERENCES

[1] "Thomas' Calculus, Single Variable (12th Edition) - PDF Free Download," *epdf.pub*. [Online]. Available: https://epdf.pub/thomas-calculus-single-variable-12th-edition.html. [Accessed: 16-Dec-2019].

[2] "Advanced Engineering Mathematics, 10th Edition - PDF Free Download," *epdf.pub*. [Online]. Available: https://epdf.pub/advanced-engineering-mathematics-10th-edition.html. [Accessed: 16-Dec-2019].

[3] D. W. Jordan and P. Smith, *Nonlinear ordinary differential equations: an introduction for scientists and engineers*, 4th ed. Oxford [England]: New York/ : Oxford University Press, 2007.

Journal of Research and Applications (JRA), UCSMTLA, 2019 Volume-01, Issue-01

Article ID - JRA190041

COMPARATIVE STUDY OF THE PROPERTIES OF SOFTWOOD AND HARDWOOD-PLASTIC COMPOSITES

Moe Tin Khaing [(1)], Wor Ma Lay[(2)]

[(1)] Department of Chemistry, Myitkyina University, Myanmar,

[(2)] MSc Student, Myitkyina University

[(1)]moetin.khaing@gmail.com

ABSTRACT

The aim of this research is to produce hand-made eco-friendly wood plastic composites (WPCs) by applying waste plastic bottles blending with sawdust particles of softwood (SW) and hardwood (HW) by compression moulding method and to compare physical, chemical and mechanical properties of composites obtained. In this research, composite preparation could be divided into two steps based on the types of hand press used. Although the procedure was similar with first step, ZnO was put as plasticizer and cotton seed oil -based polyol resin was utilized instead of cotton seed oil in the second step preparation. Three ratios applied (polyethylene (PE): softwood (SW) (or) hardwood (HW): coupling agent (CA)) were (65 : 20 :15) as ratio (a), (60 : 25: 15) as (b) and (55 : 30 : 15) as (c) respectively. Water reduction, thickness swelling, specific gravity (SG), density and hardness of prepared WPCs were examined. In addition, chemical resistance test with (94% ethanol), salt spraying test with (3.5 % NaCl solution) and biodegradable test were done on all WPCs. To compare the properties of WPCs, screening electron microscopic (SEM) and thermogravimetric (TGA) analyses were also performed.

KEYWORDS: *composites, plasticizer, coupling agent, screening electron microscopic (SEM), thermogravimetric (TGA)*

1. INTRODUCTION

Wood Plastic Composite is a material made from combination of wood and plastic wastes mixed in the right proportion and extruded inside a specially designed extruding machine at temperature of about 170°C - 200°C. The term strength applied to a material such as WPC refers to its ability to resist external forces tending to change its shape. Also, the physical and mechanical properties, which are present in wood plastic composite, decide purpose to which WPC can be sustainably put. During utilization, when external forces such as heavy loads are applied to a given sample of wood plastic composite, internal forces generated within the WPC which resist changes in size and alteration in shape.

Wood plastic composites (WPC) containing wood plastics and additives are used to substitute wood products as well as standard plastics (Bledzki, 2002, Dale, 1999 and Bledzki and Gassan, 1999). Due to their increased water absorption and thus, lower dimension stability, these composites are not suitable for all areas of application (e.g. wet areas). However, the desired stability can be achieved by chemical modification, for example, by acetylation or by adding coupling agents (Rowell, 2005). To achieve the desired composite properties, the wood fibres (particles) were modified with a cou-pling agent. By using maleic anhydride grafted PP as a coupling agent, an increase in water resistance as well as a rise in mechanical data in comparison to untreated composites could be demonstrated (Nechwatal, 2005 and Rowell, 2000).

The plastic wastes were first sort into their specific types (that is, polyethylene terephthalate (PET), high density polyethylene (HDPE), polyvinyl chloride (PVC) low density polyethylene (LDPE), polypropylene (PP), polystyrene (PS). The aim of this study is to compare the physicochemical and mechanical properties of hand made wood plastic composite (WPC) based on soft wood (Say-Khar)

and hard wood (Taung-Ta-Mar) with waste plastic bottle of low density polyethylene (LDPE) by cold pressing and hot pressing.

2. EXPERIMENT

2.1 Sample Collection and Preparation

Two kinds of wood particles from (Say-Khar) (softwood) and (Taung-Ta-Mar) (hardwood) were collected from a sawmill of Mayan, Myitkyina Township, Kachin State, Myanmar and they were grounded by applying efficient shredder (100A) to get powder. Shredded low density polyethylene (LDPE) of empty water sachet plastics were obtained from a commercial plastic waste company, Mandalay and they were also grounded. Refined cotton seed oil which was used as coupling agent in the first step of preparation was purchased from an oil mill of Pakokku. Polyol of cotton seed oil used as coupling agent in the second step was synthesized in the laboratory of Faculty of Science, Institute of Tropical Forestry and Forest Products (INTROP), University of Putra Malaysia, Malaysia.

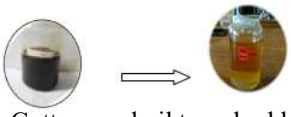

Fig1. Cotton seed oil to polyol by epoxidation and ring opening synthesis

2.3 Determination of the Physicochemical Properties of Sawdust

Determination of moisture, ash, particle density and water absorption properties were carried out and the resulting data will be discussed in the next seciton.

2.4 Characterization of Sawdust

Two sawdust samples used as raw materials in the preparation of particlboards were characterized by Energy Dispersive X-ray Fluorescence (EDXRF) and Fourier Transform Infrared(FT-IR) spectroscopy.

2.5 Preparation of Composite Panels

Fig2. PE, SW and HW powder samples

Two types of sawdust (SW, HW) and plastic particles (PE) powders (Figure 2) were dried at 80°C in an oven for 24 hr prior to the mixing process in order to achieve a moisture content of less than 3%. (1%). PE was added into a pan heated and stirring at 100°C thoroughly to activate its adhesive property. After 5 mins heating and stirring, calculated amount of cotton seed oil was added to the heated PE particles to get more compatibility between the sawdust and treated PE and then stirred for another 5 min. Finally, oven dried sawdust particles were blended with treated PE in the heated pan and they were stirred for 5 mins to produce a homogeneous PE-sawdust compound through efficient dispersion. After stirring, commercial adhesive latex ATM (A-9000), premium grade was added as additive into the mixture and they were mixed and blended thoroughly. Then the resulting mixture was transferred into the mould sprayed with liquid paraffin on which it was pre-shaped as composite panel. The composite obtained was rubbed with liquid paraffin smoothly to get the desired shape and size. The mould was heated at 70°C in an oven (model 10 lab) for two hrs, Heating in the oven and pressing by cold hand press were done alternatively in every 2 hrs for the composite processing part I.

In the part-II composite processing, PE powder was added into the heated pan and stirred at 100°C for 5 mins. Then after 5 mins, cottonseed-based polyol resin was added as a coupling agent. ZnO nanoparticles (8.5g) were added and then heated and stirred to extend the quality of the plastic particles. Finally sawdust particles were added into the above heating mixture and stirring was continued for another 5 mins. After heating, ATM (A-9000), premium grade was added and blended until homogeneous PE-sawdust compound mixture was obtained. It was placed into the mould and pre-shaped. Heating and pressing the composite sample was done by applying hot press to get more adhesion between sawdust and plastic particles.

Fig3. Cold press Fig 4. Hot press

2.6 Determination of Physical Properties of Composite Panels

Water absorption, water reduction and thickness swelling of composite panels were examined and their percentages were calculated using the following equations.

$$WA(t) = (W(t) - W_0)/ W_0 \times 100$$

$$W_R(t) = (W_0 - W(t))/W_0 \times 100$$

$$\text{Thickness swelling (\%)} = \frac{T_t - T_0}{T_0}, \ 100$$

The specific gravity (SG) of composite panels were examined at Department of Agriculture, Rubber Research and Development Center, Yangon.

2.7 Determination of Mechanical Properties of Composite Panels

The hardness and compression set of composite panels were determined according to ASTM standard method at Department of Agriculture, Rubber Research and Development Center, Yangon.

2.8 Determination of Chemical Properties of Composite Panels

Chemical resistance test, salt spray test and biodegradable test were done on the composite panel obtained to detect their chemical and corrosion resistance and biodegradable properties.

2.9 Characterization of Composite Panels

Scanning electron microscopic analysis on composite panels was done by (SEM, JSM-5610) for a visual inspection of external porosity. Thermo gravimetric analysis was performed using a TGA detector (DTG-60H) according to ASTM standard method. The composite panel (7-16mg) were heated from about 37 to 600 °C at the flow rate of 50[ml/min] under a nitrogen atmosphere.

3. ANALYSIS

3.1 Some Physical Properties of Wood Powder

Table 1 Physical Properties of Wood Powder

No	Test Parameter	Result	
		(SW)	(HW)
1.	Moisture (%)	1.35	1.85
2.	Particle Density(gcm^{-3})	0.20	0.20
3.	Water absorption (%)	17.69	16.03
4.	Ash (%)	5.90	5.80

Moisture retaining of HW (1.85%) was greater than SW (1.35%).Though particle density of SW and HW were the same (0.20) g cm^3, it was found that higher water absorption (17.69%) in SW then HW (16.03%) . Ash percent of SW and HW were similar 5.80% and 5.90% .

3.2 Characterization of Wood Powder

3.2.1 Elemental composition of wood powder

Table 2 Elemental Composition of Softwood (SK) and Hardwood (TTM)

No	Analyte	Softwood (SK)	Hardwood (TTM)
1	Si	0.148	0.152
2	Ca	0.057	0.102
3	K	0.129	0.099
4	P	0.067	0.054
5	S	0.069	0.046
6	Fe	0.004	0.006
7	Hg	-	0.002
8	Ti	0.001	0.002
9	Cu	0.001	0.001
10	Mn	0.001	0.001
11	Zn	0.000	0.000
12	Sr	-	0.000
13	Ag	0.001	-
14	CH	99.521	99.535

3.3 Some Physical and Mechanical Properties of WPCs

Table 3. Some Physical and Mechanical Properties of Soft Wood Plastic Composite (SWPCs)

Parameter	Ratios of (SK:PE:CA) in WPCs		
	(a)	(b)	(c)
Water absorption(%)	41.23	52.01	61.23
Thickness swelling(%)	36.80	45.40	53.00
Water reduction(%)	28.00	35.00	41.00
Hardness (IRHD)	78.00	94.00	94.00
Specific gravity(SG)	0.80	0.78	0.75
Density(gcm^{-3})	0.79	0.73	0.73
Thickness(mm)	10.90	8.90	10.30

IRHD = International Rubber Hardness

Table 4. Some Physical and Mechanical Properties of Hard Wood Plastic Composite (HWPCs)

Parameter	Ratios of (TTM:PE:CA) in WPCs		
	(a)	(b)	(c)
Water absorption (%)	36.56	42.61	56.32
Thickness swelling (%)	13.60	14.70	24.00
Water reduction (%)	25.00	32.00	42.00
Hardness (IRHD)	93.00	92.00	95.00
Specific gravity (SG)	0.86	0.80	0.75
Density (gcm^{-3})	0.82	0.68	0.85
Thickness (mm)	10.50	11.00	10.40

It was observed that both of water absorption of SWPCs and HWPCs tend to increase as the percentages of wood contents also increase. The densities of ratio a , b and c in HWPCs were 0.82 , 0.68 and 0.85 gcm^{-3} and the determination of ratio a , b and c in SWPCs were 0.79, 0.73 and 0.73 gcm^{-3} respectively. Water absorption inversely related with density of all WPCs. When the density was lower, more water entered into the cell wall of WPCs and therefore there was more swelling along the hydrophilic sawdust grains. Water absorption of SWPC was higher than those of HWPCs.

As the amount of wood increased, thickness swelling properties of SWPCs and HWPCs were also increased. Density inversely effected on the thickness swelling properties of all WPCs. Due to the increasing order of wood contents in the formulation of ratio a , b and c, the highest swelling was found in ratio c not only for SWPCs but also for HWPCs. It was found clearly that the highest water reduction rates in SWPCs and HWPCs were accompanied with the highest amount of sawdust (SD) filler because of the porous contained SD. Ratios (c) of both WPCs samples response the best water reduction qualities in this determination.

It is significant in the determination of variance of WPCs properties. In this study, slightly decreased specific gravities were obtained with the increased amount of wood contents in the analyzed SWPCs and HWPCs.

Alternatively, higher plastic contents associated with the higher density and specific gravities of applied SWPCs and HWPCs in this study.

3.4 Mechanical Properties

3.4.1 Hardness

Hardness of a material is the measure of the resistance to indentation and therefore it is one of the important properties of composites. Among the HWPCs, ratio (c) gave the highest hardness , 95 and the similar results were shown in the three tested SWPCs , ratio (b) and (c) also expressed their hardness as 94. It was because the more the content of wood in the composition of WPCs , the more adhesion between the sawdust fiber and PE matrix. Good hydrophilic sawdust short fiber dispersion within hydrophobic polyethylene gained the effective interfacial bonding. And therefore it could reduce the softness and enhance the stiffness of all WPCs examined in this study.

3.5 Characterization on WPCs

3.5.1 Screening electron microscopic analysis(SEM)

In the SEM micrograms of both of SW and HW composites, morphological structure of ratio (c) was found as better dispersion than (a) and (b) (Figures 5-10). The best ratio (c) from the production of part-I was carried to the second step preparation.

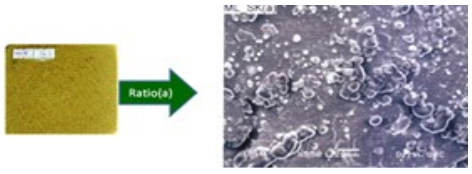

Fig5. SEM micrograph of SWPC ratio (a) and SW composite panel

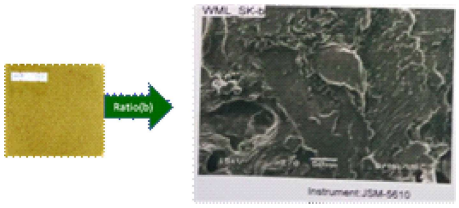

Fig6. SEM micrograph of SWPC ratio (b) and SW composite panel

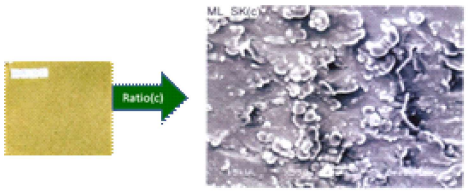

Fig7. SEM micrograph of SWPC ratio (c) and SW composite panel

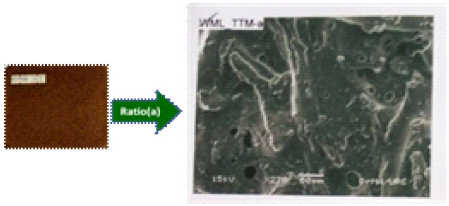

Fig8. SEM micrograph of HWPC ratio (a) and HW composite panel

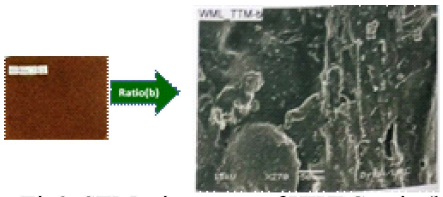

Fig9. SEM micrograph of HWPC ratio (b) and HW composite panel

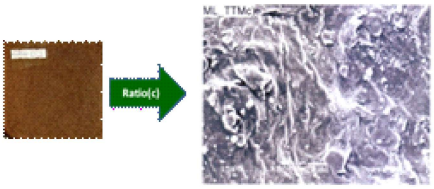

Fig10. SEM micrograph of HWPC ratio (c) and HW composite panel

Fig11. SEM micrograph of PE only

Fig12. SEM micrograph of SW only

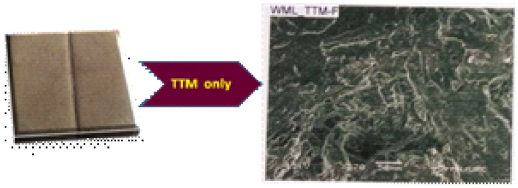

Fig. 13 SEM micrograph of HW only

3.5.2 Thermogravimetric analysis (TGA) (or) Thermobalance

A technique in which the mass of the sample is recorded versus time or temperature while the temperature of the sample is programmed, in a controlled atmosphere. In the TGA thermograms of SW and HW, similar patterns of mass loss by dehydration and decomposition as the function of constant temperature were obtained and do not differ significantly (Figures 14 -22).

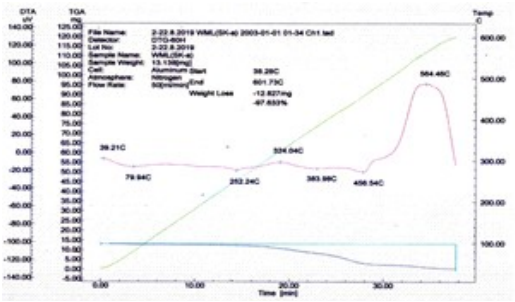

Fig. 14 TGA thermogram given by SW ratio (a)

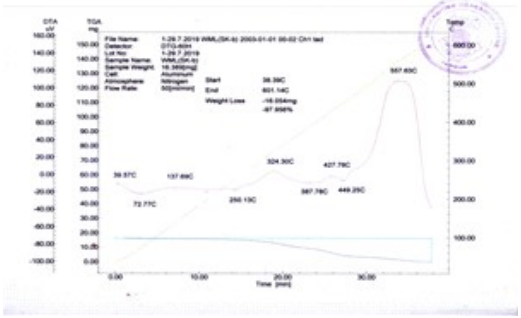

Fig15. TGA thermogram given by SW ratio (b)

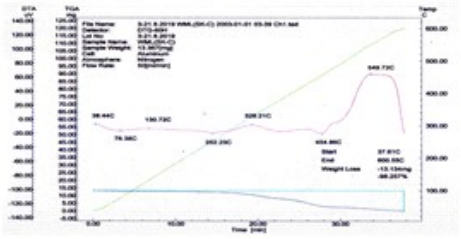

Fig16. TGA thermogram given by SW ratio (c)

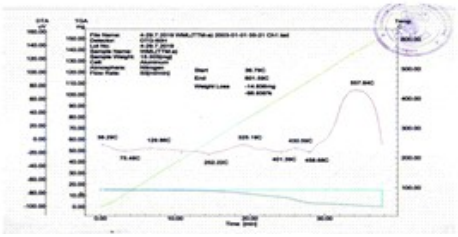

Fig17. TGA thermogram given by HWPC ratio (a)

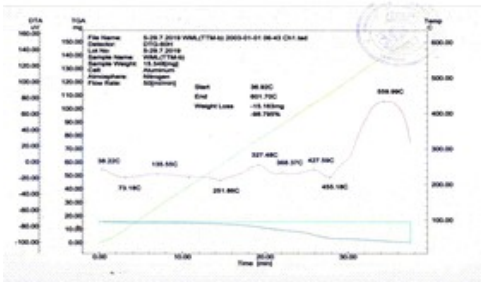

Fig18. TGA thermogram given by HWPC ratio (b)

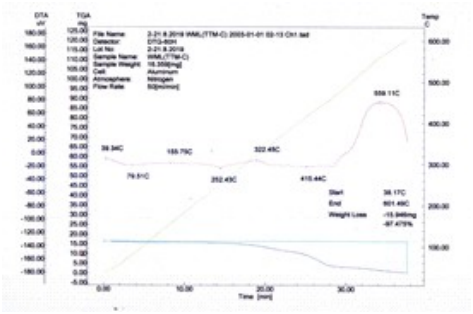

Fig. 19 TGA thermogram given by HWPC ratio (c)

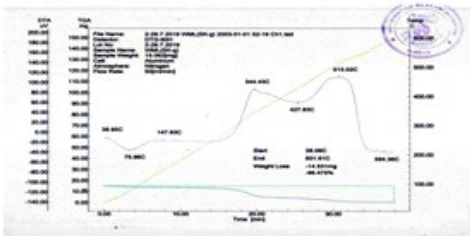

Fig20. TGA thermogram of SW only

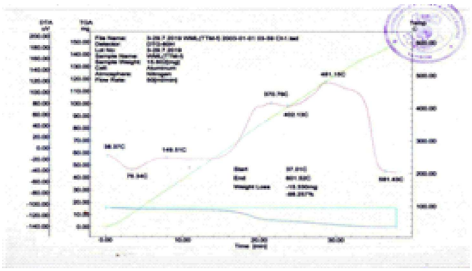

Fig21. TGA thermogram of HW only

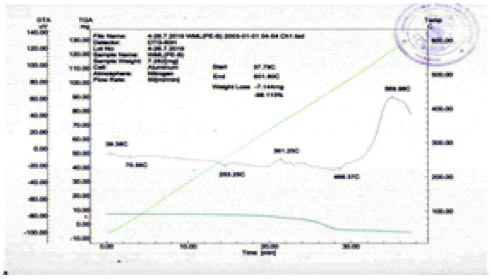

Fig22. TGA thermogram of PE only

3.6 Salt Spray Test

After spraying 3.5 % NaCl solution for 3 days, the resulting observation at at 0 day and 3 days were shown (Figure 23). All samples showed no sign of corrosion and it could be concluded that these composites panel showed their resistance on NaCl salt solution.

Fig23. Salt spray test with 3.5 % NaCl solution

3.7 Chemical Resistance Test

After spraying onto the surface of composite panels with 94 % ethanol, it was found that there was no change in color of the composites and therefore the composites obtained showed their chemical resistant properties on ethanol were good.

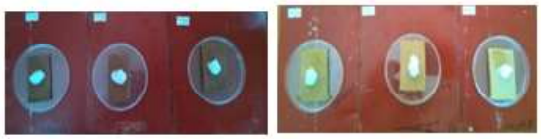

Fig. 24 Chemical resistance test with 94% ethanol

Fig25. Hand-made WPC materials by cold press

3.8 Determination of Physical and Mechanical Properties of SWPCs*and HWPCs*

SWPCs* and HWPCs* were sent to Rubber Research and Development Center, Department of agriculture, Ministry of Agriculture Livestock and Irrigation, Yangon, to examine mechanical properties of WPCs*. For the determination of SEM and TGA, WPCs* were sent to university Research center (URC), Yangon.

Table5. Mechanical Properties of SWPC* and HWPC*

Sample	Hardness (IRHD)	S.G
SWPCs*	94	0.81
HWPCs*	89	0.70

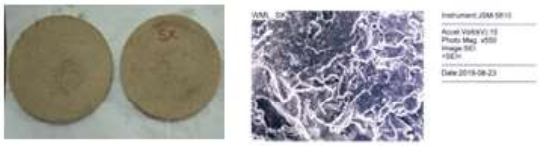

Fig26. SWPC* by hot press and its SEM microgram

By comparing the SEM micrograms of SWPC* and HWPC*, it was found that more porous and better dispersion of ZnO nanoparticles between plastic and softwood and hardwood sawdust particles in the morphology of SWPC* (Figure 26) than that of HWPC* (Fig27).

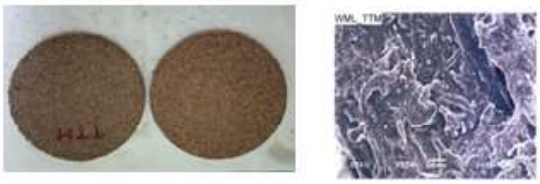

Fig27. HWPC* by hot press and its SEM micrograph

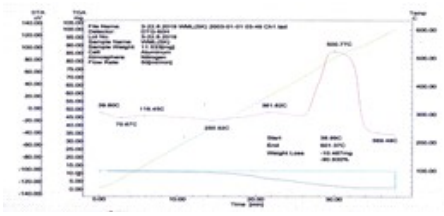

Fig.28. TGA thermogram given by SWPC*

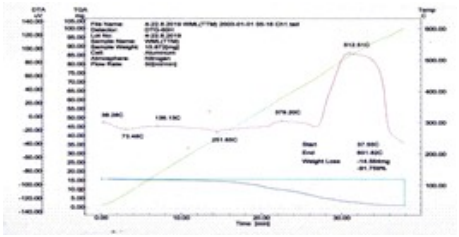

Fig29. TGA thermogram given by HWPC*

Two thermograms of SW and HW were similar in mass loss by dehydration, and decomposition as the function of constant temperature.

4. CONCLUSION

Hand-made SWPCs and HWPCs of various compositions were fabricated by cold press in part - I production and hot press by part-II production. In part-I, it was found that water absorption, water reduction and thickness swelling properties were related with the concentration of wood particles in the composition of WPCs. Alternatively increased amount of density and specific gravity associated with an increase of PE concentration. SEM micrograms clearly pointed out that HWPCs had lower porosity than SWPCs and also HW only showed lesser amount of porosity than SW only composite. In the part -I production, same size of sawdust and plastic particles were utilized and therefore the dispersion of these particles within composite matrix were similar. But in mechanical properties, HWPCs had better qualities than SWPCs. Presence of more hollow feature character within the fiber cell wall of SW than HW induced the lesser hardness of SWPCs than HWPCs and also the other qualities. Thermal decomposition of HWPCs by TGA analysis and SWPCs composites did not show significant differences. Among three ratios, both of HWPCs and SWPCs informed the best response in ratio (c) and therefore this ratio was brought for the composite production part-II. More porous character of SWPC and well uniform dispersions of nanoparticles filler, ZnO were matched and this fact enhanced the hardness mechanical property than HWPCs. In TGA analysis, both of SWPCs and HWPCs gave the similar thermograms. It could be concluded that SW could produce with better mechanical properties than HW by hot compression method in the same condition.

ACKNOWLEDGEMENT

I owe a great deal of gratitude to Dr Aung Win, Rector, Dr Aye Aye Ko and Dr Soe Myint Aye, Prorectors, Myitkyina University for their encouragements. Then we would like to express our gratitude to Dr Ni Ni Aung, Professor and Head and Dr Nant Si Si Htay, Professor, Department of Chemistry, Myitkyina University for their invaluable advices, kind guidance and encouragements for this research.

REFERENCES

[1] Ardanuy, M., Claramunt, J. and Filho, R.D.T. "Cellulosic fiber reinforced cement-based composites: a review of recent research".

[2] Bledzki A. K., Gassan J.: Composites reinforced with cellulose based fibres. Progress in polymer Science, 24, 221–274 (1999). DOI: 10.1016/S0079-6700 (98) 00018-5.

[3] Bledzki A. K., Sperber V. E., Faruk O.: (2002). Natural and wood fibre reinforcement in polymers. Rapra, Shrewsbury.

[4] Bledzki A. K., Sperber V. E., Specht K., Letman M., Viksne A. (2005), Effect of defined waxes and couplingagents on moisture behavior of injection molded wood fiber reinforced PP composites. in '8th International Conference on Woodfiber-Plastic Composites (and other Natural Fibers), Madison, USA' 229–238.

[5] Bledzki, A.K., Letman-Sakiewicz, M., Murr, M. (2010). Influence of static and cyclic climate condition on bending properties of wood plastic

composite (WPC). eXPRESS Polymer Letters Vol.4, No.6, 364-372.

[6] BYK Additives & Instruments. (201). "Modifiers for Wood Plastic Composites (WPC)". Application Information TP-A1.

[7] Cantero G., Arbelaiz A., Mugika F., Valea A., MondragonI. (2003) Mechanical behavior of wood/polypropylenecomposites: Effects of fibre treatments and ageing processes. Journal of Reinforced Plastics and Composites, **22**, 37–50. DOI: 10.1177/0731684403022001495

[8] Dale Ellis W., O'Dell J. L.: Wood-polymer composites made with acrylic monomers, isocyanate, and

[9] Gozdecki, C., Wilczynski, A., Kociszewski, M. and Zajchowski, S. (2015). "Properties of wood-plastic composite made of milled particleboard and polypropylene", 73:87-95, DOI 10.1007/ s00107-014-0852-2.

[10] Oladejo, K.O. and Omoniyi T.E. (2017). "Dimensional Stability and Mechanical Properties of Wood Plastic Composites Produced from Sawdust of *Anogeissus leiocarpus* (Ayin) with Recycled Polyethylene Teraphthalate (PET) Chips". European Journal of Applied Engineering andScientific Research, ISSUE 5(1): 28-33.

[11] Oladele, I.O., Daramola, O.O. and Fasooto, S. (2014). "Effect of Chemical Treatment on the Mechanical Properties of Sisal Fibre Reinforced Polyester Composites". Leonardo Electronic Journal of Practices and Technologies, Issue 24, pp.1-12, ISSN 1583-1078.

[12] Rowell R. M., (2005). Handbook of wood chemistry and wood composites. Taylor and Francis, New York, maleic anhydride. Journal of Applied Polymer Science, **73**, 2493–2505 (1999). DOI: 10.1002/(SICI)1097-4628 (19990919)73:12<2493::AID-APP18>3.0.CO;2-C

[13] Rowell R. M., Lange S. E., Jacobson R. E.: Weathering performance of plant fiber/ thermoplastic composites. Molecular Crystals

Journal of Research and Applications (JRA), UCSMTLA, 2019 Volume-01, Issue-01

Article ID - JRA190042

ANALYSIS ON RESIDUAL NETWORK MODELS FOR IMAGE DESCRIPTION GENERATION

Phyu Phyu Khaing [(1)], Myint San[(2)], Mie Mie Aung[(2)]

[(1)]Myanmar Institute of Information Technology, Mandalay, Myanmar

[(2)]University of Computer Studies (Monywa), Myanmar

[(1)]phyu_phyu_khaing@miit.edu.mm

ABSTRACT

Image description generation is the process in which the sentence is generated for the context of the image. In this process, there are two important parts: feature extraction from the image and sentence generation based on the image features. The process of image description generation works as the combination of computer vision and natural language processing. This paper intends to represent the image description generation framework based on the pre-trained Convolutional Neural Network trained by Deep Residual Network (ResNet) for feature extraction and Two Long-Short Term Model (Two-LSTM) for sentence description. The experiment of the system is implemented on the Flickr8Kdatasets and the performance of the system is measured using standard evaluation metrics, such as: BLEU, METEOR, CIDEr, and ROUGE-L.

KEYWORDS: *Image Description Generation, Convolutional Neural Network, ResNet, Long-Short Term Memory, LSTM.*

1. INTRODUCTION

Image description generation process is still challenging in the artificial intelligence processes and is used both computer vision process and natural language process. Computer vision is utilized to extract the features from the image, and natural language processing helps in generating the sentence description that further describes what the image shows. The process of the image description generation requires the model to acknowledge objects in an image, to comprehend the relationship between objects and to communicate them in a natural language sentence.

Deep learning model has become as core component any advanced applications, and the usage of this learning method is also much more available. Image captioning can produce a single significant and comprehensive grammar phrase and increase description precision by using a profound learning model. This paper presents the image description generation framework by using deep Residual Network (ResNet) and Long-Short Term Model (LSTM). The system is implemented on the benchmark datasets: Flickr8k; and evaluated the performance of the model using BLEU, METEOR, CIDEr, and ROUGE-L.

The rest of the paper is prepared with the following sections. The related works of this research is reviewed in Section 2. Section 3 shows the structure of the image description generation framework and explains the methodologies. The experimentation is implemented in Section 4. Section 5 concludes about the methods with the limitation and future works of the system.

2. RELATED WORKS

Vinyals et al. [1] suggested an end-to-end neural image caption generator model called NIC by integrating deep CNN with LSTM. NIC first utilizes a convolutional neural network to encode the image and then utilizes a recurrent neural network to produce a natural language sentence that matches with the image. This measured efficiency with the conventional assessment metrics and also assessed individual judgments on five benchmark datasets.

Mao et al. [2] initiated the multimodal recurrent neural network (m-RNN) technique to extract new image caption. The proposed m-RNN technique

consists of two networks. A convoluted neural network that encodes images and adeep recurrent neural network generates sentences. The two subnets communicate with each other in the multimodal layer to form the entire m-RNN model. The input to this method is the image and the sentence. The probability distribution is calculated to form the next captioning word for the sentence. The model includes five additional layers: a two-word embedded layer, a recurrent layer, a multimodal layer, and a SoftMax layer.

Donahue et al. [3] proposed the Long-term Recurrent Convolutional Network (LRCN) that is similar with m-RNN [4]. for visual recognition and description, LRCN incorporates long-range temporal recursion with convolutional layers. LRCN uses AlexNet for feature extraction of the image and a stacked two-layer LSTM for image description generation by feeding the image content. In a stacked two-layer LSTM, bottom LSTM is supplied only with the prior word to embed, and the top LSTM takes the feature of the image as input and the bottom LSTM output the result. The benefit of the stacked architecture is that top LSTM merges the image and the context information to predict the distribution of word, and bottom LSTM can concentrate on text information modelling.

Jia et al. [5] suggested the alternative LSTM extension which is called guided LSTM (gLSTM) and long sentences can be generated by using this gLSTM. This model brings the semantic image-extracted information into LSTM cell state and each gate to produce image descriptions as input together with entire image. It also examines the various strategies for controlling the captioning length by normalizing with the semantic information. Multimodal embedding space can also be used to extract semantic based information from the image.

Wang et al. [6] indicated the architecture by integrating the benefits of simple RNN and LSTM used throughout parallel fusion for image captioning, namely parallel-fusion RNN-LSTM. This strategy enhances performance and effectiveness through evaluation on Flickr8 K dataset with BLEU and METEOR. Future research must examine the restriction of simultaneous threads by using more complicated image features to concentrate the greater efficiency.

Aneja et al. [7] studied convolutional image captioning technology, which has proven to be consistent with current LSTM techniques. Validity and comparison performance is shown by verifying on the MSCOCO datasets. Models can be used to carefully improve performance. Wang et al. [8] found a framework for producing the caption of the image using a convolutional neural network (CNN). MSCOCO has been extensively studied to examine the effects of model size and thickness. Compared to the LSTM-based model using a similar attention process, the proposed design can be compared in terms of BLEU, METEOR and CIDER scores.

There are few important literatures on image description processes but mostly lack of explicit concluding remrks and scope for research directions that can be implemented. Thus, an extensive comparison is required to assess what methodology could be considered as benchmark with suitable datasets.

3. IMAGE DESCRIPTION GENERATION MODEL

This system presents the analysis of image description generation model by using deep residual network (ResNet) and long-short term model (LSTM) as shown in Fig 1.

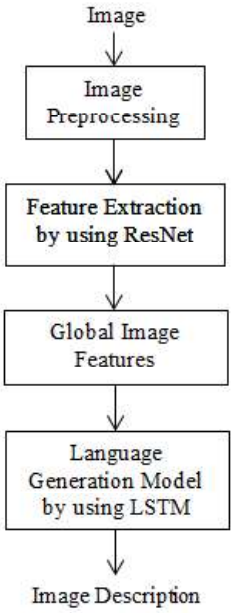

Fig 1.Image Description Generation Model

3.1 Convolutional Neural Network

Convolutional Neural Network (CNN) is fundamental type of deep learning method similar to ordinary neural network with hidden layers. In convolutional neural network, increasing the number of hidden layers poses several challenges which are overcome in CNN. In CNN, convolutional layers, pooling scheme, normalization scheme and fully connected layers are main components. Pooling is most important component that helps in reducing the repeating number of features and allowing the hidden layers to increase. CNN works much better than ordinary SVM or any other training method.

There are many pre-trained model for Convolutional Neural Network (CNN). Among them, some pre-trained model that contained in Keras. Keras is a neural-network library, which is open-source and is written with Python. There have been many research areas that used Keras. For image captioning, many researchers used Keras pre-trained model for image encoding that extracts the features of image. It supports convolutional neural networks, recurrent neural networks, and also combinations of two networks; and runs impeccably on CPU and GPU. There are many pre-trained models for image captioning. Among them, this study is applied deep Residual Networkfor the feature extraction of the image.

The Residual Network (ResNet) [9] is a specialized neural network that helps to manage more advanced deep learning tasks and models. ResNet is implemented by adding the corresponding residual version to the normal network. In the network, the layer uses the reference as a layer input to learn the redundant function instead of learning the function without reference. ResNet can achieve precision from a greatly increased depth and is easy to optimize. ResNet is available in 18, 34, 50, 101 and 152 versions. 34-layer ResNet is better than 18-layer ResNet. The 34-tier ResNet reduced the previous error by 3.5%. The 18-layer ResNet is faster than an 18-layer normal network. ResNet 50/101/152 is more sensitive than ResNet 34. Therefore, ResNet50, ResNet101, and ResNet152 are implemented in the feature extractor.

3.2Long-Short Term Memory

Long-Short Term Memory (LSTM) is used that can handle long term dependence and also address the problems of hidden states. LSTM was actually suggested by Hachreiter (1997) mainly to deal with long term dependency issues and the information can retain for very long time also [10]. LSTM is designed in chain like structure with four important layers, namely Forget Gate (f); Input Gate (I); Candidate Layer (C); Output Gate (O). Except Candidate layer, other layers are all single layered networks that use Sigmoid function whereas Candidate layer utilizes Tanh function for activation purposes. Generally, three major steps are executed in LSTM operation. The information that has to be thrown away is processed in first step and second step determines what information has to be stored as new information. Output is appropriately decided by third step.The output of the LSTM cell is calculated with the following equations.

$$f_t = \sigma(x_t * W_{xf} + h_{t-1} * W_{xf}) \quad (1)$$

$$\bar{c_t} = \tanh(x_t * W_{xc} + h_{t-1} * W_{hc}) \quad (2)$$

$$i_t = \sigma(x_t * W_{xi} + h_{t-1} * W_{hi}) \quad (3)$$

$$o_t = \sigma(x_t * W_{xo} + h_{t-1} * W_{ho}) \quad (4)$$

$$c_t = f_t * c_{t-1} + i_t * \bar{c_t} \quad (5)$$

$$h_t = o_t * \tanh(c_t) \quad (6)$$

In the equations,f_t is forget gate, $\bar{c}_t$ is cell state, i_t is input gate and o_t is output gate, c_t is current cell memory, h_t is current cell output, c_{t-1} is previous cell memory, h_{t-1} is previous cell output, x_t is input vector. W_x and W_h are the weights of input and the previous cell output respectively.

4. EXPERIMENT

4.1 Dataset

There has been many popular datasets that is used for image description generation model such as Flickr8k [11], Flickr30k [12], MSCOCo [12], etc. Among them, this study presents on Flickr8k [11] benchmark datasets. That is very popular and mostly used for image annotation. The images from Flickr.com website is collected for Flickr8k dataset. Flickr8k dataset consists of 8,092 images; and divided into 6,000 images to train, 1,000 images to test and 1,000 images to validate. Five sentences are created for each image in the dataset by characterizing with events scenes, situation, and entities (animals, people and objects). The grammar of images from the dataset is tested with the help of the workers and spelling is checked with United State format.

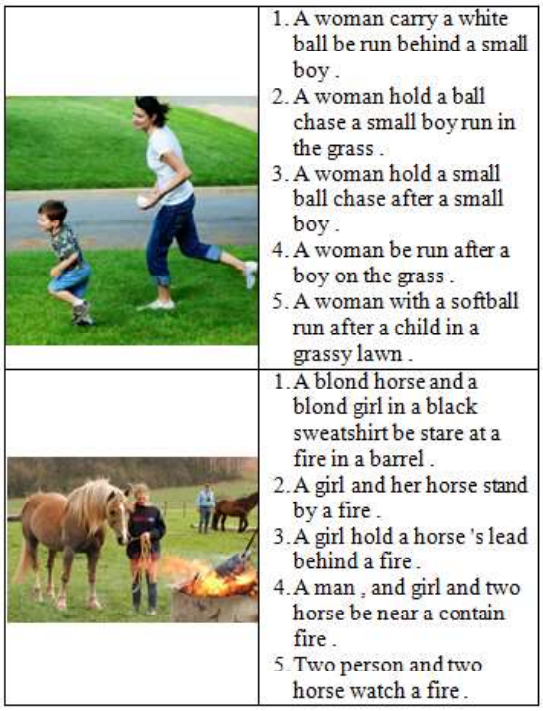

Fig 2. Sample images and descriptions from the dataset

4.2Evaluation Metrics

The evaluation metrics are mostly implemented to measure the performance of image captioning model. There are many popular evaluation metrics. Among them, this study is evaluated with Bilingual Evaluation Understudy (BLEU), Metric for Evaluation based Image Description Evaluation (METEOR), Consensusbased Image Description Evaluation (CIDEr), and Recall-Oriented Understudy for Gisting Evaluation (ROUGE).

BLEU [13] measures by the similarity between machine-generated sentences and sentences in a data set. It is part of the N-gram. This is very similar to human judgment. Therefore, this is often referred to as a humanoid assessment for machine translation. In this experiment, the performance of the model will be verified at 1, 2, 3 and 4 grams, respectively.

To overcome the BLEU metric problem, METEOR [14] was designed based on the harmonic averages of unigram precision and recall rates. It is used the same resources to evaluate the target language and create a statistical translation system. Open source software is freely available for that. Unlike BLEU indicators, METEOR seeks compliance at the corpus level.

CIDEr [15] is used to evaluate definitions created using human consensus. The purpose of CIDEr is to automatically evaluate the description for the image. The metric specifies the number of units of ideas that match the candidate sentence in the image description set.

ROUGE-L [16] is designed for measurement of a general result of maximum length between the target and source statements. There are four different ROUGE measurements: ROUGE-L, ROUGE-N, ROUGE-S, and ROUGE-W. Because the survey has a sentence-level LCS, ROUGE-L is used for the most common sequence of results (LCS) in this experiment.

4.3 Experimental Results

To implement the image description generation model, we have used the machine with Intel Core I7 processor with 8 cores and 8GB RAM running on Window 10 OS. Keras library based on tensorflow is used for creating and training deep neural networks. Tensorflow is a deep learning library developed by Google [17]. Tensorflow uses the graph definition to implement the deep learning network. It can be executed on any supported devices by defining one graph at once.

For the image description generation model, we are using by combining CNN and LSTM. ResNetsare used for the image features extraction task and act as an image encoder. That model is trained with 10 epochs. Table 1 shows the experimental results for image description generation.Generally, ResNet50 is better than the other two and ResNet152 is better than ResNet101. However, BLEU-2, BLEU-3, BLEU-4 of ResNet152 is the better than ResNet50 and ResNet101. Sample generated descriptions of the images are shown in Fig.3.

This work compares few image description generation models in terms of various performance metrics and it can be evidently seen that ResNet50 outperforms all the models. So, the comparison of literature suggests that we need to expensively evaluate and based on that the suitable model can be recommended.

Table 1. Experimental results of image description generation

Models	BLEU-1	BLEU-2	BLEU-3	BLEU-4	METEOR	CIDEr	ROUGE_L
ResNet50	**0.576308**	**0.305348**	**0.167662**	**0.085092**	**0.207652**	**0.213671**	**0.454116**
ResNet101	0.568494	0.303183	0.167712	0.088484	0.201189	0.188736	0.447229
ResNet152	0.575645	0.31071	0.169603	0.087169	0.20544	0.197922	0.453826

Generated Caption:
1) dog is running through the grass

Generated Caption:
1) man is riding his bike on the snow

Generated Caption:
1) man is sitting on the street

Fig 3.Some Generated Captions for Sample Images

5. CONCLUSIONS

This paper studies the analysis for image description generation models and the study used the encoder-decoder framework for image description generation. Deep residual networks (ResNets)are used as the encoder to extract features from image and LSTM is used as the decoder to generate a sentence that described the image. This study is implemented on Flickr8k dataset and evaluate with BLEU, METEOR, CIDEr, and ROUGE-L evaluation metrics. We have evaluated different models in term of performance evaluation parameters and observed that the model ResNet50 does well in comparison with other models.The work, however, doesn't consider the attention mechanism on the model. For the extension, we will test with different datasets and other different models, and we will also add the attention models in the encoder-decoder framework. Though, the test and experimentation were carried out for a dataset which is significantly used by numerous researchers.

ACKNOWLEDMENT

The authors are grateful for the constructive advice and comments to all the esteemed reviewers who have anonymously helped a lot for making the manuscript of very good quality.

REFERENCES

[1] O. Vinyals, A. Toshev, S. Bengio, and D. Erhan, "Show and tell: A neural image caption generator," in *2015 IEEE Conference on Computer Vision and Pattern Recognition (CVPR)*, Boston, MA, USA, 2015, pp. 3156–3164.

[2] J. Mao, W. Xu, Y. Yang, J. Wang, Z. Huang, and A. Yuille, "Deep Captioning with Multimodal Recurrent Neural Networks (m-RNN)," *ArXiv14126632 Cs*, Jun. 2015.

[3] J. Donahue *et al.*, "Long-Term Recurrent Convolutional Networks for Visual Recognition and Description," p. 10.

[4] T.-Y. Lin *et al.*, "Microsoft COCO: Common Objects in Context," in *Computer Vision – ECCV 2014*, vol. 8693, D. Fleet, T. Pajdla, B. Schiele, and T. Tuytelaars, Eds. Cham: Springer International Publishing, 2014, pp. 740–755.

[5] X. Jia, E. Gavves, B. Fernando, and T. Tuytelaars, "Guiding Long-Short Term Memory for Image

Caption Generation," Sep. 2015.

[6] M. Wang, L. Song, X. Yang, and C. Luo, "A parallel-fusion RNN-LSTM architecture for image caption generation," in *2016 IEEE International Conference on Image Processing (ICIP)*, 2016, pp. 4448–4452.

[7] J. Aneja, A. Deshpande, and A. G. Schwing, "Convolutional Image Captioning," in *2018 IEEE/CVF Conference on Computer Vision and Pattern Recognition*, Salt Lake City, UT, 2018, pp. 5561–5570.

[8] Q. Wang and A. B. Chan, "CNN+CNN: Convolutional Decoders for Image Captioning," *ArXiv180509019 Cs*, May 2018.

[9] K. He, X. Zhang, S. Ren, and J. Sun, "Deep Residual Learning for Image Recognition," in *2016 IEEE Conference on Computer Vision and Pattern Recognition (CVPR)*, Las Vegas, NV, USA, 2016, pp. 770–778.

[10] S. Hochreiter and J. Schmidhuber, "Long Short-term Memory," *Neural Comput.*, vol. 9, pp. 1735–80, Dec. 1997.

[11] M. Hodosh, P. Young, and J. Hockenmaier, "Framing Image Description as a Ranking Task Data, Models and Evaluation Metrics Extended Abstract," p. 5.

[12] B. A. Plummer, L. Wang, C. M. Cervantes, J. C. Caicedo, J. Hockenmaier, and S. Lazebnik, "Flickr30k Entities: Collecting Region-to-Phrase Correspondences for Richer Image-to-Sentence Models," p. 9.

[13] K. Papineni, S. Roukos, T. Ward, and W.-J. Zhu, "BLEU: a method for automatic evaluation of machine translation," in *Proceedings of the 40th Annual Meeting on Association for Computational Linguistics - ACL '02*, Philadelphia, Pennsylvania, 2001, p. 311.

[14] M. Denkowski and A. Lavie, "Meteor Universal: Language Specific Translation Evaluation for Any Target Language," in *Proceedings of the Ninth Workshop on Statistical Machine Translation*, Baltimore, Maryland, USA, 2014, pp. 376–380.

[15] R. Vedantam, C. L. Zitnick, and D. Parikh, "CIDEr: Consensus-based Image Description Evaluation," *ArXiv14115726 Cs*, Jun. 2015.

[16] C.-Y. Lin, "ROUGE: A Package for Automatic Evaluation of Summaries," in *Text Summarization Branches Out*, Barcelona, Spain, 2004, pp. 74–81.

[17] M. Abadi *et al.*, "TensorFlow: A system for large-scale machine learning," p. 21.

Journal of Research and Applications (JRA), UCSMTLA, 2019 Volume-01, Issue-01

Article ID - 190056

EXPLICIT RUNGE-KUTTA METHODS FOR FIRST ORDER INITIAL VALUE PROBLEMS

Khin Kyawt Kyawt San [(1)], Khin Hnin Thwe [(2)], Cho Cho Soe Wai [(3)]

[(1)]University of Computer Studies (Monywa), Myanmar

[(2)(3)] Pakokku University (Pakokku), Myanmar

[(1)]*kyawtkyawt7419@gmail.com*

ABSTRACT

This paper is concerned with the numerical properties of explicit Runge-Kutta methods (ERK) for the first order initial value problems. The derivatives of each method will be presented by Butcher tableau of the coefficients in the system of algebraic equations of s-stage ERK methods. Besides, it is examined that the order of accuracy and convergence of ERK methods. It is also examined the regions of absolute stability of s-stage ERK methods of order s for s = 1, 2, 3, 4 for $y' = f(t, y)$ by applying these methods to the test equation + ay + r(t)=0. It will be found that the regions of higher order methods are more broader from the point of stability as well as the higher order methods are more closer to the exact solutions by calculating ERK methods. At last, Numerical and graphical comparisons between these methods with the exact solution have been presented for the initial value problems.

KEYWORDS: *explicit Runge-Kutta methods, Butcher tableau, stability regions, approximations, errors*

1. INTRODUCTION

Differential equations can nearly describe all system undergone change. Many mathematicians have studied the nature of these equations and many complicated systems can be described quite precisely with compact mathematical expressions. However, many systems involving differential equations are so complex. It is in these complex systems where computer simulations and numerical approximations are useful. The techniques for solving differential equations based on numerical approximations were developed before programmable computers existed. The problem of solving ordinary differential equations is classified into initial value and boundary value problems, depending on the conditions specified at the end points of the domain. There are numerous methods that produce numerical approximations to solution of initial value problems in ordinary differential equations such as Euler's method which was the oldest and simplest method originated by Leonhard Euler in 1768 and Runge-Kutta methods. The Runge-Kutta methods are an important family of iterative methods for the approximation of solutions of ordinary differential equations (ODEs), that were developed around 1900 by the German mathematicians C. Runge and M.W. Kutta[1] [2].

We start with the consideration of the explicit methods. Let us consider an initial value problem (IVP)

$$\frac{dy}{dt} = f(t, y(t)), \qquad (1)$$

$y(t) = (y_1(t), y_2(t),..., y_n(t))^T$, $f \in [a,b]\times \mathbb{R}^n \to \mathbb{R}^n$, with an initial condition

$$y(t_0) = y_0. \qquad (2)$$

Here, it is interested in a numerical approximation of the continuously differentiable solution y(t) of the IVP(1)-(2) over the time interval $t \in [a,b]$. To this aim we subdivide the interval [a, b] into M equal subintervals and select the mesh points t_j .

$$t_j = a + jh, j = 0,1,...,M, h = \frac{b-a}{M}. \quad (3)$$

The value h is called a *step size*. Traditionally it is assumed that the function f of (1) is continuous and satisfies a Lipschitz condition with constant L,

$$\| f(t,u) - f(t,v) \| \leq L \| u - v \|.$$

The stability of solution of (1) in this class of problems is easily established. It will be sketched in a form analogous to developments which follow. Any solution y(t) of (1) can be represented in the form

$$y(t) = y(t_n) + \int_{t_n}^{t} f(\theta, y(\theta))d\theta$$ in [8], [9], [10].

Standard introductory texts are Stoer & Bulirsch [1], Dekker & Verwer [2], Morecver, Bosede, Emmanuel & Temitayo [3] , Sankara Rao [4], Islam [5] ,Sastry [6] and Scott [7] give a more complete recent survey of the field.

2. EXPLICIT RUNGE-KUTTA METHODS

2.1 Definition

The family of explicit Runge-Kutta (ERK) methods of the s- stage is given by

$$y(t_{n+1}) = y_{n+1} = y_n + h\sum_{i=1}^{s} b_i k_i, \quad (4)$$

where

$$k_1 = f(t_n, y_n)$$

$$k_2 = f(t_n + c_2 h, y_n + h a_{21} k_1(t_n, y_n)),$$

$$k_3 = f(t_n + c_3 h, y_n + h(a_{31} k_1(t_n, y_n) + a_{32} k_1(t_n, y_n))),$$

$$\vdots$$

$$k_s = f(t_n + c_s h, y_n + h\sum_{j=1}^{s} a_{sj} k_j).$$

To specify a particular method, we need to provide the integer s (the number of stages), and the coefficients $c_i (i = 2,3,...,s)$, $a_{ij} (1 \leq j < i \leq s)$, and $b_i (i = 1,2,...,s)$.

These data are usually arranged in a co-called *Butcher tableau* (after John C. Butcher):

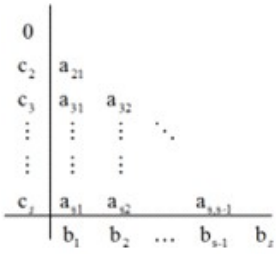

2.2 First, Second, third and Fourth Order of

Let s =1 then,

$$k_1 = f(t_n, y_n),\ y_{n+1} = y_n + hb_1 f(t_n, y_n). \quad (5)$$

On the other hand, the Taylor expansion yields

$$y_{n+1} = y_n + h\, y|_{t_n} + ... = y_n + hf(t_n, y_n) + O(h^2).$$

This implies $b_1 = 1$.

Thus, the first stage RK method is equivalent to the explicit Euler's method. Note that the Euler's method is the first order of accuracy. Thus, it is the RK method of the first order.

Now consider the case s= 2. In this case (4) is equivalent to the system

$$k_1 = f(t_n, y_n),\ k_2 = f(t_n + c_2 h, y_n + h a_{21} k_1),$$

$$y_{n+1} = y_n + h(b_1 k_1 + b_2 k_2).$$

Now, let us write down the Taylor series expansion of y in the neighborhood of t_n up to the h^2 term, i.e.,

$$y_{n+1} = y_n + h\left.\frac{dy}{dt}\right|_{t_n} + \frac{h^2}{2}\left.\frac{d^2y}{dt^2}\right|_{t_n} + O(h^3).$$

However, we know that $y' = f(t, y(t))$, so that

$$\frac{d^2y}{dt^2} = \frac{df(t, y)}{dt} = \frac{\partial f(t, y)}{\partial t} + f(t, y)\frac{\partial f(t, y)}{\partial y}.$$

Hence the Taylor series expansion can be rewritten as

$$y_{n+1} - y_n = hf(t_n, y_n) + \frac{h^2}{2}\left(\frac{\partial f}{\partial t} + f\frac{\partial f}{\partial y}\right)\Bigg|_{(t_n, y_n)} + O(h^3).$$

(6)

On the other hand, the term in the proposed RK method can also expanded to $O(h^3)$ as

$$k_2 = f(t_n + c_2 h, y_n + h a_{21} k_1)$$

$$= hf(t_n, y_n) + hc_2\left.\frac{\partial f}{\partial t}\right|_{(t_n, y_n)} + ha_{21} f\left.\frac{\partial f}{\partial y}\right|_{(t_n, y_n)} + O(h^3).$$

Now, substituting this relation for k_2 into the last equation of (5), we achieve the following expression:

$$y_{n+1} - y_n = h(b_1 + b_2)f(t_n, y_n) + h^2 b_2 c_2\left.\frac{\partial f}{\partial t}\right|_{(t_n, y_n)}$$

$$+ h^2 b_2 a_{21}\left.\frac{\partial f}{\partial y}\right|_{(t_n, y_n)} + O(h^3).$$

Making comparison in the last equation and (6) we can write down the system of algebraic equations for unknown coefficients

$$b_1 + b_2 = 1,\ b_2 c_2 = \frac{1}{2},\ b_2 a_{21} = \frac{1}{2}.$$

The system involves four unknowns in three equations. That is, one additional condition must be supplied to solve the system. We discuss two useful choices, namely

a) Let $c_2 = 1$. Then $b_2 = 1/2, b_1 = 1/2, a_{21} = 1$. The corresponding Butcher tableau is

0		
1	1	
	1/2	1/2

Thus, in this case the two-stages RK method takes the form

$$y_{n+1} = y_n + \frac{h}{2}\big((f(t_n, y_n) + f(t_n + h, y_n + hf(t_n, y_n))\big),$$

and is equivalent to the Heun's method, so we refer the last method of two-stages to RK-method of the second order.

a) Now, let $c_2 = 1/2$. In this case $b_2 = 1, b_1 = 0,\ a_{21} = 1/2$. The corresponding Butcher tableau is

0		
1/2	1/2	
	0	1

In this case the second-order RK method (4) can be written as

$$y_{n+1} = y_n + h(f(t_n + \frac{h}{2}, y_n + \frac{h}{2} f(t_n, y_n))$$

and is called the second order RK method (*RK2 method*).

Otherwise, the method becomes

$$y_{n+1} = y_n + \frac{1}{2}(k_1 + k_2), \quad (7)$$

where, $k_1 = hf(t_n, y_n)$, $k_2 = hf(t_n + h, y_n + k_1)$.

This formula (7) is also called Heun's formula (or) the improved Euler's method (or) Trapezoidal method.

So, the choice of the parameter (coefficients) is arbitrary and we have several s-stage RK-formulas.

Therefore, we choose the coefficients for the most commonly used formulas for third-stage and fourth-stage RK methods.

For s =3, by applying Taylor series expansion we can compute the equations of the coefficients as follow:

$$b_1 + b_2 + b_3 = 1, \qquad b_3 c_2 a_{32} = \frac{1}{6},$$

$$b_2 c_2 + b_3 c_3 = \frac{1}{2}, \qquad c_2 = a_{21},$$

$$b_2 c_2^2 + b_3 c_3^2 = \frac{1}{3}, \qquad c_3 = a_{31} + a_{32}.$$

If we choose $c_2 = 1/2$ and $c_3 = 3/4$, then, we get

$b_1 = 2/9$, $b_2 = 1/3$, $b_3 = 4/9$, $a_{21} = 1/2$, $a_{31} = 0$ and $a_{32} = 3/4$.

The corresponding Butcher tableau is

0			
1/2	1/2		
3/4	0	3/4	
	2/9	1/3	4/9

Therefore third-stage RK method is

$$y_{n+1} = y_n + \frac{2}{9}k_1 + \frac{1}{3}k_2 + \frac{4}{9}k_3, \quad (8)$$

where

$$k_1 = hf(t_n, y_n),\ k_2 = hf(t_n + \frac{1}{2}h, y_n + \frac{1}{2}k_1),$$

$$k_3 = hf(t_n + \frac{3}{4}h, y_n + \frac{3}{4}k_1).$$

This method is called the third order RK method (*RK3 method*). It is also called Simpson method.

Let s = 4, then there are fourth-stage RK methods. One member of the family of Runge–Kutta methods (4) is often referred to *RK4 method* or *classical RK method* and represents one of the solutions corresponding to the case s = 4. In this case, by matching coefficients with those of the Taylor series one obtains the following system of equations

$$
\left.
\begin{aligned}
&b_1 + b_2 + b_3 + b_4 = 1 \\
&b_2c_2 + b_3c_3 + b_4c_4 = \frac{1}{2} \\
&b_2c_2^2 + b_3c_3^2 + b_4c_4^2 = \frac{1}{3} \\
&b_2c_2^3 + b_3c_3^3 + b_4c_4^3 = \frac{1}{4} \\
&b_3c_2a_{32} + b_4(c_2a_{42} + c_3a_{43}) = \frac{1}{6} \\
&b_3c_2c_3a_{32} + b_4c_4(c_2a_{42} + c_3a_{43}) = \frac{1}{8} \\
&b_3c_2^2a_{32} + b_4(c_2^2a_{42} + c_3^2a_{43}) = \frac{1}{12} \\
&c_2 = a_{21}, c_3 = a_{31} + a_{32} \\
&b_4c_2a_{32}a_{43} = \frac{1}{24}.
\end{aligned}
\right\}
$$

The system involves thirteen unknowns in eleven equations. That is, two additional conditions must be supplied to solve the system. The most useful choices are

$$c_2 = 1/2, \qquad a_{31} = 0.$$

The corresponding Butcher tableau is presented in the following table. The tableau yields

0				
1/2	1/2			
1/2	0	1/2		
1	0	O	1	
	1/6	1/3	1/3	1/6

Then the equivalent corresponding equations defining the classical RK4 method is

$$y_{n+1} = y_n + \frac{1}{6}(k_1 + 2k_2 + 2k_3 + k_4), \quad (10)$$

where $k_1 = hf(t_n, y_n)$,

$$k_2 = hf(t_n + \frac{1}{2}h, y_n + \frac{1}{2}k_1)$$

$$k_3 = hf(t_n + \frac{1}{2}h, y_n + \frac{1}{2}k_2)$$

$$k_2 = hf(t_n + h, y_n + k_3).$$

Hence, this method is the most commonly used method and called the fourth order RK method (*RK4 method*).

Now, we will accommodate the convergence and stability of ERK methods as the following sections.

3. CONVERGENCE OF EXPLICIT RUNGE-KUTTA (ERK) METHODS

2.2 Convergence of RK methods

3.1 Definition

A Runge-Kutta method has *accuracy order p* if for sufficiently smooth problem (1),

$$\| y(t_n + h) - y_{n+1} \| \le Kh^{p+1} \qquad (11)$$

i.e., if the Taylor series for the exact solution $y(t_n + h)$ and for y_{n+1} coincide up to (and including) the term h^p.

3.2 Lemma (Gronwall)

Let $\chi : [a,b] \to \square$ be continuous, $\alpha,\beta > 0$ and

$$\chi(t) \le \alpha + \beta \int_{t_0}^{t} \chi(s)\,ds, \qquad t_0 \le t \le b.$$

Then $\chi(t) \le \alpha e^{\beta(t-t_0)}, \quad \forall t \in [t_0,b].$ (12)

Proof. Let $u(t) = \alpha + \beta \int_{t_0}^{t} \chi(s)\,ds$.

Then $u(t_0) = \alpha$. By hypothesis, $\chi(t) \le u(t)$.

The equation can be written as

$$u'(t) = \beta\chi(t) \le \beta u(t), \text{ since } \beta > 0,\ t \in [t_0,b].$$

Multiply throughout this inequality by $e^{-\beta(t-t_0)}$, we get

$$u'(t)e^{-\beta(t-t_0)} - u(t)\beta e^{-\beta(t-t_0)} \le 0.$$

Equivalently, $\frac{d}{dt}\left[u(t)e^{-\beta(t-t_0)} \right] \le 0.$

Integrating from t_0 to t, we obtain

$u(t)e^{-\beta(t-t_0)} - u(t_0) \le 0.\ u(t) \le \alpha e^{\beta(t-t_0)}$, since $u(t_0) = \alpha$

$$\chi(t) \le \alpha e^{\beta(t-t_0)}, \forall t \in [t_0,b].$$

3.3 Theorem

Let f be Lipschitz continuous with L and x(t), y(t) the solutions of IVP (1) with $x(t_0) = x_0$ and $y(t_0) = y_0$.

Then $\| x(t) - y(t) \| \le e^{L(t-t_0)} \| x_0 - y_0 \|, \ \forall t \in [t_0,b].$ (13)

Proof. Take any $t \in [t_0,b]$.

Consider

$$\| x(t) - y(t) \|$$

$$= \| x_0 + \int_{t_0}^{t} f(s,x(s))\,ds - [y_0 + \int_{t_0}^{t} f(s,y(s))\,ds] \|$$

$$\le \| x_0 - y_0 \| + \int_{t_0}^{t} \| f(s,x(s)) - f(s,y(s)) \|\,ds$$

$$\le \| x_0 - y_0 \| + L\int_{t_0}^{t} \| x(s) - y(s) \|\,ds$$

By Gronwall Lemma, we have

$$\| x(t) - y(t) \| \le e^{L(t-t_0)} \| x_0 - y_0 \|.$$

This theorem is known as Gronwall theorem.

3.4 Theorem (Convergence)

Suppose f is Lipschitz continuous. Then the Runge-Kutta method is convergent if its accuracy order p is at least 1.

Proof.

Consider a RK method of accuracy order p with residual vector

$r_n = y_{n+1} - \Phi(\tau, t_n)y_n$, $\| r_n \| \le C\,\tau^{p+1}$ where Φ is solution operator.

Next consider two solutions y(t) and x(t) in which

$y' = f(y, t), \quad x' = f(x, t), \quad y(0) = y_0 \quad x(0) = x_0$

and let $g(t) = \| y(t) - x(t) \|^2$.

Computing this equation,

we get $\frac{1}{2} g'(t) =$

$< y(t) - x(t), y'(t) - x'(t) >$

$\leq \| y(t) - x(t) \| \| f(y, t) - f(x, t) \|$

$\| f(y, t) - f(x, t) \| \leq Lg(t).$

By using Gronwall Theorem,

$\| y(t) - x(t) \| \leq e^{Lt} \| y(0) - x(0) \|.$

In terms of the solution operator, this becomes

$\| \Phi(t; 0) y(0) - \Phi(t; 0) x(0) \| \leq e^{Lt} \| y(0) - x(0) \|.$

(14)

Now we consider the error at time

$t_n, e_n = y_n - y(t_n).$

We prove by induction that $\| e_n \| \leq \frac{C}{L} \tau^p (e^{n\tau L} - 1).$

Since the initial condition is exact, this obviously holds for $n = 0$. Assume it is true for n and consider the error at t_{n+1}:

$e_{n+1} = y_{n+1} - y(t_{n+1}) = y_{n+1} - \Phi(\tau; t_n) y(t_n)$

$e_{n+1} = [y_{n+1} - \Phi(\tau; t_n) y_n] + [\Phi(\tau; t_n) y_n - \Phi(\tau; t_n) y(t_n)].$

We put the first term in brackets as the residual r_n.

Taking norms and applying the triangle inequality, we obtain

$\| e_{n+1} \| \leq \| r_n \| + \| \Phi(\tau; t_n) y_n - \Phi(\tau; t_n) y(t_n) \|.$

Applying (14), we get

$\| e_{n+1} \| \leq \| r_n \| + e^{\tau L} \| e_n \| \leq C\tau^{p+1} + e^{\tau L} \| e_n \|$

$\leq C \tau^{p+1} + e^{\tau L} \frac{C}{L} \tau^p (e^{n\tau L} - 1)$

$\leq \frac{C}{L} \tau^p (e^{(n+1)\tau L} - L\tau - e^{\tau L}) \leq \frac{C}{L} \tau^p (e^{(n+1)\tau L} - 1).$

By mathematical induction, we have

$$\| e_n \| \leq \frac{C}{L} \tau^p (e^{n\tau L} - 1), \quad n = 0, ..., N.$$

Thus $\| e_n \| \leq \frac{C}{L} \tau^p (e^{TL} - 1)$, ere $T = N\tau$.

Convergence follows since for any $p > 0$,

$$\lim_{\substack{h \to 0 \\ h = \frac{T}{N}}} \max_{n=0,1,...,N} \| e_n \| = 0.$$

4. STABILITY OF EXPLICIT RUNGE-KUTTA (ERK) METHODS

3.1 STABILITY OF EXPLICIT RUNGE-KUTTA (ERK) METHODS

Let $\varphi(t)$ be a smooth solution of $y' = f(t, y)$. Using Taylor expansion, we obtain

$$y'(t) = f(t,\varphi(t)) + \frac{\partial f}{\partial y}(t,\varphi(t))(y(t) - \varphi(t)) + \cdots$$

(15)

And introduce $y(t) - \varphi(t) = \overline{y}(t)$ to obtain

$$\overline{y}'(t) = \frac{\partial f}{\partial y}(t,\varphi(t))\overline{y}(t) + \cdots = J(t)\overline{y}(t) + \cdots$$

(3.4) As a first approximation we consider the Jacobian J(t) as constant and neglect the error terms.

Omitting the bars we arrive at $y' = Jy$. (16)

By applying the Runge-Kutta method (4) to the test equation (16), we obtain0

$$y_{n+1} = y_n + hJ\sum_{i=1}^{s} b_i k_i$$

$$k_i = y_n + hJ\sum_{j=1}^{i-1} a_{ij}k_j, \qquad i = 1,2,\ldots,s. \qquad (17)$$

Inserting k_i repeatedly from the second line into the first equation, this becomes $y_{n+1} = R(h\,J)\,y_n$ (18)

Let $z = hJ$ then

R(z)=1+z

$$\sum_i b_i + z^2\sum_{i,k} b_i a_{ik} + z^3\sum_{i,k,l} b_i a_{ik}a_{kl} + \cdots \qquad (19)$$

is a polynomial of degree $\le s$.

4.1 Definition

The function R(z) in the equation (18) is called the *stability function* or the *stability polynomial* of the method. It can be interpreted as the numerical solution $y_{n+1} = R(z)$ after one step for

$$y' = \lambda y, \qquad y_0 = 1, \qquad z = h\lambda \qquad (20)$$

the famous Dahlquist test equation.

The set $\mathbf{S} = \left\{ z \in C/\,\middle|\, R(z) \right| \le 1 \}$,

is called the *stability domain* or the *stability region* of the method.

4.2 Theorem

If the Runge-Kutta method is order p, then

$$R(z) = 1 + z + \frac{z^2}{2!} + \cdots + \frac{z^p}{p!} + O(z^{p+1}).$$

Proof. From the equation (9) ,we have the coefficients of RK method as follow:

$$\sum_i b_i = 1$$

$$\sum_{i,k} b_i a_{ik} = \sum_i b_i c_i = b_1 c_1 + b_2 c_2 = \frac{1}{2}$$

$$\sum_{i,k,l} b_i a_{ik} a_{kl} = \sum_{i,k} b_i a_{ik} c_i = b_3 a_{32} c_2 + b_4(a_{42}c_2 + a_{43}c_3) = \frac{1}{6}$$

$$\sum_{i,k,l} b_i a_{ik} a_{kl} c_l = b_4 a_{43} a_{32} c_2 == \frac{1}{24}.$$

The stability function in (19) becomes

$$R(z) = 1 + z + \frac{z^2}{2!} + \frac{z^3}{3!} + \frac{z^4}{4!} + \cdots . \qquad (21)$$

Since the RK method is order p, and the exact solution of (20) is e^z and therefore the numerical solution $y_{n+1} = R(z)$ must satisfy ccc

$e^z - R(z) = O(\tau^{p+1}) = O(Z^{p+1})$.

As a consequence, all explicit Runge-Kutta methods of order $p = s$ possess the stability function

$$R(z) = 1 + z + \frac{z^2}{2!} + \cdots + \frac{z^s}{s!}.$$

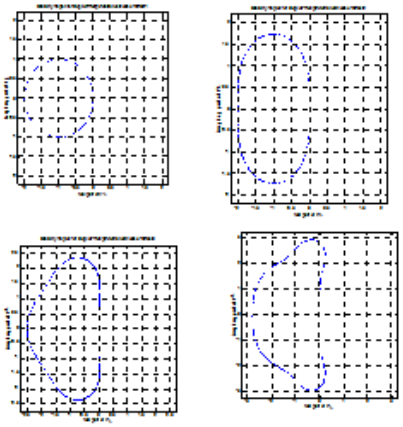

The corresponding stability domains for $s = 1, \ldots, 4$ are represented in Fig.1.

Fig1.Stability domains for ERK methods of order 1, 2,3,4

It is noted that the stability regions of higher order methods more safe for the accuracy than lower order methods of ERK methods.

Moreover, the another way which applies the formulas of ERK methods means higher order methods are more accurate than the lower order methods in solving ODEs. So, we will illustrate the approximations by means of the following examples.

4.3 Example

Consider the initial-value problem $y' = y + t$, with the initial condition $y(0) = 0$.

The exact solution of this IVP is $(e^t - t - 1)$.

It is computed by applying the explicit Runge-Kutta methods for order 1, 2, 3 and 4 with $h = 0.1$ for time-steps and its exact solution and the approximate solutions are given as the following table and the figures. Here, this problem is computed on the interval $0 \le t \le 1$, for the step size $h = 0.1$. The intermediate data is only given to six decimal places even though the computation has been done to many more.

Table 1. Comparison of numerical approximations and exact solution for $y' = t + y$, h= 0.1

t	Exact	RK1	RK2	RK3	RK4	Error			
						RK1	RK2	RK3	RK4
0.1	0.00 5171	0.01	0.0 05	0.0 05	0.00 5167	-0.00 4829	0.00 0171	0.00 017	4.25 E-06
0.2	0.02 1403	0.03 1	0.02 1025	0.02 1025	0.02 1393	-0.00 9597	0.00 0378	0.00 0378	9.39 E-06
0.3	0.04 9859	0.06 41	0.04 9233	0.04 9233	0.04 9843	-0.04 2697	0.00 0626	0.00 0626	1.55 8E-05
0.4	0.09 1825	0.11 051	0.09 0902	0.09 0902	0.09 1802	-0.01 8685	0.00 0923	0.00 0923	2.29 5E-05
0.5	0.14 8721	0.17 1561	0.14 7447	0.14 7447	0.14 8690	-0.02 2840	0.00 1274	0.00 1274	3.17 E-05
0.6	0.22 2119	0.24 87171	0.22 0429	0.22 0429	0.22 2077	-0.09 9996	0.00 1690	0.00 1690	4.21 E-05
0.7	0.31 3753	0.34 3389	0.31 1374	0.31 1374	0.31 3699	-0.02 9836	0.00 2179	0.00 2179	5.42 2E-05
0.8	0.42 5541	0.45 7948	0.42 2789	0.42 2789	0.42 5472	-0.03 2407	0.00 2752	0.00 2752	6.84 9E-05
0.9	0.55 9603	0.59 3743	0.55 6182	0.55 6182	0.55 9518	-0.16 8202	0.00 3421	0.00 3421	8.51 5E-05
1	0.71 8282	0.75 3117	0.71 4081	0.71 4081	0.71 8177	-0.03 4835	0.00 4201	0.00 4201	0.00 01046

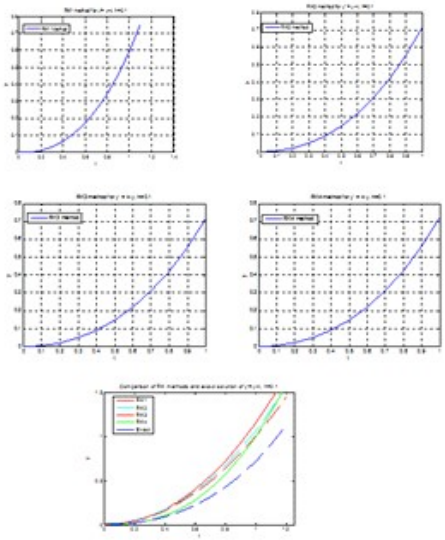

Fig2. RK1, RK2, RK3, RK4 methods and Comparison of exact solution and these methods for $y' = y + t$, h=0.1

4.4 Example

Consider the initial-value problem

$y' = 2(1 + y^2)$, with the initial condition $y(0) = 0$.

The exact solution of this IVP is $\tan 2x$. It is computed by applying the explicit Runge-Kutta

methods for order 1, 2, 3 and 4 with $h = 0.1$ and 0.05 for time-steps and its exact solution and the approximate solutions are given as the following tables and the figures. Here, this problem is computed on the interval $0 \le t \le 0.5$ for the step size

$h = 0.1$and 0.05. The intermediate data is only given to six decimal places even though the computation has been done to many more.

Table 2. Comparison of numerical approximations and exact solution for $y' = 2(1 + y^2)$, h= 0.1

t	Exact	RK1	RK2	RK3	RK4	Error			
						RK1	RK2	RK3	RK4
0.1	0.20 271	0.2	0.2 04	0.20 2707	0.20 2707	0.00 271	-0.00 129	3.24 E-06	2.64 E-06
0.2	0.42 2793	0.4 08	0.4 25	0.42 277	0.42 2789	0.01 4793	-0.00 2207	2.33 E-05	4.31 E-06
0.3	0.68 4137	0.64 1293	0.68 6973	0.68 3997	0.68 4133	0.04 2844	-0.00 2836	0.00 014	3.4 1E-06
0.4	1.02 9639	0.92 3544	1.03 0473	1.02 8933	1.02 9637	0.10 6095	-0.00 0834	0.00 0706	1.95 E-06
0.5	1.55 7408	1.29 413	1.54 4841	1.55 376	1.55 7352	0.26 3278	0.01 2567	0.00 3648	5.6 E-05

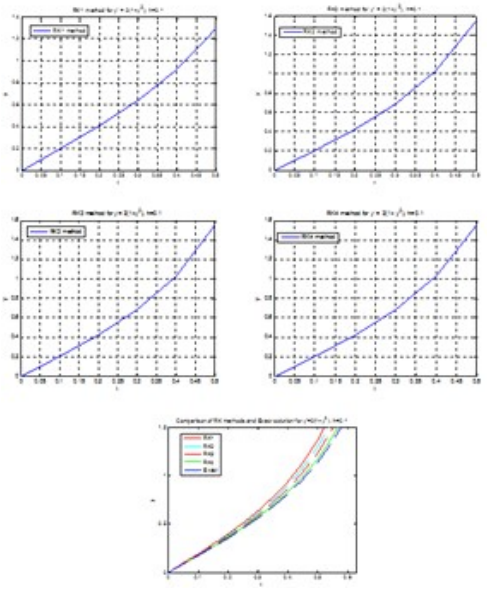

Fig3. RK1, RK2, RK3, RK4 methods and Comparison of exact solution and these methods for $y' = 2(1 + y^2)$, h=0.1

Table 3. Comparison of numerical approximations and exact solution for $y' = 2(1 + y^2)$, h= 0.05

t	Exact	RK1	RK2	RK3	RK4	Error			
						RK1	RK2	RK3	RK4
0.1	0.20 271	0.20 1	0.20 3035	0.20 271	0.20 271	0.00 171	-0.00 0325	3.35 E-07	1.65 E-07
0.2	0.42 2793	0.41 4345	0.42 3408	0.42 279	0.42 2793	0.00 8448	-0.00 0615	2.95 E-06	2.2 E-07
0.3	0.68 4137	0.67 9764	0.68 4899	0.68 4118	0.68 4137	0.02 4373	-0.00 0762	1.93 E-05	1.05 E-07
0.4	1.02 9639	0.96 7821	1.02 9887	1.02 9537	1.02 9639	0.06 1818	-0.00 0248	0.00 0102	-5.1 E-07
0.5	1.55 7408	1.39 6394	1.55 379	1.55 6847	1.55 7406	0.16 1014	0.00 3618	0.00 0561	1.28 E-06

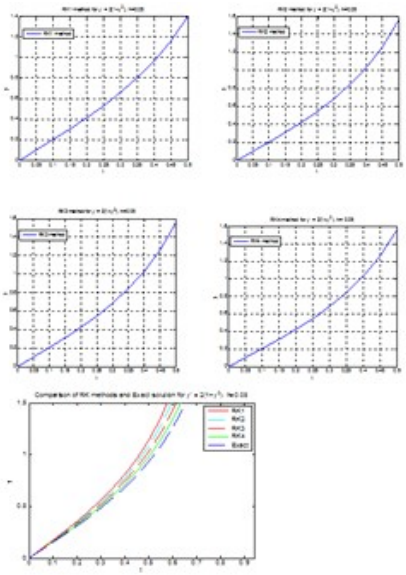

Here, although it cannot be compared with the exact solutions and the stability regions of IVPs in the examples, it is presented that the more the orders, the closer to the exact solutions and then the results of the formulas can create a good situation according to the theory of stability regions. It can be observed that the explicit Runge-Kutta methods of order 1, 2, 3 and 4 are accurate to the analytical solutions of the first order initial value problems from these tables and figures. The tables and the figures for the comparison of approximate solutions and the exact solutions are obtained by MATLAB. It is also found that the less the step-size, the closer to the exact solutions by calculating with the formulas. Hence, the fourth order Runge-Kutta method (RK4 method) gives more accuracy than the three methods.

5. CONCLUSIONS

It can be concluded that the stability regions of the explicit Runge-Kutta methods get bigger as the order increase. And it is also attained that the approximations of the explicit Runge-Kutta methods are applied to solve the first order initial value problems of the ordinary differential equations. Therefore, it is also concluded that finding more accurate result of higher order numerical methods is more appropriate than lower order methods from any point of views (the stability region and the formulas of ERK methods).

ACKNOWLEDMENT

We would like to express our gratitude to Dr Hnin Oo Lwin, Professor, Department of Mathematics, Banmaw University for her guidance, helpful advice and discussion throughout this work. In addition, our special thanks are due to our families for their kind encouragement and helpful advice.

REFERENCES

[1] F. B. Hildebrand, *Introduction to Numerical Analysis: Second Edition*, Second edition. New York: Dover Publications, 1987.

[2] "Stability of Runge-Kutta methods for stiff nonlinear differential equations (Book, 1984) [WorldCat.org]." [Online]. Available: https://www.worldcat.org/title/stability-of-runge-kutta-methods-for-stiff-nonlinear-differential-equations/ oclc/11090889. [Accessed: 10-Dec-2019].

[3] "(PDF) On Some Numerical Methods for Solving Initial Value Problems in Ordinary Differential Equations." [Online]. Available: https://www.researchgate.net/publication/271248188_On_Some_Numerical_ Methods_for_ Solving_Initial_Value_Problems_in_Ordinary_Differential_Equations. [Accessed: 10-Dec-2019].

[4] "9788120332171: Numerical Methods for Scientists and Engineers - IberLibro - K. Sankara Rao: 8120332172." [Online]. Available: https://www. iberlibro.com/9788120332171/Numerical-Methods-Scientists-Engineers-Sankara-8120332172/plp. [Accessed: 10-Dec-2019].

[5] "A Comparative Study on Numerical Solutions of Initial Value Problems (IVP) for Ordinary Differential Equations (ODE) with Euler and Runge Kutta Methods." [Online]. Available: https://www. scirp.org/journal/PaperInformation.aspx?PaperID=59961. [Accessed: 10-Dec-2019].

[6] "(PDF) Introductory methods of numerical analysis by S S Sastry .pdf | Rayhan Hossen - Academ ia.edu." [Online]. Available: https://www.acade mia.edu/37066104/Introductory_methods_of_numerical_analysis_by_S_S_Sastry_.pdf. [Accessed: 10-Dec-2019].

[7] "Numerical analysis - PDF Free Download." [Online]. Available: https://epdf.pub/numerical-analysis a5ea0ed4a0e223189988cae8 2b2c624020534 . html. [Accessed: 10-Dec-2019].

[8] "Computing stability regions—Runge-Kutta methods for delay differential equations | IMA Journal of Numerical Analysis | Oxford Academic." [Online]. Available: https://academic.oup.com/ imajna/article-abstract/14/3/347/650278? redirectedFrom=fulltext. [Accessed: 10-Dec-2019].

[9] "Stability of explicit Runge—Kutta methods - ScienceDirect." [Online]. Available: https://www.sciencedirect.com/science/article/pii/0898122184900725. [Accessed: 10-Dec-2019].

[10] A. Bellen and M. Zennaro, *Numerical Methods for Delay Differential Equations*. Oxford University Press, 2003.

Journal of Research and Applications (JRA), UCSMTLA, 2019 Volume-01, Issue-01

Article ID - JRA190079

SOL-GEL PROCESSED ZINC OXIDE FILMS AS ELECTRON TRANSPORT LAYER FOR PLANAR PEROVSKITE SOLAR CELL APPLICATIONS

Thiri Thu [(1)], Win Win Aye [(2)], Than Zaw Oo [(3)]

[(1)]University of Technology (Lashio), Myanmar

[(2)]Hakha College (Hakha), Myanmar

[(3)]Universities' of Research Center (Yangon), Myanmar

[(1)] *thirithuchoo@gmail.com*

ABSTRACT

Zinc Oxide (ZnO) films with difference thickness (13, 23, 51 nm) were prepared by sol-gel spin-coating method. The optical properties, phase and structure of ZnO films were investigated by UV-vis spectroscopy and X-ray Diffractometry. The electrical conductivity of the films were determined from the I-V characteristics of ZnO based two terminal device. The wettability of organometallic halide perovskite solution toward on the ZnO thin films were also evaluated by contact angle measurement. According to the result of UV-vis spectroscopy measurement, the optical transmission and band-gap energy 90% and 3.1 eV for thinner ZnO films (13 nm). X-ray Diffractometry study indicated that ZnO film has hexagonal structure and the calculated crystallite size was 43.13 nm for ZnO films annealed at 700C for 3 hr. The electrical conductivity is about 1.0×10^{-4} S/m for ZnO film (13 nm thick). The contact angle measurement showed lower the contact angle of ZnO towards the perovskite solution indicating that ZnO surface is hydrophilic. A series of investigation suggests that ZnO is promising as compact electron transport layer in perovskite solar cell applications.

KEYWORDS: *sol-gel, perovskite solar cell, optical transmission, band-gap energy, conductivity, wettability.*

1. INTRODUCTION

Global warming is one of the main problem in human being life that come from energy consume from fossil fuels. The energy from fossil fuels is the main reason for environmental damages. In many countries, wind, photovoltaics and hydropower are green and renewable energies. Among them, solar energy is one of the important resources. Photovoltaic is the most important technology to use the solar energy. The technology of solar cell is one of the most promising renewable energy [1], [2].

Solar cells are usually divided into three main generations. Organic solar cells and organic-inorganic hybrid perovskite solar cells (PSCs), as the third-generation solar cells, are attracting due to low-cost, flexibility and high output. Most technologies in this generation have not yet been commercialized, but there is a lot of research going on in this area [3].

Solar energy technology is very important to improve the power conversion efficiency (PCE) and reduce the cost. In order to enhance the photovoltaic performance of perovskite solar cells, a lot of researchers have been extensively studied to the interface engineering, device architecture, perovskite deposition methods, perovskite composition engineering, etc. [4]. Photovoltaic solar cells harvest sun light and convert into electrical energy. The general components of perovskite solar cells are fluorine-doped tin oxide (FTO), electron transporting layer (ETL), absorber layer (perovskite), hole transporting layer (HTL), and anode [5].

The perovskite layer can harvest the light on the basis of electron excitation. Afterwards, the electron and hole are collected at the charge transport materials. The electron and hole transport materials play, therefore, as a crucial role in determining the light harvesting and charge transport properties. There are many kinds of metal oxides and ternary metal oxides are used as ETL and HTL. Metal oxide

such as TiO_2, ZnO, SnO_2, Fe_2O_3, WO_3, etc., have received a grate attention over the last few years [6]. The favorable characterize of charge transporting window layer in solar cells are high optical transmittance, high electrical conductivity, mobility and good energy level alignment.

Among these metal oxides, ZnO possesses several advantages such as high-specific surface area, nontoxicity, chemical stability, electrochemical activity, high electron communication, high optical and electrical properties. The thin films of ZnO gave many applications such as solar cells, luminescent, electrical and acoustic devices, transparent electrodes, field effect transistors, display devices, chemical sensors, gas sensor devices, catalysis, optoelectronics transducers, and biomedical science. Moreover, ZnO has high-electron Hall mobility, wide optical band-gap, and relatively low refractive index nearly and transmittance in the visible region [7]-[8].

There are many techniques used for preparation of ZnO thin films such as physical vapor deposition, RF magnetron sputtering, chemical vapor deposition, spray pyrolysis and sol-gel technique. Among them sol-gel method especially spin coating has much attention due to simple deposition procedure, easy control of chemical components and low-cost [9], [10].

In this paper, we report the fabrication of zinc oxide layers by sol-gel spin-coating method. Moreover, the optical, electrical, structural and wetting properties of fabricated ZnO layers were carried out by using UV-vis spectrophotometer, current-voltage characteristic of a two terminal device, X-ray diffractometry and Digital Microscope. It was expected that the ZnO layers will be used as electron transporting layer in perovskite solar cells as a further study.

2. EXPERIMENT

2.1 Preparation of ZnO solution

There are three stages of thin film coating process. They are solution preparation, coating and drying of coated film. Zinc chloride [$ZnCl_2$] was used as a precursor for preparation of ZnO solution. This solution was prepared by dissolving 0.24M of $ZnCl_2$ in acetonitrile solvent (40 ml). The mixed solution was stirred using magnetic stirrer for 60 minutes. The solution was kept in a beaker for 3 hours to obtain a homogenous and transparent clear solution.

2.1.1 Spin-coating for synthesis ZnO thin films

Before the spin-coating process, we need to clean the substrates. Substrate cleaning process is the important step to get homogenous film. The glass slides as substrate were cut with size 2 cm´2 cm and were cleaned with distilled water, detergent, chromic acid, acetone and isopropyl alcohol in ultrasonic cleaner for 15 minutes each. They were also treated with 1M NaOH solution for 15 minutes to make it hydrophilic nature. Then the substrates were dried by nitrogen blow and followed by UV treatment. Figure 1 shows the substrate cleaning process before the spin-coating.

Cleaned glass substrates were span with prepared ZnO solution. The speed range of spin coater is 3000 rpm and spinning duration is 30 seconds in this research. The WS-400-6NPP-Lite spin coater (special spinning container) was used to coat the ZnO layer on substrate. The ZnO coated glasses were dried at 100 °C for 10 minutes on hot-plate. The spin-coating process repeat again and again in order to get desire thickness and then deposited films were annealed at 700 °C for 3 hours. Figure 2 shows the flow chat for synthesis of ZnO solution and thin film by spin-coating method.

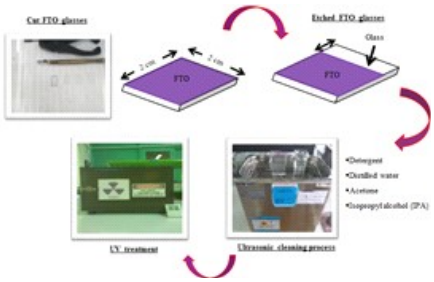

Fig1. Substrate cleaning process

3. CHARACTERIZATION OF ZnO THIN FILMS

The optical property of ZnO films was measured by UV-Vis spectrophotometer (UV-1600). The transmission spectra of ZnO films were recorded in the wavelength ranging from 400 nm-900 nm. The thickness of films were determined by surface profiler which is computerized by Alpha-Step IQ software. The electrical conductivity of films were calculated by measuring I-V characteristic of device with two terminals configuration (FTO/ZnO/Al). The structure and phase of the films were analyzed by X-ray diffractometry. The determination of wetting properties of perovskite solution (CH3NH3PbI3) on ZnO films were captured by a video camera which is attached with Digital Microscope (U500X).

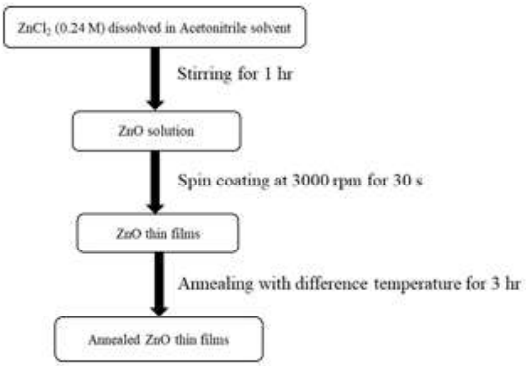

Fig2. Flow chat for synthesis of ZnO thin film

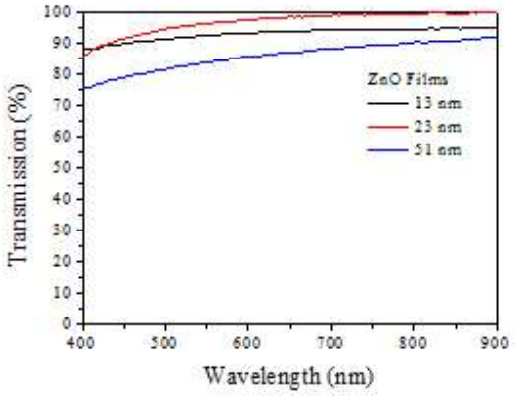

Fig3. Transmission spectra of ZnO films with difference thickness (13 nm, 23 nm, 51 nm)

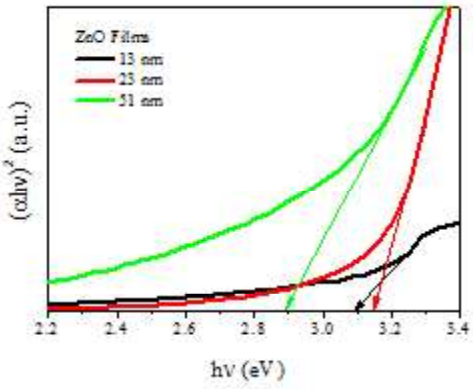

Fig4. Optical band-gap energies of ZnO films with difference thickness (13 nm, 23 nm, 51 nm)

4. RESULTS AND DISSUSIONS

4.1 Transmission and optical band-gap energy of ZnO films

The optical properties of ZnO films with difference thickness in wavelength range (400-900 nm) by using UV-Vis spectrophotometry. Figure 3 show the transmission spectra of ZnO films with difference thickness (13 nm, 23 nm, 51 nm). The transmission of ZnO films with various thickness are 90, 98 and 87% respectively. The band-gap energy is main point to select the material which can match or not with that of photosensitizer. We calculated band–gap energy E_g from absorption spectra of ZnO films by using the following equation (1).

$$\alpha h\nu = A\,(h\nu - E_g)^n \qquad (1)$$

where α is absorption coefficient, $h\nu$ is the incident photon energy, A is the proportionality constant, E_g is the band-gap energy and n is either 1/2 for direct band-gap semiconductor or 2 for indirect band-gap semiconductor [11]. Band-gap energy means the different between the conduction band and valance band of ZnO film. Figure 4 shows the optical band-gap energy of the ZnO films. The calculated band-gap energies of ZnO films with various thickness are 3.10, 3.15, 2.88 eV. Table 1 shows the transmission and optical band-gap of ZnO films with difference thickness. The calculated band-gap energies are confirmed with the references [12].

Table1. The transmission and optical band-gap of ZnO films with difference thickness

ZnO with difference thickness (nm)	Tranmission (%)	Optical band-gap energy (eV)
13	90	3.10
23	98	3.15
51	87	2.88

4.2 Electrical conductivity of ZnO films

The electrical conductivity of ZnO films were determined by measuring the current- voltage characteristic of a two terminal device (FTO/ZnO/ Ag). The device structure is shown in Figure 5. Figure 6 shows the slop of current- voltage curve of two terminal device (FTO/ZnO/Ag). The reciprocal of the slope is the resistance of the ZnO as seen in equation (2).

$$\text{Slope} = \frac{1}{R} = \frac{\Delta I}{\Delta V} \qquad (2)$$

where, R is resistant, I is current, V is voltage. The cross- sectional area (active area) of ZnO in the device is 0.24 cm^2 and the thickness (t) of ZnO films are about 13 nm, 23 nm, 51 nm by measured by surface profiometry. Using R and t values, the electrical resistivity and conductivity of ZnO were obtained using equation (3) and (4).

$$\rho = \frac{RA}{l} \qquad (3)$$

$$\sigma = \frac{1}{\rho} = \frac{l}{RA} \qquad (4)$$

where, ρ is resistivity, A is active area, σ is conductivity.

The calculated electrical conductivity values of ZnO are in table 2. According to the result, the conductivity for ZnO film with 51 nm thickness is not reasonable. According to my opinion, it may be due to experimental error during the experiment.

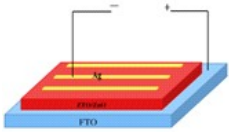

Fig 5. Structure of two terminal device

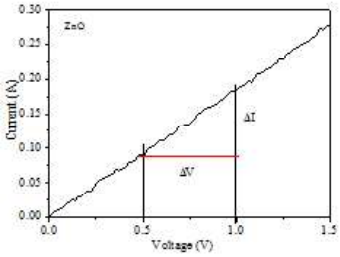

Fig6. Slop of current- voltage curve of two terminal device

Table2. The band-gap energies and electrical conductivities of ZnO

ZnO Films (nm)	Optical Band-gap Energies (eV)	Electrical Conductivity x 10^{-4} (S/m)
13	3.10	1.0
23	3.15	2.1
51	2.88	49.6

4.3 XRD characterization of ZnO films

The phase and structural characteristics of samples were examined with the X-ray diffractometry (XRD). Figure 7 shows the XRD patterns of ZnO film annealed at 700°C. ZnO with 23 nm thickness will be used to characterize the structural property of film in this paper. The samples were annealed with a fixed annealing time of 3 hr in muffle furnace. The observed XRD patterns were examined using Joint Committee on Powder Diffraction Standard (JCPDS) reference data of ZnO (JCPDS, 36-1451). In prepared ZnO film, the observed peaks can be confirmed as the ZnO hexagonal structure. The peaks of ZnO were indexed as (100), (002), (101), (102), (110), (103), (200), (112), and (201) as shown in Figure 7. The ZnO film at 700°C have sharp and narrow diffraction peaks, indicating that the materials exhibit high crystallinity and the average lattice constant were (a=3.2701 Å, c=5.2148 Å).

The strongest peak of corresponding to the plane (100) was selected to determine the crystallite size of using Debye-Scherrer's equation (3):

$$t = \frac{0.9\lambda}{\beta \cos\theta} \qquad (3)$$

where, t is the crystallite size, λ is the X-ray wavelength, β is the full-width half-maximum (FWHM) of the peak and θ is the Bragg's angle. The calculated crystallite size was 43.13 nm for ZnO film at 700°C for 3 hr. It is a good agreement with references [13], [14].

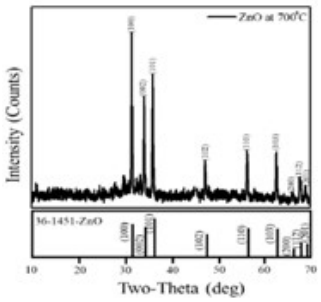

Fig 7. XRD patterns of ZnO film at 700°C

4.4 Wettability of perovskite towards ZnO films

The topic of wetting plays an important role in many industrial processes. In recent years, there has been an increasing interest in the study of super hydrophilic surfaces, due to their potential applications. Wettability studies indicates the degree of wetting when a solid and liquid interact. Small contact angles (£90°) correspond to high wettability, while large contact angles (³90°) correspond to low wettability [15]. All contact angle measurements were performed immediately after the formation of $CH_3NH_3PbI_3$ (perovskite solution) drop at the substrate. The obtained contact angles at three different locations of the same sample were averaged out. In Figure 8, the contact angles of $CH_3NH_3PbI_3$ solution on ZnO films were measured. The contact angles of $CH_3NH_3PbI_3$ solution on ZnO films is very small about 5°. Table 3 shows the contact angles of $CH_3NH_3PbI_3$ solution on ZnO films. According to this result, ZnO films are hydrophilic surfaces for $CH_3NH_3PbI_3$ solution.

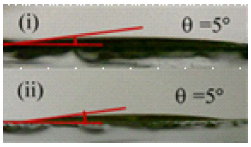

Fig 8. Contact angles of perovskite solution on ZnO thin films with difference concentrations

Table 3. The contact angles of $CH_3NH_3PbI_3$ solution on ZnO films.

Different concentrations of perovskite solution	Contact angles of perovskite solution on ZnO films
0.07 M	5°
0.24 M	5°

5. CONCLUSIONS

In this research work, synthesis and characterization of ZnO films by sol-gel spin coating method have been successfully studied. As a result of UV-vis spectrum, the optical transmission are about 90% and band-gap energy are 2.88-3.15 eV according to different thickness. From XRD analysis, ZnO was found with hexagonal structure. The average crystallite size of ZnO is about 43.13 nm. The conductivities of ZnO layers are 1 to $2´10^{-4}$ S/m. In addition, the contact angle is very small and that means the ZnO film is hydrophilic surface.

ACKNOWLEDMENT

One author, Thiri Thu, thanks the members of Materials Research Lab, Department of Physics, and University of Mandalay for their helps in experimental works.

REFERENCES

[1] J. Fan, B. Jia, and M. Gu, "Perovskite-based low-cost and high-efficiency hybrid halide solar cells," *Photonics Res.*, vol. 2, p. 111, Oct. 2014.

[2] N. K. Elumalai, A. Mahmud, D. Wang, and A. Uddin, "Perovskite Solar Cells: Progress and Advancements," 2016.

[3] S. Gamliel and L. Etgar, "Organo-metal perovskite based solar cells: sensitized versus planar architecture," *RSC Adv.*, vol. 4, no. 55, pp. 29012–29021.

[4] T. Salim, S. Sun, Y. Abe, A. Krishna, A. Grimsdale, and Y.-M. Lam, "Perovskite-Based Solar Cells: Impact of Morphology and Device Architecture on Device Performance," *J. Mater. Chem. A*, vol. 3, Dec. 2014.

[5] W. Yin, L. J. Pan, T. Yang, and Y. Liang, "Recent Advances in Interface Engineering for Planar Heterojunction Perovskite Solar Cells," *Molecules*, vol. 21, p. 837, Jun. 2016.

[6] K. Bush *et al.*, "23.6%-efficient monolithic perovskite/silicon tandem solar cells with improved stability," *Nat. Energy*, vol. 2, p. 17009, Feb. 2017.

[7] J. Duan, Q. Xiong, H. Wang, J. Zhang, and J. Hu, "ZnO nanostructures for efficient perovskite solar cells," *J. Mater. Sci. Mater. Electron.*, vol. 28, no. 1, pp. 60–66, Jan. 2017.

[8] D. Liu and T. L. Kelly, "Perovskite solar cells with a planar heterojunction structure prepared using room-temperature solution processing techniques," *Nat. Photonics*, vol. 8, no. 2, pp. 133–138, Feb. 2014.

[9] W. Hadouchi, J. Rousset, D. Tondelier, B. Geffroy, and Y. Bonnassieux, "Zinc Oxide as hole blocking layer for Perovskite solar cells deposited in atmospheric conditions," *RSC Adv*, vol. 6, Jul. 2016.

[10] H. Ebrahimi, H. Yaghoubi, F. Giammattei, and A. Takshi, "Electrochemical Detection of Piezoelectric Effect from Misaligned Zinc Oxide Nanowires Grown on a Flexible Electrode," *Electrochimica Acta*, vol. 134, pp. 435–441, Jul. 2014.

[11] "Mesoscopic CH3NH3PbI3/TiO2 Heterojunction Solar Cells." [Online]. Available: https://pubs.acs.org/doi/pdf/10.1021/ja307789s. [Accessed: 10-Dec-2019].

[12] S. Wali, H. olavanahalli Murthy, M. Bangalore, and S. Sharma, "Investigation of Influence of Spin Coating Parameters on the Morphology of ZnO Thin Films by Taguchi Method," *Int. J. Thin Films Sci. Technol.*, vol. 2, pp. 143–154, May 2013.

[13] S. T. Shishiyanu, T. S. Shishiyanu, and O. I. Lupan, "Sensing characteristics of tin-doped ZnO thin films as NO2 gas sensor," *Sens. Actuators B Chem.*, vol. 107, no. 1, pp. 379–386, May 2005.

[14] J. Alvarado, A. Maldonado, H. Juárez, and M. Pacio, "Synthesis of Colloidal ZnO Nanoparticles and Deposit of Thin Films by Spin Coating Technique," *J. Nanomater.*, vol. 2013, pp. 1–9, Dec. 2013.

[15] L. Loh, J. Briscoe, and S. Dunn, "Perovskite enhanced solid state ZnO solar cells," *J. Phys. Conf. Ser.*, vol. 476, p. 2008, Dec. 2013.